Estimating Seismic Performance of Friction Damped Braced Frames by Pushover Analysis

Er Mao Gong

A Thesis

in

The Department

of

Building, Civil and Environmental Engineering

Presented in Partial Fulfillment of the Requirement

For the Degree of Master of Applied Science at

Concordia University

Montreal, Quebec, Canada

March 2004

Your file Votre référence
ISBN: 0-612-94687-8
Our file Notre référence
ISBN: 0-612-94687-8

ABSTRACT

Estimating Seismic Performance of
Friction Damped Braced Frames by Pushover Analysis

Er Mao Gong

In previous investigations [Chopra and Goel, 2001], the Modal Pushover Analysis (MPA) procedure was demonstrated to be accurate enough in estimating floor displacements and story drifts, and identifying locations of most plastic hinges for Moment Resistant Frame (MRF) systems. The principal objective of this investigation is to implement MPA procedure to analyze Friction Damped Braced Frame (FDBF) Systems.

First, the pushover analysis procedure based on structural dynamics theory is introduced to predict the performances of one-story FDBF systems. To extend the use of pushover analysis from single-degree-of-freedom (SDF) systems to multi-degree-of-freedom (MDF) systems, the basic theory and the detail procedure of the MPA is presented with emphasis on applications to multi-story FDBF systems.

Comparing the nonlinear history responses computed by DRAIN-2DX [Allahabadi and Powell, 1988] with that of the similar MRF system, the earthquake resistance of the selected 10-story FDBF system, such as the lateral displacement resistance and the damage control potential of the structure has been increased dramatically by the friction damped bracing.

The comparisons of the seismic responses of the FDBF determined by MPA with Nonlinear Response History Analysis (NL-RHA) procedure illustrate that for a FDBF system, the MPA procedure is probably accepted in estimating floor displacements, but for the story drift of the structure, the accuracy of the MPA is too poor to be accepted. This leads to the introduction of an improved modal pushover analysis (IMPA) procedure.

Based on the MPA procedure, the IMPA procedure is implemented by pushing the structure again to the roof displacement that has been estimated by the capacity spectrum method from ATC-40 [Applied Technology Council, 1996] or by analysis of the equivalent SDF system. Therefore, the modal floor displacement is not linearly related to the mode shape. Comparing the results by IMPA and NL-RHA, the errors are much smaller than that of MPA procedure, especially in calculating the story drift of the structure. Comparing the seismic demands determined by IMPA procedure, FEMA-273 pushover analysis [Building Seismic Safety Council, 1997], and NL-RHA, it is demonstrated that the IMPA procedure is also better than FEMA-273 pushover analysis in determining the floor displacement, story drifts and the plastic slip of the friction damped bracing.

ACKNOWLEDGEMENTS

The author acknowledges with gratitude the valuable guidance, support and encouragement provide by his supervisor, Professor O. A. Pekau, during the entire course of this research. His critical review, together with his excellent sense of engineering judgement, have proved invaluable to the quality of this work.

The financial support for this work was provided by National Sciences and Engineering Research Council of Canada under Grant No. A8258. The Avtar S.Pall Award is also gratefully acknowledged. The excellent computing facilities offered at the Building, Civil and Environmental Engineering Department at Concordia University have been very useful in conducting the work.

Finally, the deepest gratitude goes to the author's wife Jian Zhen for her utmost patience and understanding throughout this study. The encouragement and inspiration demonstrated by author's lovely daughters, Jennifer and Jin, deserve greatest appreciation.

TABLE OF CONTENTS

LIST OF FIGURES

LIST OF TABLES

LIST OF ABBREVIATIONS

BMRF	Braced Moment Resistant Frame
ELF	Equivalent Lateral Force Distribution
FDBF	Friction Damped Braced Frame
IMPA	Improved Modal Pushover Analysis Procedure
MDF	Multi-degree-of-freedom
MPA	Modal Pushover Analysis Procedure
MRF	Moment Resistant Frame
NL-RHA	Nonlinear Response History Analysis Procedure
SDF	Single-degree-of-freedom
SRSS	Square-Root-of-Sum-of-Squares Rule

LIST OF NOTATIONS

$\{1\}$	unity vector
a_{np}	spectral acceleration of the demand performance point for the *n*th-mode
a_p	spectral acceleration of the demand performance point
a_{pi}	acceleration of trial point *i*
a_y	acceleration of yield point
A_b	cross section of the brace
$A_n(t)$	pseudo-acceleration history of the *n*th-mode inelastic SDF system
$[c]$	damping coefficient matrix
c	damping coefficient
C_A, C_V	the seismic coefficients
d_{np}	spectral displacement of the demand performance point for the *n*th-mode
d_p	spectral displacement of the demand performance point
d_{pi}	displacement of trial point *i*
d_y	displacement of yield point
$D_n(t)$	deformation history of the *n*th-mode inelastic SDF system
D_{no}	peak deformation of the *n*th-mode inelastic SDF system
E	the Young's modulus of elasticity
f_{jn}	lateral force for the *n*th-mode
f_D	damping force
f_I	inertia force
f_S	lateral force

$\{f_s(u)\}$	lateral force vector for nonlinear system
F_{sn}	resisting lateral force for nonlinear system
F_y	yield stress
h	height of each floor
h_j	height of the jth floor above the ground
$I_{b,}$ $\mathrm{I_c}$	moment of inertia of beam and column
k	structural stiffness, the exponent for ELF distribution
K_b	stiffness of the brace
K_f	stiffness of the frame
K_{FDBF}	stiffness of the FDBF
K_{MRF}	stiffness of the MRF
L	bay length of the frame
$[m]$	mass matrix
m	structural mass
m^*	structural mass for the equivalent SDF system
m_j	mass at the jth floor
M_n^*	effective modal mass
$\sum_i m_i$	total value of mass for the system
Mp_b, Mp_c	yield moment of beam and column
M_f^*	controlling yield moment of the column for the equivalent SDF system
P_s	slip load of the brace
$q_n(t)$	modal coordinate

$\{s_n^*\}$	force distribution vector
s_j^*	FEMA-273 force distribution
S_a	spectral acceleration
S_d	spectral displacement
SR_A , SR_V	spectral reduction factors
T_n	natural period of the structure
T_s	control period
$\{u(t)\}$	displacement vector
$u^t(t)$	total displacement of the mass
$\{\dot{u}(t)\}$	velocity vector
$\{\ddot{u}(t)\}$	acceleration vector
$\ddot{u}^t(t)$	total acceleration of the mass
$u_g(t)$	displacement of ground motion
$\ddot{u}_g(t)$	acceleration of ground motion
u_m	peak value of the displacement
u_{no}	peak roof displacement for the *n*th-mode SDF system
u	displacement
u_o	roof displacement
u_{oi}	roof displacement at point *i* in the capacity curve
u_F^r	peak roof displacement of the FDBF
u_M^r	peak roof displacement of the MRF
u_y	displacement at yield point

V	base shear force
V_i	base shear force at point *i* in the capacity curve
V_b, V_f	shears resisted by the brace and the frame
V_{jn}	shear at the *j*th floor for the *n*th-mode
V_o	base shear when the displacements reach u_o
V_y	base shear when the displacements reach u_y
V_f^*	yield force of the column for the equivalent SDF system
ZEN	shaking intensity
α	reduction factor of stiffness
α_n	modal mass coefficient
Γ_n	modal participation factor
ζ	viscous damping ratio of linearly elastic system
ζ_{eq}	equivalent viscous damping ratio
$\hat{\zeta}_{eq}$	effective viscous damping ratio used in equivalent linear procedures
ζ_n	damping ratio for the *n*th-mode
ω_F	first natural frequency of the FDBF
ω_M	first natural frequency of the MRF
ω_n	natural period of the structure for the *n*th-mode
$\{\phi_n\}$	mode shape
ϕ_{no}	roof level amplitude of the *n*th-mode
ρ	beam to column stiffness ratio

λ	stiffness ratio of the brace to the frame
σ_s	normal stress
φ	angle between the brace and the beam
□	damping modification factor

CHAPTER 1

INTRODUCTION

1.1 GENERAL

Over the past two decades, two subjects, 1) Pushover Analysis procedure, and 2) Friction Damped Braced Frames (FDBFs) have become more and more popular in earthquake engineering.

Pushover analysis is a nonlinear static procedure by which the structure is pushed to a predetermined target displacement by increasing lateral forces with a constant static force distribution. The predetermined target displacement can be estimated by the capacity spectrum method (CSM) [Applied Technology Council, 1996], but the CSM procedure itself also depends on pushover curve that is obtained from pushover procedure. For the lateral force distributions, several pushover analysis procedures have been developed, such as the FEMA-273 pushover procedure and modal pushover analysis procedure (MPA). Modal pushover analysis procedure is a simplified computational method for seismic performance evaluation of structures [Chopra and Goel, 2001]. For MPA procedure, first of all, a Multi-Degree-of-Freedom (MDF) system is separated into several equivalent Single-Degree-of-Freedom (SDF) systems, and each SDF system represents one mode of the MDF system. By utilizing the orthogonal property of modes, only the *n*th mode contributes to the response of the *n*th SDF system. The peak value of the total response can be obtained by combining the several modal contributions by the

Square-Root-of-Sum-of-Squares (SRSS) rule. Up to now, many investigations [Saiidi and Sozen, 1981; Rao et al., 1996; Tso and Moghadam, 1998; Kuramoto et al., 2000; Chopra and Goel, 2001] have demonstrated that pushover analysis procedures are accurate enough for practical evaluation and design for normal structures, such as Moment Resistant Frames (MFRs).

By incorporating friction damped braces in a moment resistant frame, the seismic performance of a FDBF System, such as the lateral displacement resistance and damage control potential of the structure, are increased dramatically. During a major earthquake, most of the seismic energy is dissipated by the friction damped braces which slip at predetermined loads. Because this kind of slipping can be designed so that it occurs before yielding in main members of the frame, beams and columns are protected from yielding and hinge formation. Many researchers [Pall and Marsh, 1982; Baktash, 1989; Pall and Pall, 1993; Adam and Ziegler, 1996; Pall and Pall, 1996; Lin et al., 2000] have focused on comparisons of seismic performances of FDBF with that of MRF by dynamic analysis. It was demonstrated that the FDBF systems have better seismic performance than the MRF systems in resisting floor displacements, story drifts and decreasing damage of the structures.

1.2 OBJECTIVE

However, little research has concerned combination of the above two issues, i.e., to implement pushover analysis procedures to analyze the friction damped braced frames (FDBF) systems. Hence, the principal objective of this investigation is an attempt to

apply pushover analysis procedures for determining the performance evaluation of FDBF systems and check the accuracy by comparing the results calculated by MPA procedure, Nonlinear Response History Analysis (NL-RHA) and FEMA-273 Pushover Analysis procedure. Moreover, an Improved Modal Pushover Analysis procedure (IMPA) is introduced to analyze FDBF systems, because the MPA procedure can provide good estimate of floor displacements for the FDBF systems, but for the story drifts, the accuracy is not acceptable.

1.3 SCOPE

1.3.1 Types of Structures

This research is focused on the behavior of FDBF systems, such as the earthquake resistance, the control potential of the lateral displacement and damage of the structure. For comparison purposes, two types of structures are considered in this investigation. One is the moment resistant frame and another one is the friction damped braced frame. Single-bay, one-story and 10-story structures are selected for detailed study.

1.3.2 Analytical Procedures

Nonlinear Response History Analysis (NL-RHA)

NL-RHA procedure is the most rigorous procedure to determine the response of structures subjected to ground motions during an earthquake. The results computed by NL-RHA procedure are considered as the references for comparisons with MPA and FEMA-273 pushover analysis procedures. DRAIN-2DX [Allahabadi and Powell, 1988] is used for NL-RHA for the structures during this investigation. Although the NL-RHA

procedure is becoming much easier than before, it is still time consuming especially when the system is considered to be subjected to a long duration of ground motion (e.g. for a 1-bay, 10-story FDBF system assumed subjected to a 30 seconds ground motion, the total computer time for the structure is about 22 minutes).

Capacity Spectrum Method (CSM)

The capacity spectrum method (CSM) is a graphical and approximate method [Nagao et al., 2000] that is used to find the performance point of a structure by comparing the capacity spectrum of the structure and demand spectrum of the design earthquake.

In ATC-40, three procedures (procedure A, B and C) are introduced to determine the performance point. In this thesis, procedure A is chosen for implementation in case studies in Chapters 4 and 5 because it is the most direct application of the methodology and the iteration can be done by hand or by spreadsheet methods.

The step by step procedure A of CSM [Applied Technology Council, 1996] for estimating the performance point of a structure for *n*th-mode is illustrated in flow chart 1.1. This includes:

1. Develop the 5 percent damped (elastic) response spectrum appropriate for the site.
   1.1. Develop the elastic traditional spectrum, with S_a versus T, by

$$\begin{cases} S_a = 2.5 \cdot C_A & T \le T_s \\ S_a = \dfrac{C_V}{T} & T > T_s \\ T_s = \dfrac{C_V}{2.5 \cdot C_A} \end{cases} \tag{1.1}$$

where the seismic coefficients, C_A, and, C_V, are depended on the soil profile type and the shaking intensity ZEN. They can be obtained from Appendices B.1 [Table 4-7, ATC-40] and B.2 [Table 4-8, ATC-40]. T_s is the control period.

1.2. Transform the elastic traditional spectrum to the elastic response spectrum *(ζ=5%)* with S_a versus S_d, by

$$S_a = \omega^2 S_d \tag{1.3}$$

$$S_d = \frac{1}{4\pi^2} S_a T^2 \tag{1.4}$$

where ζ is the viscous damping ratio of linearly elastic system, S_a and S_d are the spectral acceleration and displacement.

2. Develop the capacity curve by pushing the structure to a target roof displacement.
3. Transform the capacity curve into a capacity spectrum by

$$S_{ai} = \frac{V_i}{M_n^*} = \frac{V_i}{\alpha_n \cdot \sum M}, \qquad S_{di} = \frac{u_{oi}}{\Gamma_n \cdot \phi_{no}} \tag{1.5}$$

where α_n and Γ_n are respectively the modal mass coefficient and participation factors for nth mode of the structure, M_n^* is the effective modal mass, $\sum M$ is the total mass of the structure, ϕ_{no} is the roof level amplitude of the nth mode, S_{di}, S_{ai} are the horizontal axis and vertical axis of any point i in the capacity spectrum, and u_{oi}, V_i are the horizontal axis and vertical axis of any point i in the capacity curve, respectively.

4. Plot the capacity spectrum for the nth mode on the same chart as the 5 percent damped (elastic) response spectrum.

5. Select a trial performance point and develop the bilinear spectrum which represents the portion of the capacity spectrum from the beginning point (0,0) to the trial performance point.

6. Calculate the effective viscous damping $\hat{\zeta}_{eq}$ which will be used in equivalent linear procedures

$$\hat{\zeta}_{eq} = \frac{63.7\kappa(a_y d_{pi} - d_y a_{pi})}{a_{pi} d_{pi}} + 5 \tag{1.6}$$

where a_y, d_y, a_{pi}, d_{pi} are the coordinates of the yield point and the trial point for any bilinear spectrum; κ is the value for damping modification factor shown in Appendix B.3 [Table 8-1, ATC, 1996].

7. Calculate the spectral reduction factors SR_A and SR_V by

$$SR_A = \frac{3.21 - 0.68\ln(\hat{\zeta}_{eq})}{2.12} \geq \text{Value in Appendix B.4 [ATC, 1996]} \tag{1.7}$$

$$SR_V = \frac{2.31 - 0.41\ln(\hat{\zeta}_{eq})}{1.65} \geq \text{Value in Appendix B.4 [ATC, 1996]} \tag{1.8}$$

where $\hat{\zeta}_{eq}$ is the effective viscous damping ratio.

The demand spectrum is developed by

$$\begin{cases} S_a = 2.5 \cdot SR_A \cdot C_A & T \leq T_s \\ S_a = \dfrac{SR_V \cdot C_V}{T} & T > T_s \\ T_s = \dfrac{SR_V \cdot C_V}{2.5 \cdot SR_A \cdot C_A} \end{cases} \tag{1.9}$$

8. Plot the demand spectrum on the same plot as the capacity spectrum.
9. Compare the intersection point of the demand spectrum and the capacity spectrum with the initial trial performance point. If the error of the displacement between these two points is less than *5%*, i.e., the demand spectrum intersects the capacity spectrum within acceptable tolerance. The initial trial performance point, a_{p1}, d_{p1}, can be considered as the demand performance point, a_p, d_p.
10. If the demand spectrum does not intersect the capacity spectrum within acceptable tolerance, then select the intersection point as a new trial performance point and return to step 5, until the demand spectrum intersects the capacity spectrum within acceptable tolerance.

FEMA-273 Pushover Analysis

FEMA-273 Pushover Analysis [Building Seismic Safety Council, 1997] is one kind of non-linear static analysis procedure by which the pushover curves of structures are developed. In this procedure, the structures are assumed to be subjected to three kinds of distributions for lateral forces: 1) uniform force distribution, 2) equivalent lateral force distribution and 3) SRSS force distribution. For each force distribution, the response of a structure, such as floor displacements, story drifts, joint rotations and plastic hinge rotations are simply calculated for a target roof displacement which can be estimated by the capacity spectrum method described in ATC-40 [Applied Technology Council, 1996].

Modal Pushover Analysis (MPA)

In 2001, a modal pushover analysis (MPA) procedure was presented by Chopra and Goel. In their report [Chopra and Goel, 2001], the detailed step-by-step MPA procedure was listed as follows, and it is also shown in flow chart 1.2:

1. Compute natural frequency, ω_n, and mode, $\{\phi_n\}$, for each mode by the modal analysis of the building by modal analysis.
2. For the nth-"mode", define the force distribution $\{s_n^*\}$ as

$$\{s_n^*\} = [m] \cdot \{\phi_n\} \tag{1.10}$$

   where $[m]$ is the matrix of the mass and $\{\phi_n\}$ is mode shape.
3. Applying force distribution incrementally, the pushover curve for the nth-"mode", a plot of the base shears and associated roof displacements, is developed by pushing the structure just beyond the target roof displacement. Since the target roof displacement may not be known at the start of the procedure, an assumption of it would be judged and iterations may be necessary. The final target roof displacement for pushover analysis should bigger than the roof displacement determined in step 7.
4. Idealize the pushover curve as a bilinear curve using the rule of equal area that is described in FEMA-273 procedure [Building Seismic Safety Council, 1977].
5. Develop the properties of the equivalent SDF system with unit mass and stiffness associated with the natural frequency.
6. Compute the peak deformation, D_{no}, of the nth "mode" inelastic SDF system. Compute deformation history, $D_n(t)$, and pseudo-acceleration history, $A_n(t)$, for the nth-mode SDF system developed from step 5 by any software, e.g., DRAIN-2DX [Allahabadi and Powell, 1988], SAP2000 [Willson, 1998] .

7. Calculate the peak roof displacement u_{no} associated with the nth-mode inelastic SDF system by

$$u_{no} = \Gamma_n \phi_{no} D_{no} \tag{1.11}$$

in which Γ_n is the participation factor for nth mode and ϕ_{no} is value of the nth mode at roof level,

8. At u_{no}, the values of floor displacements can be extracted by mode shape $\{\phi\}$ times the peak roof displacement, u_{no}, and so on for the other responses of the structure.
9. Repeat step 4 to 8 for as many "modes" as required for sufficient accuracy. Typically, the first three "modes" will be sufficient, which was demonstrated by Lopez and Cruz, 1996.
10. Determine the total response by combining the peak "modal" responses using the SRSS combination rule. From the total hinge rotation, subtract the yield hinge rotation to determine the plastic hinge rotation.

The peak deformation, or the peak roof displacement, can also be simply estimated by hand or in a spreadsheet using the capacity spectrum method which is described in detail in ATC-40 [Applied Technology Council, 1996]. The capacity spectrum method directly applies the concepts and does not require any structural analysis software so that it is preferred for use for the multi-story FDBF system in this investigation.

Improved Modal Pushover Analysis (IMPA)

After the peak roof displacement for each mode is obtained by the capacity spectrum method, in the IMPA procedure the structure is pushed again to the peak roof

displacement with the same modal lateral force distribution as MPA. The SRSS rule is used to compute the peak responses of structures, such as floor displacements, story drifts, joint rotations and plastic hinge rotations, etc.

1.4 ORGANIZATION OF THE THESIS

Chapter 1 Introduction

Chapter 1 provides the statement of the objective and scope of this investigation, followed by the brief description of each chapter.

Chapter 2 Literature Review

Chapter 2 presents existing literature related to the FDBF system and pushover analysis procedures. At same time, the detailed step-by-step implementation of FEMA pushover analysis, MPA and IMPA procedure are introduced.

Chapter 3 One-Story Systems

The basic concepts of single-degree-of-freedom (SDF) system will be introduced in this chapter; they are also the foundation of MPA since all the multi-degree-of-freedom (MDF) systems finally transfer to the equivalent SDF systems according MPA procedure. An approach to optimize the slip load and stiffness of the brace for the one-story FDBF will be proposed. For the selected one-story FDBF system, the MPA procedure will be implemented to demonstrate that it can provide good estimation for the seismic response.

Chapter 4 Multistory Moment Resisting Frame (MRF) System

Chapter 4 presents a case study of a single bay, 10-story MRF system for which the MPA procedure is implemented. The capacity spectrum method from ATC-40 [Applied Technology Council, 1996] is introduced and used to estimate the peak value of the roof displacement for MPA for the MRF system. It is employed because it is the most direct application of the concepts and it is not necessary to use any structural analysis software.

Chapter 5 Multistory Friction Damped Braced Frame (FDBF) System

In Chapter 5, a multi-story FDBF system is optimized for the maximum amount of energy which will be dissipated by the friction damped braces. The comparisons of the roof displacement and story drifts determined by MPA and NL-RHA are illustrated in figures and tables. Because of the limitations of the MPA procedure, an improved modal pushover analysis (IMPA) procedure is proposed in this chapter in order to obtain more accurate estimation of the seismic performance of the FDBF system,

Chapter 6 Conclusions

The conclusions of this investigation are presented in chapter 6, and the recommendations of the future work are also discussed in this chapter.

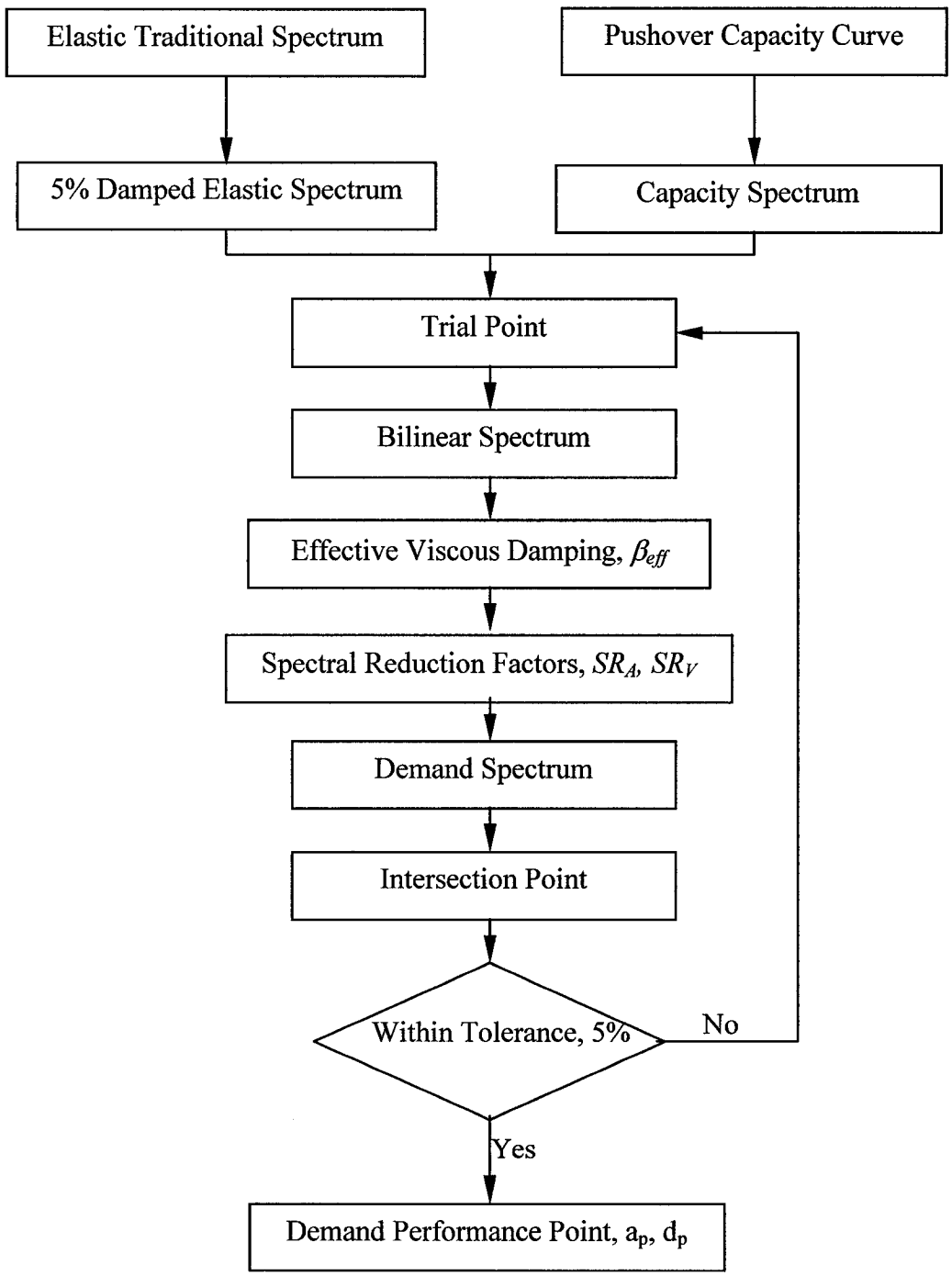

Flow Chart 1.1 Capacity Spectrum Method (CSM) Procedure A

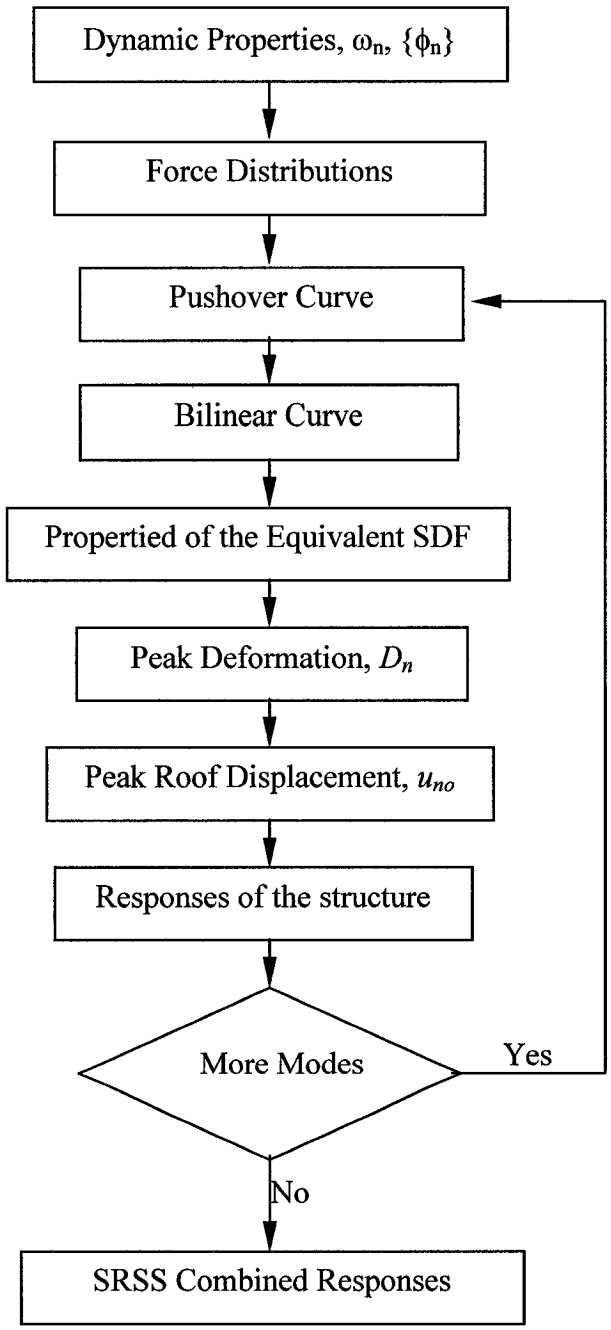

Flow Chart 1.2 Modal Pushover Analysis (MPA) Procedure

CHAPTER 2

LITERATURE REVIEW

2.1 FDBF SYSTEMS

2.1.1 The Behavior of FDBF Systems

Different from moment resistant frames, each brace in a FDBF system is connected by a friction joint. In order to obtain the behavior of the FDBF systems, it is necessary to model the performance of the friction devices in earthquakes. Figure 2.1 illustrates the simple hysteretic behavior of a friction joint which slips in tension and compression. It shows that the force displacement relation of the friction brace is linear before the force reaches the slip force, P_s. After that, the brace slips at constant slip force; therefore, the seismic energy is dissipated by the slipping joint which acts as a damper. Unloading from the maximum displacement, the hysteretic loop of the force displacement relationship is changed to a path parallel to the initial elastic branch until slip of the friction joint occurs in the opposite direction.

By optimizing the slip force and the stiffness of the braces, maximum seismic energy can be dissipated by the friction damped braces. For an earthquake considered, the main frame can be pre-designed to be elastic so that no permanent damage will occur in the main structure. If the shaking intensity in the site is higher than that of the design earthquake, as the shear resistance increases, the main frame is brought into action which leads to first yield in main elements of the frame. As yielding in the main frame provides

additional dissipation of the seismic energy, it is possible for FDBF systems to control the margin of safety of the building compared to other frames.

2.1.2 Previous Research and Application of FDBF Systems

In 1982, an investigation of the response of FDBF system was presented by Pall and Marsh [Pall and Marsh, 1982]. Three types of 10-story frames, namely moment resisting frame (MRF); braced moment resisting frame (BMRF) and FDBF, were compared by dynamic analysis assuming that the structures were subjected to the same earthquake ground motion. The comparisons were focused on peak roof displacements and their time-history responses, the maximum moments in the beams, the maximum shear envelope of the columns and the damage of the structures. The results are summarized in Table 2.1. It was shown that the earthquake resistance of FDBF was dramatically enhanced by using the friction damped braces in the frames.

In 1989, a thesis of Friction Damped Braced Frames was presented by Baktash [Baktash, 1989]. In her research, three types of FDBF, Z-Braced, K-Braced and X-Braced frames were analyzed. The methodology of optimizing the slipping loads of the braces was introduced in order to dissipate maximum energy by friction damped braces. The comparisons in tables and diagrams were also made by nonlinear dynamic analysis between the FDBF and traditional frames without friction dampers. For all types of FDBF systems, the floor displacements, the forces in elements and the damage of the structures were much lower than that of the frames without friction dampers. In that investigation, a steel model of FDBF was designed and tested on a shaking table. It was

shown that the performance of the FDBF system was in good agreement with the computer predictions.

In 1996, two semi-active schemes, the "off-on" friction damper and the "Semi-Active Friction Damper"(SAFD), were proposed by Dowdell and Cherry. In the "off-on" system, the slip force was switched between zero and a pre-determined constant value, while in the SAFD system it was considered continuously in response to the deformation state of the structure. It was demonstrated that these two systems could significantly enhance the performance of a passive friction damped structure.

By redistribution of the slip load of the friction devices over the plan layout of the building, the application of the FDBF was extended from symmetric structures to un-symmetric structures [Martin and Pekau, 1996; Pekau and Guimond, 1991].

From the middle of the 1980's, a novel Pall damper [Pall and Pall, 1996] had been developed and, in 1987, it was applied for the first time in constructing the 10-story concrete frames in Concordia University Library in Montreal. Up to 1996, it had been extensively used in the seismic design, construction and retrofit of structures for more than 15 buildings. The buildings with Pall Friction-Dampers were summarized in Table 1 [Pall and Pall, 1996]. The practical applications show that the FDBF systems are efficient in energy dissipation, saving cost of construction and retrofit of structures.

2.1.3 Simplified Method for FDBF

In 1996, a simplified design method for retrofit of gravity load design RC frame with friction dampers was introduced [Rao et al., 1996]. In this study, the CSM [Applied Technology Council, 1996] was introduced to predict the performance of a 3-story retrofitted frame with friction damper in the report. It was also used to calculate the slipping load for the dampers. It was shown that the earthquake performance of the structure was great optimized by implementing the friction dampers, which can increase the stiffness and control the strength of the structure. For design of building structures with supplemental lead dampers, another group [Lin et al., 2000] proposed four types of lateral load distributions for pushover analysis, such as only one lateral force acting on the top floor (case-I), parabolic load distribution (case-II), inverted-triangular load distribution (case-III) and uniform distribution (case-IV). The comparisons of the structural responses were made in tables and showed that the simplified method using an equivalent SDF system was efficient to predict the responses of the MDOF structures.

2.2 PREVIOUS RESEARCH AND APPLICATION IN FEMA-273 AND CSM

Over the past two decades, pushover analysis procedures have become more and more popular as simplified computer methods for seismic performance evaluation of structures. Up to now, there are so many investigations focused on the implementation of pushover analysis procedures in the analysis of the seismic performances of structures [Kuramoto et al., 2000; Kelly and Chambers, 2000; Kim et al., 1999; Nagao et al., 2000]. The results of analysis proved that although these methods were not very accurate, they could

provide fair estimate for the evaluation of structural behavior during strong earthquakes, such as the deflections and the plastic mechanism of the structure.

The application of pushover analysis procedures was also extended to different structures, such as asymmetric structures, steel building, RC buildings and masonry buildings [Kilar and Fajfar, 1997; Moghadam and Tso, 2000; Magenes, 2000; Sheu et al., 2000; Peter and Badoux, 2000; Skokan and Hart, 2000].

To eliminate the errors in the ATC-40 (CSM) procedures, an improved CSM method which used the well-known constant-ductility design spectrum for the demand diagram was proposed by Chopra and Goel [1999].

To check the accuracy of pushover analysis procedures, a 1:12 scale 10-story reinforced concrete frame was tested by Lee and Kang [2000]. The comparisons between the experimental and analytical results showed that the pushover analysis can predict the overall responses such as story shear versus inter-story drift with very high reliability, but for the local inelastic behavior or damage patterns, it seemed to have some limitations.

2.3 PREVIOUS RESEARCH AND APPLICATION IN MPA

A simple nonlinear seismic analysis methodology for R/C structures was proposed by Saiidi and Sozen in 1981, when the computer was not as powerful as today. It is necessary to develop a simple procedure with conceptual simplicity and computational economy. That kind of necessity led to the development of the Q-model by involving two

simplifications: (1) Reduction of a multi-degree-of-freedom (MDOF) model of a structure to a single-degree-of-freedom (SDOF) oscillator; and (2) approximation of the equivalent stiffness of the SDOF oscillator by a single nonlinear spring. The Q-model illustrated in [Saiidi and Sozen, 1981] is shown in Figure 2.2. The two main attributes of the Q-model procedure, conceptual simplicity and computational economy, are also the principal objectives of the modern modal pushover analysis (MPA) procedure described in [Chopra and Goel, 2001]. The Q-model procedure was tested by eight small-scale reinforced concrete structures and the experimental results, as shown as in Figures and Tables in [Saiidi and Sozen, 1981], demonstrated that the overall performance of this methodology for estimating the response of structures subjected to strong ground motion was satisfactory.

A 9-story SAC building was selected by Chopra and Goel [2001] and analyzed by MPA procedure, FEMA-273 pushover analysis [Building Seismic Safety Council, 1997] and rigorous nonlinear response history analysis (RHA) using DRAIN-2DX [Allahabadi and Powell, 1988], respectively. The comparisons of the peak inelastic response determined by those analysis procedures, as shown as in Tables 2.2, 2.3 and 2.4, demonstrated that the MPA procedure provided better results than FEMA-273 pushover analysis procedure in estimating the floor displacements, story drifts and identified locations of most plastic hinges of the MRF structures. However, Chopra and Goel [2001] reported that both of those two simplified pushover analysis procedures were less accurate in estimating the plastic hinge rotations.

2.4 IMPA PROCEDURE AND SOME RESULTS

Modal pushover analysis (MPA) procedure, as one of the pushover analysis procedures, depends on two basic assumptions: (1) The response of the structure is related to the response of an equivalent single-degree-of-freedom system, (2) the mode shape vector remains constant throughout the time history response. Obviously, both assumptions are incorrect, which led to an improved pushover analysis procedure presented by Yang and Wang [2000]. In order to decrease the errors for these assumptions, a lateral load pattern was introduced as the approximation of the distribution of the inertia force obtained from results of dynamic analysis of the story equivalent MDOF system of the structure, which was time dependent. It was similar to the SRSS distribution in FEMA-273 [Building Seismic Safety Council, 1977], which will be introduced in case studies in Chapters 4 and 5.

The improved modal pushover analysis procedure (IMPA) will be emphasized and implemented in this investigation. It is based on MPA procedure mentioned before (Section 1.3.2). The only difference between MPA and IMPA procedures is in step 8, which becomes:

8. After the peak roof displacement u_{no} associated with nth "mode" inelastic SDF system is obtained by step 7, apply the same force distribution as step 2 and push the structure again to the peak roof displacement, u_{no}. The responses of floor displacements are calculated as well as the story drifts. It is noted that the distribution of floor displacements of the nth mode is different from the mode shape of that mode,

and this nonlinear distribution would be closer to the NL-RHA distribution than that of MPA procedure.

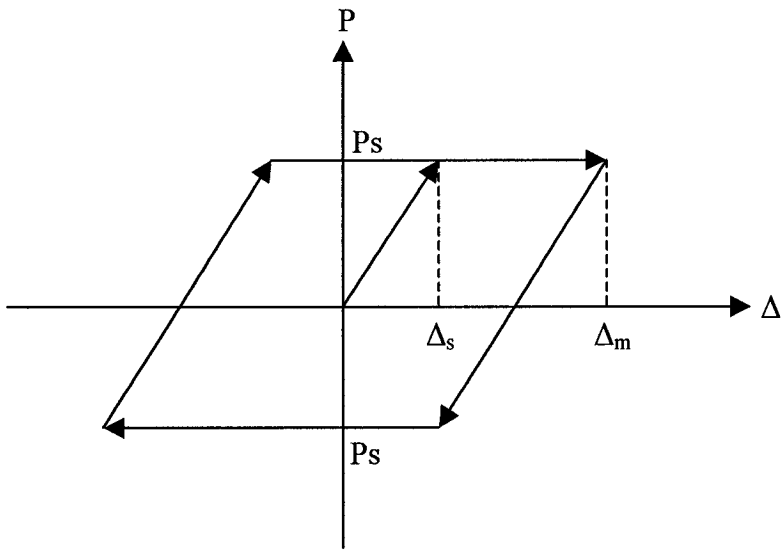

Figure 2.1. Axial Force/Displacement Behaviors of Braces in FDBF [Baktash, 1989], P_s=slip force

Table 2.1. Behavior of MRF, BMRF and FDBF

Frame	Roof Displacement	Maximum Base Shear	Maximum Base Moment	Axial Forces	Damage in Beams	Damage in Columns	Damage in Braces
MRF	100.0%	87.5%	90.7%	60.0%	90.0%	10.0%	-
BMRF	80.0%	100.0%	100.0%	100.0%	80.0%	-	100.0%
FDBF	40.0%	70.0%	68.0%	75.0%	40.0%	-	-

* Data developed from [Pall and Marsh, 1982]

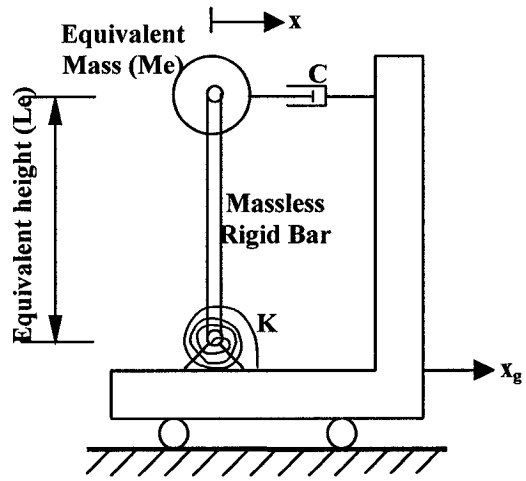

Figure 2.2. Q-Model [Saiidi and Sozen, 1981]

Table 2.2. Peak Values of Floor Displacement Ratios (as % of building height=37.14 m) from FEMA and MPA for 1.5 El-Centro for the 9-story MRF[Chopra and Goel, 2001]

Floor	Displacement/Height (%)					Error (%)			
	FEMA			MPA 3 modes	NL-RHA	FEMA			MPA 3 modes
	Uniform	ELF	SRSS			Uniform	ELF	SRSS	
0	0	0	0	0	0.000	0	0	0	0
1	0.344	0.195	0.209	0.263	0.270	27.6	-27.7	-22.5	-2.6
2	0.597	0.351	0.355	0.466	0.490	21.8	-28.4	-27.5	-4.8
3	0.809	0.524	0.487	0.667	0.686	17.9	-23.7	-29.1	-2.8
4	0.975	0.708	0.611	0.854	0.836	16.7	-15.3	-26.9	2.2
5	1.089	0.875	0.724	0.998	0.913	19.3	-4.2	-20.6	9.4
6	1.178	1.015	0.840	1.109	0.953	23.7	6.5	-11.9	16.4
7	1.262	1.154	1.007	1.214	0.998	26.5	15.6	0.9	21.7
8	1.341	1.294	1.221	1.330	1.098	22.2	17.9	11.2	21.2
9	1.399	1.399	1.399	1.436	1.199	16.7	16.7	16.7	19.8

Table 2.3. Peak Values of Story Drifts Ratios (as % of story height) from FEMA and MPA for 1.5 El-Centro for the 9-story MRF[Chopra and Goel, 2001]

Floor	drift/story height (%)					Error (%)			
	FEMA			MPA 3 modes	NL-RHA	FEMA			MPA 3 modes
	Uniform	ELF	SRSS			Uniform	ELF	SRSS	
1	2.335	1.323	1.417	1.783	1.830	27.6	-27.7	-22.5	-2.6
2	2.367	1.462	1.372	1.927	2.064	14.7	-29.2	-33.5	-6.6
3	1.992	1.623	1.234	1.938	1.858	7.2	-12.6	-33.6	4.3
4	1.560	1.730	1.168	1.860	1.414	10.3	22.3	-17.4	31.5
5	1.067	1.562	1.061	1.530	1.207	-11.6	29.4	-12.1	26.8
6	0.839	1.314	1.083	1.310	1.128	-25.6	16.5	-3.9	16.2
7	0.789	1.306	1.566	1.530	1.353	-41.7	-3.5	15.8	13.1
8	0.736	1.318	2.011	1.888	1.877	-60.8	-29.8	7.1	0.5
9	0.547	0.984	1.672	1.673	1.515	-63.9	-35.0	10.4	10.5

Table 2.4. Peak Values of Plastic Hinge Rotations from FEMA and MPA for 1.5 El-Centro for the 9-story MRF[Chopra and Goel, 2001]

Floor	Rotation (rad)					Error (%)			
	FEMA			MPA 3 modes	NL-RHA	FEMA			MPA 3 modes
	Uniform	ELF	SRSS			Uniform	ELF	SRSS	
1	1.53E-2	4.51E-3	4.94E-3	8.35E-3	1.23E-2	24.2	-63.4	-59.9	-32.3
2	1.10E-2	4.65E-3	2.34E-3	8.11E-3	1.04E-2	5.2	-55.3	-77.6	-22.2
3	7.93E-3	7.03E-3	2.16E-3	9.00E-3	8.26E-3	-4.0	-14.8	-73.8	9.0
4	1.62E-3	5.45E-3	0.00	5.19E-3	3.78E-3	-57.2	44.1	-100.0	37.2
5	0.00	3.09E-3	0.00	1.23E-3	1.17E-3	-100.0	163.4	-100.0	4.3
6	0.00	4.52E-3	2.58E-4	3.35E-10	9.19E-4	-100.0	-50.9	-71.9	-100.0
7	0.00	1.50E-3	6.59E-3	3.55E-3	5.13E-3	-100.0	-70.8	28.4	-30.8
8	0.00	0.00	5.78E-3	3.88E-3	5.75E-3	-100.0	-100.0	0.5	-32.5
9	0.00	0.00	0.00	1.00E-10	0.00	0.0	0.0	0.0	-

CHAPTER 3

ONE-STORY SYSTEMS

3.1 SINGLE-DEGREE-OF-FREEDOM SYSTEM

3.1.1 Idealized one-story structure

For any structure, the components of structural mass (m), stiffness (k) and damping coefficient (c) are contributed to by each structural member, such as a beam, a bar, a column, a wall. The idealized one-story structure which was selected in the investigation in [Chopra and Goel, 2001] is shown in Figure 3.1. In this simplified structure, the total mass (m) is considered to concentrate at the roof level, the frame is massless and provides the stiffness (k) of the structure with a linear damper of damping coefficient (c).

3.1.2 Force-displacement Relation

In 1971, an experimental force-displacement relationship for a structural steel component undergoing cyclic deformation was proposed by Krawinkler et al., as shown as in [Figure1.3.4, Chopra, 2001]. It is obvious that the force-displacement relation for the structural steel would be linear at small deformation but would change to be nonlinear as the deformation increases.

For the linear system, the relationship between the lateral force f_S and the lateral displacement is still linear, that is,

$$f_S = k \cdot u \tag{3.1}$$

In this investigation, a bilinear hysteretic relationship is considered as the idealized lateral force-deformation relation and shown in Figure 3.2. It is clear that the system is still elastic with stiffness k before yielding, as the increasing load reaches the yielding force f_y, the system begins yielding and the stiffness of the structure is reduced to αk, where $0<\alpha<<1$. Unloading the system from the maximum deformation, a path is taken parallel to the initial elastic curve. Similarly, reloading the system from the minimum deformation, another path would be taken parallel to the initial elastic curve. For the lateral force-deformation relationship illustrated in Figure 3.2, the yield strength is considered the same in the two directions of deformation.

After yielding, the structure is changed to an inelastic system where the force f_S is not single valued corresponding to the deformation u, i.e., the lateral force depends not only the deformation itself but its velocities as well [Chopra, 2001]. That relationship can be expressed as

$$f_S = f_S(u, \dot{u}) \tag{3.2}$$

3.1.3 Equation of Motion

Considering the behavior of the idealized one-story structure subjected to earthquake ground motion, as shown as in Fig. 3.1, the total displacement of the mass at each instant of time is

$$u^t(t) = u(t) + u_g(t) \tag{3.3}$$

where, $u^t(t)$ is the total displacement of the mass, $u_g(t)$ is the ground motion.

Differentiating Equation (3.3) twice, the total acceleration of the mass is,

$$\ddot{u}^t(t) = \ddot{u}(t) + \ddot{u}_g(t) \tag{3.4}$$

For the free-body diagram of the forces shown in Fig.3.1.b, the equation of dynamic equilibrium is

$$f_I + f_D + f_s = 0 \tag{3.5}$$

where, the inertia force f_I is related to the acceleration of the mass by

$$f_I = m \cdot \ddot{u}^t(t) \tag{3.6}$$

The damping force f_D is related to the velocity across the linear viscous damper by

$$f_D = c \cdot \dot{u} \tag{3.7}$$

Substituting Equations (3.6), (3.7) and Equation (3.2) in Equation (3.5) gives

$$m \cdot \ddot{u}(t) + c \cdot \dot{u}(t) + f_S(u) = -m \cdot \ddot{u}_g(t) \tag{3.8}$$

This is the governing equation for SDF non-linear system subjected to horizontal ground motion. And the incremental equation of motion for the nonlinear system is

$$m \cdot \Delta\ddot{u}(t) + c \cdot \Delta\dot{u}(t) + k \cdot \Delta u(t) = -m \cdot \Delta\ddot{u}_g(t) \tag{3.9}$$

3.2 GROUND EXCITATION CONSIDERED

All structures in this investigation are subjected to the north-south component of the El Centro (1940) ground motion, shown in Figure 3.3 (data from http://www.vibration data.com/elcentro.htm)

3.3 ONE-STORY MRF SYSTEM

The one-story moment resistant frame considered in this investigation is chosen from [Chopra and Goel, 2001] and shown in Fig.3.4.

Reviewing the results in [Chopra and Goel, 2001], the history response of the roof displacement, *u(t),* is shown in Figure 3.5, with the damping ratio $\zeta=5\%$, the peak value of the deformation is $u_m=73.6\ mm$ and the natural period of the structure is $T_n=0.502\ sec.$ The force-deformation relationship is illustrated in Figure 3.6, where the recycling pushover curve is almost the same as that of dynamic analysis because the beam and the columns in this case are designed to yield at the same time when f_S reaches the yield strength.

3.4 ONE-STORY FDBF SYSTEM

3.4.1 System description

The one-story Friction Damped Braced Frame (FDBF) considered in this investigation, as shown as in Figure 3.7a, is similar to the one-story moment resistant frame from [Chopra and Goel, 2001] with an additional friction damped brace. The concentrated mass, $m=17.32\ k\ kg.$ The main properties of the elements: moment of inertia, $I_b=3.134x10^7\ mm^4$, $I_c=6.077x10^7\ mm^4$, yield moment, $Mp_b=21.65\ kN\text{-}m$, $Mp_c=50.18\ kN\text{-}m$, for the beam and columns, respectively. The yielding stiffness of each structural element is defined as 3% of its initial stiffness, the Young's modulus of elasticity $E=2.0x10^5\ MPa$, and the yield stress $F_y=250\ MPa.$

3.4.2 Optimum Slip Load and Stiffness of the Brace

Slip Load of the Brace

It was demonstrated by [Baktash, 1989] that the friction damped bracing system provides maximum energy dissipation when the shear resisted by the brace is equal to that of the frame without bracing

$$V_b = V_f \tag{3.10}$$

For one-story FDB-Frame shown in Figure 3.7a, considering the free-body diagram of the forces shown in Figure 3.7b, the shear resisted by the frame is,

$$\frac{V_f}{2} = \frac{M_{pb} + M_{pc}}{h} \tag{3.11}$$

with Mp_b=*21.65 kN-m* , Mp_c=*50.18 kN-m* , the yield moments for the beam and column, respectively, $V_f = 39.26kN$, so that, the shear resisted by the brace from Equation (3.10), $V_b = 39.26kN$.

By the geometric relation, the slip load of the brace P_s is

$$P_s = \frac{V_b}{\cos\varphi} \tag{3.12}$$

where, φ is the angle between the brace and the beam, *cosφ=0.8944,* the slip load for this example is $P_s = 43.89kN$.

Stiffness of the Brace

For the slip force determined in the previously paragraph, by the strength design formula, the cross section of the brace is calculate by

$$A_b = \frac{P_s}{F_y} \tag{3.13}$$

in which, the yield strength of the steel, F_y=*250 MPa*, so that $A_b = 175.6mm^2$.

The stiffness of the brace, K_b, is

$$K_b = \frac{EA_b}{L} \cdot \cos^2 \varphi \tag{3.14}$$

where Young's modulus of elasticity, $E = 2.0 \times 10^5 MPa$ and the bay length of the frame, *L=7.32m*. Substituting all the components into Equation (3.14), the stiffness of the brace is $K_b = 3.838 \times 10^6 N/m$.

The lateral stiffness of any beam/column frame can be determined by [Chopra, 2001]

$$K_f = \frac{24EI_c}{h^3} \cdot \frac{12\rho + 1}{12\rho + 4} \tag{3.15}$$

where $\rho = {I_b}/{4I_c}$ is the beam to column stiffness ratio. $I_b = 3.134 \times 10^7 mm^4$ and $I_c = 6.077 \times 10^7 mm^4$ are the moments of inertia for the beam and column, respectively, the height of the frame *h=3.66m*, then $\rho = 0.1289$ and $K_f = 2.732 \times 10^6 N/m$.

Denoting λ as the stiffness ratio of the brace to the frame

$$\lambda = \frac{K_b}{K_f} \tag{3.16}$$

Here, λ=1.4, which is too small, generally, to decrease the lateral deformation of the system. The optimum stiffness ratio of the brace to the frame, *λ=4~5,* so that the optimum stiffness of the brace becomes $K_b = 4K_f = 10.928 \times 10^6 N/m$.

Substituting K_b into Equation (3.14), the cross section of the optimum brace is $A_b = 500.4mm^2$.

Assuming the brace begins to slip as the axial force in it reaches the slip load, the normal stress of the brace is

$$\sigma_s = \frac{P_s}{A_b} \tag{3.17}$$

Substituting the value of P_s and A_b into Equation (3.17), the stress, $\sigma_s = 87.7MPa = 0.35F_y$, which is defined the slip or yield strength of the brace, and it should remain constant as the brace slips.

3.4.3 Non-linear Response History Analysis

The optimized friction damped bracing frame from the previous section 3.4.2 is analyzed by DRAIN-2DX [Allahabadi, and Powell, 1988]. The system is also subjected to the north-south component of the El-Centro (1940) ground motion with the scaled factor of 2.0. The history response of the roof displacement *u(t)* is shown in Figure 3.8. The peak amplitude of *u(t)* , u_m=*23.8mm* with the elastic damping ratio ζ=*5%* and the natural period of the system T_n=*0.240 sec.*

Comparing the history responses of friction damped braced frame (FDBF) with the moment resistant frame(MRF) shown in Figure 3.5, the roof displacement of FDBF is much smaller than that of MRF, with the peak value of the roof displacement only *32%* of that of MRF. The comparison is shown in Figure 3.9. It is demonstrated that the friction damped member is very effective in controlling the deformation of the system.

3.4.4 Modal Pushover Analysis (MPA)

In this section, the modal pushover analysis procedure [Chopra and Goel, 2001] which was introduced step by step in section 1.3.2 will be implemented to compute the responses of the FDBF mentioned in section 3.4.1.

1. From the results of modal analysis of the structure, the natural period of the FDBF system $T_n=0.240\ sec$, and for one-story structure $\phi_1=1.0$.
2. Define the force distribution related to the mode shape: $s_n^*=m\phi_n$, so that $s_1^*=1.0$, a unit force distribution.
3. Using DRAIN-2DX [Allahabadi, and Powell, 1988] push the system under the unit force distribution until the roof displacement reaches a target displacement. In engineering practice, however, the target displacement is unknown because there is no dynamic analysis at the beginning, so the iteration method should be used. First, assuming a target displacement for modal pushover, a calculated roof displacement will be obtained at the step 7 of the MPA procedure. Comparing the assuming roof displacement and the calculated roof displacement, if the error is less than 5%, the assumed roof displacement sufficiently closes to the calculated roof displacement which would be considered as the correct roof displacement for MPA procedure. Otherwise, the calculated roof displacement is considered as the second assumed roof displacement to push the system and repeat the procedure from step 3 to step 7 until the calculated roof displacement can meet the assumed roof displacement with an error less than 5%.

For this example, an assumed target roof displacement, u_o=60mm is chosen. Plotting the relation of the base shear and displacement in a diagram, the pushover curve will be obtained as shown in Figure 3.10.

4. The actual pushover curve of the one-story FDBF is not bilinear because the frame is accompanied with a friction damped brace which slips before the main members of the system yield. It should also be idealized as a bilinear curve using the FEMA-273 procedure [Building Seismic Safety Council, 1997]. Briefly, it is an area balance procedure, by iterative method, the area under the idealized bilinear curve should finally be equal to that under the actual pushover curve. The bilinear curve of the one-story FDBF is also shown in Figure 3.10.

5. In order to compute the response of the equivalent SDF system for the one-story FDBF, as shown as in Figure 3.11, it is necessary to develop the properties of the equivalent SDF system from the bilinear curve. They are:

   the frequency, $\omega_n=2\pi/T_n=26.180$ *rad/s*,

   the damping ratio, $\zeta_n=5\%$,

   the post-yielding strain-hardening ratio, α, is

$$\alpha = \frac{(V_o / V_y) - 1}{(u_o / u_y) - 1} \tag{3.18}$$

   in which, u_o, u_y are the target roof displacement, displacement at yield point, respectively and V_o, V_y are the base shears when the displacements reach u_o, u_y.

   For this example, $u_o=0.060m$, $u_y=0.006m$, $V_o=98.56$ *kN*, $V_y=74.28kN$, and $\alpha=0.038$.

   The stiffness of the equivalent SDF system with unit mass ($m^*=1.0$), k, is

$$k = m^* \cdot \omega_n^2 = \omega_n^2 \tag{3.19}$$

For the equivalent SDF system shown in Fig.3.11,

$$k = \frac{12EI_c}{h^3}, \qquad I_c = \frac{k \cdot h^3}{12E} \tag{3.20}$$

Substituting all the known components into Equation (3.20), the moment of inertia of the column, $I_c = 1.4036 \times 10^{-5} m^4$.

The yield force for the equivalent SDF system with unit mass *(m^*=1.0)*, $V_f^* = 4.289kN$ from

$$V_f^* = \frac{V_y}{m} \cdot m^* \tag{3.21}$$

and the controlling yield moment of the column, $M_p^* = 7.8487kN - m$ by

$$M_p^* = \frac{V_f^* \cdot h}{2} \tag{3.22}$$

6. With all the properties obtained in step 5, the equivalent SDF system is very simple to analyze by DRAIN-2DX [Allahabadi, and Powell, 1988]. The peak deformation, D_n, of the 1st-mode inelastic SDF system, *D_1=26.3mm.*
7. The peak roof displacement is *u_{no}=26.3mm.* It is obvious that the calculated roof displacement is not equal to that assumed target roof displacement, *u_o=60mm* on step 3, so the iteration method should be used, and repeat step 3 to 7 again. Finally, the peak roof displacement, u_{no}=26.4mm is found. The history response of the roof displacement is shown in Figure 3.12.

For the one-story FDBF system, steps 8 to 10 of the procedure are not necessary. Figure 3.13 shows the comparison of the nonlinear history responses of roof displacement of FDBF analyzed by the approximate MPA (Figure 3.12) and the nonlinear response history analysis (Figure 3.8). The difference of the absolute peak value of the roof displacement is about *11.0%*. It is demonstrated that for the one-story FDBF system, the MPA procedure can also provide good estimation for maximum seismic response.

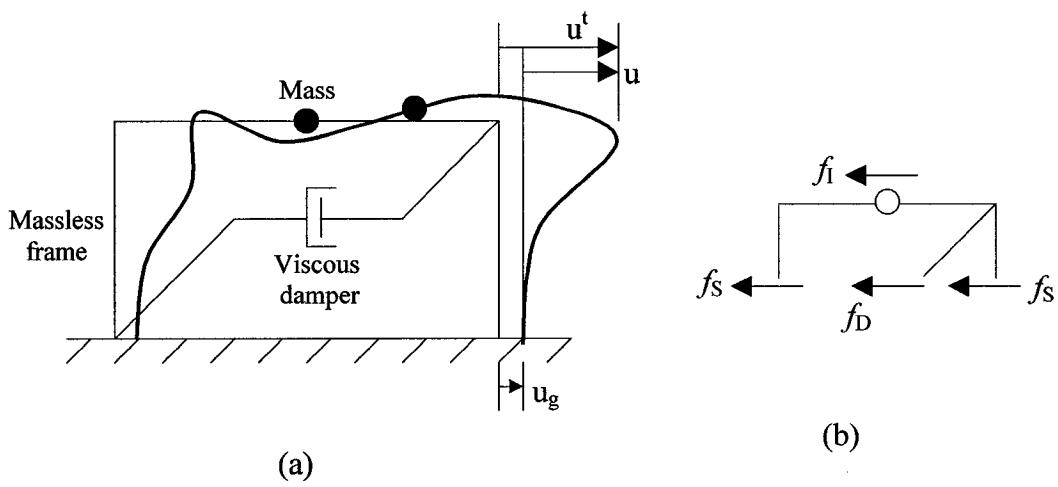

Figure 3.1. Single-degree-of-freedom System: (a) Earthquake Induced Ground Motion; (b) Free-body Diagram of the Forces

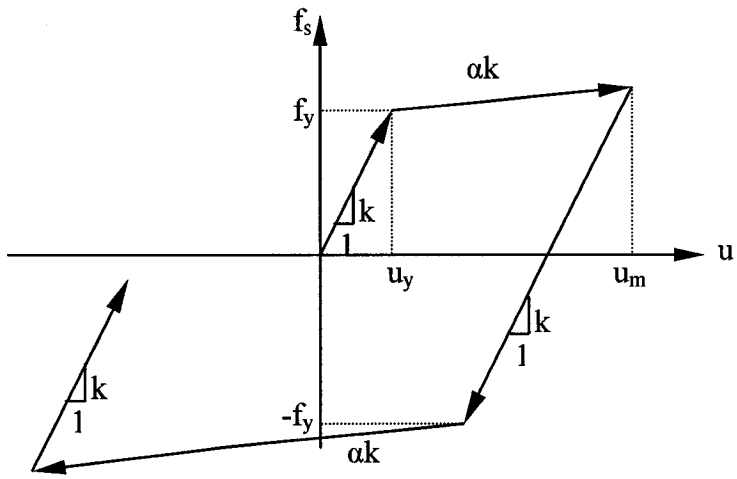

Figure 3.2. Idealized Bilinear Hysteretic Force-deformation Relation

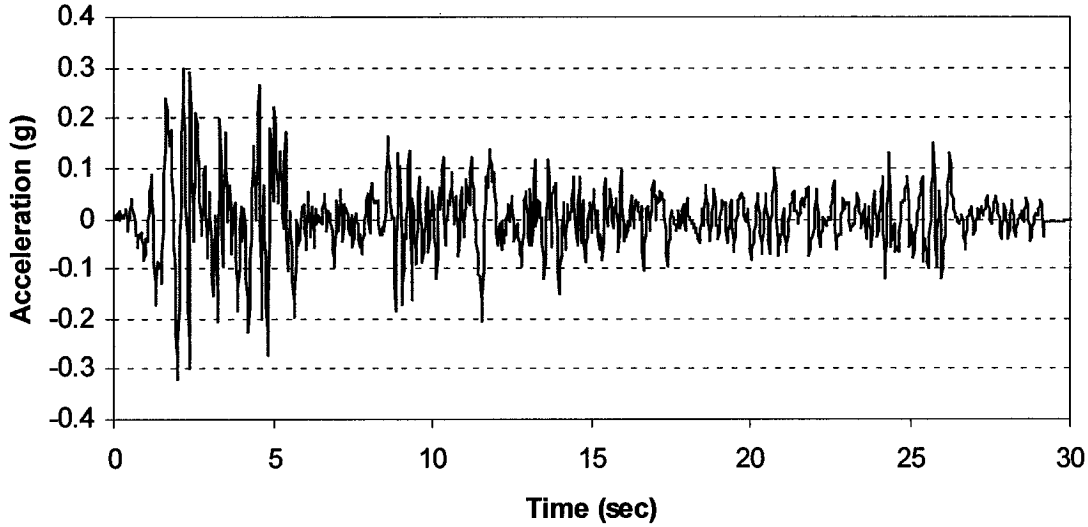

Figure 3.3. EL-Centro Earthquake May, 1940, North-South Component

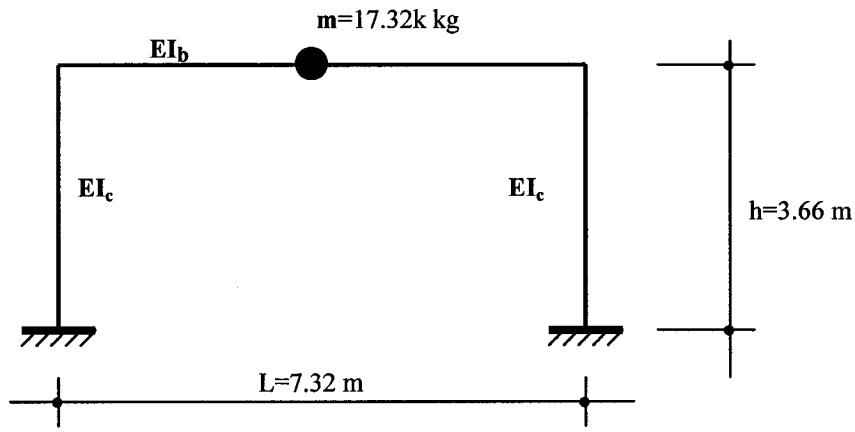

Figure 3.4. One-story, One-bay MRF System

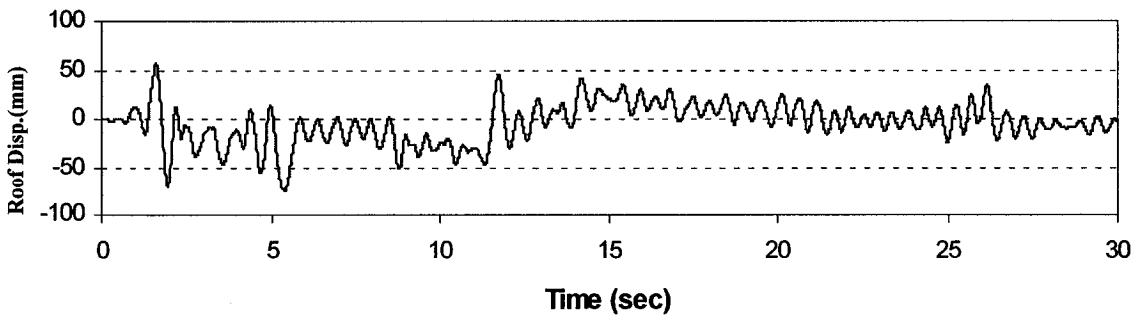

Figure 3.5. Response of NL Analysis of One-story MRF to 2.0 EL-Centro Ground Motion

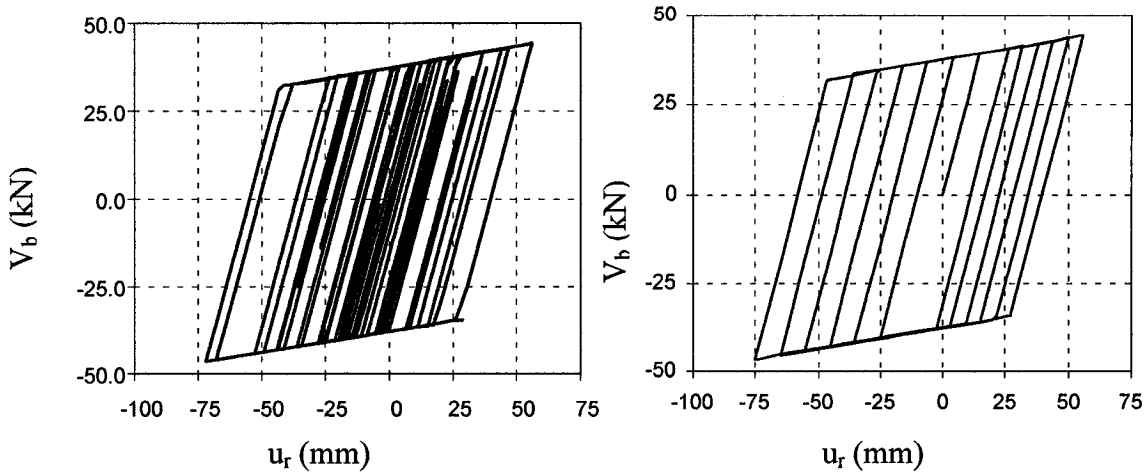

(a) Dynamic Analysis **(b) Recycling Pushover Curve**

Figure 3.6. Force-deformation Relationship of One-story MRF to 2.0 EL-Centro Ground Motion

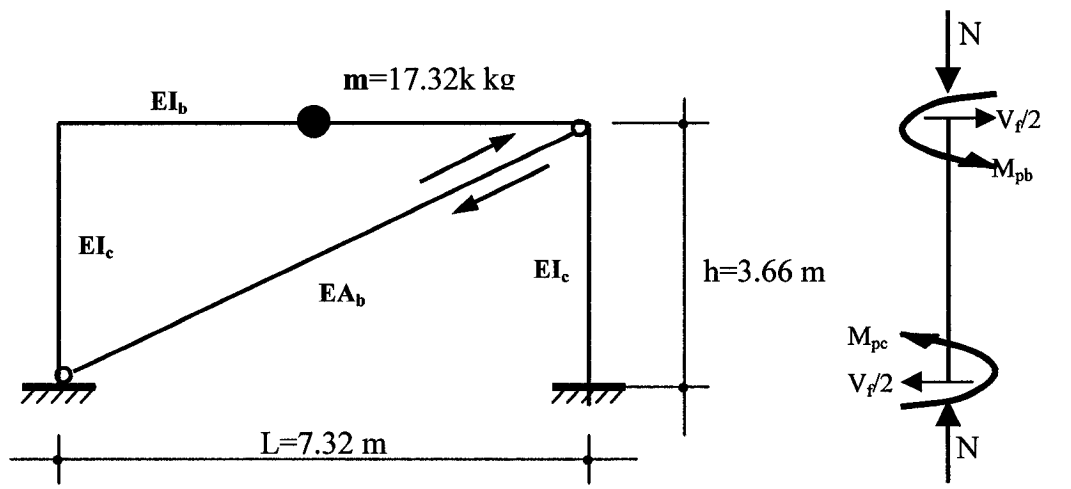

(a) Structure **(b) Free-body Diagram of the Column**

Figure 3.7. One-story, One-bay FDBF System

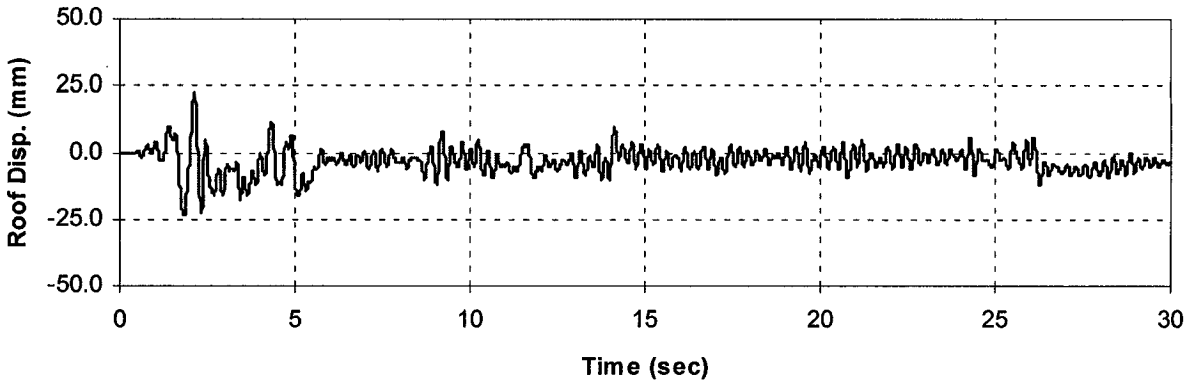

Figure 3.8. Response of NL Analysis of One-story FDBF to 2.0 EL-Centro Ground Motion

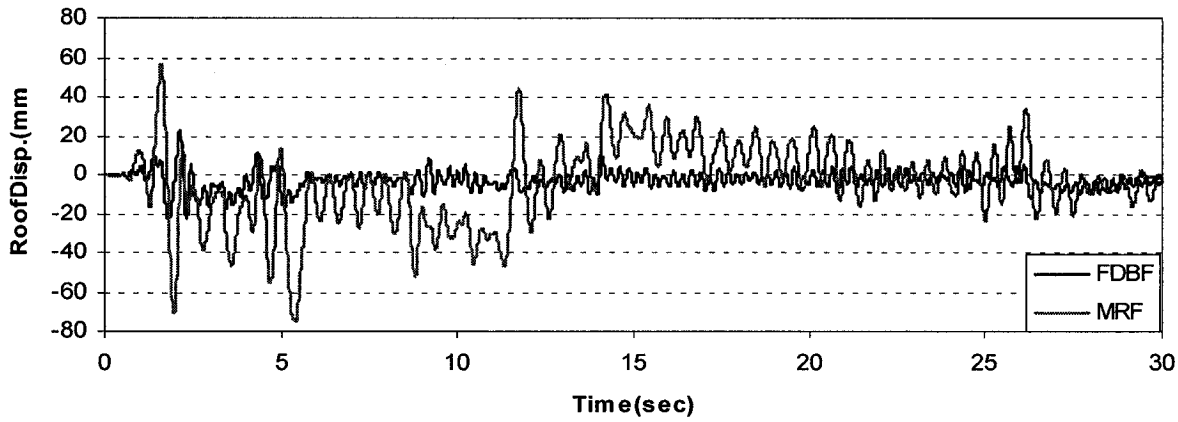

Figure 3.9. Comparison of Response of NL Analysis of One-story FDBF with MRF to 2.0 EL-Centro Ground Motion

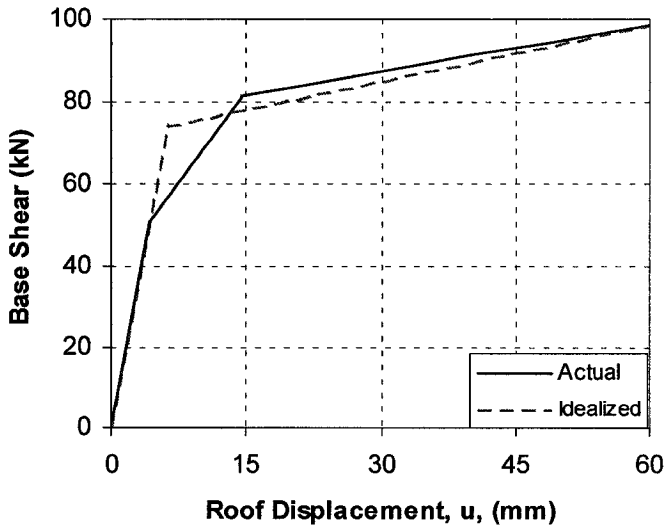

Figure 3.10. Pushover Curve of One-story FDBF

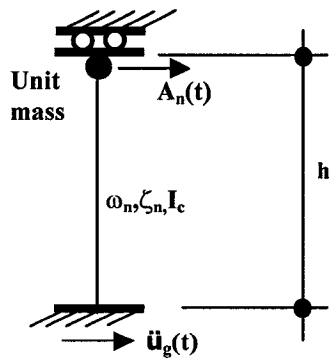

Figure 3.11. Equivalent SDF System

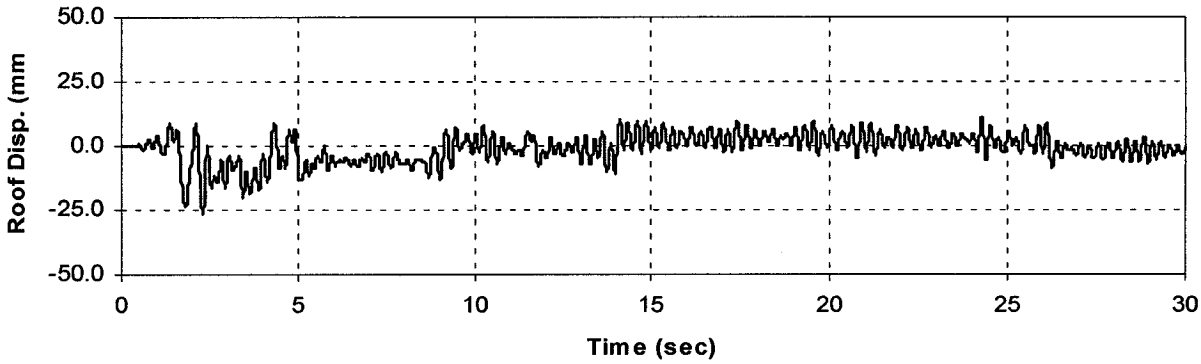

Figure 3.12. Response of Dynamic Analysis of Equivalent SDF System of One-story FDBF to 2.0 EL-Centro Ground Motion

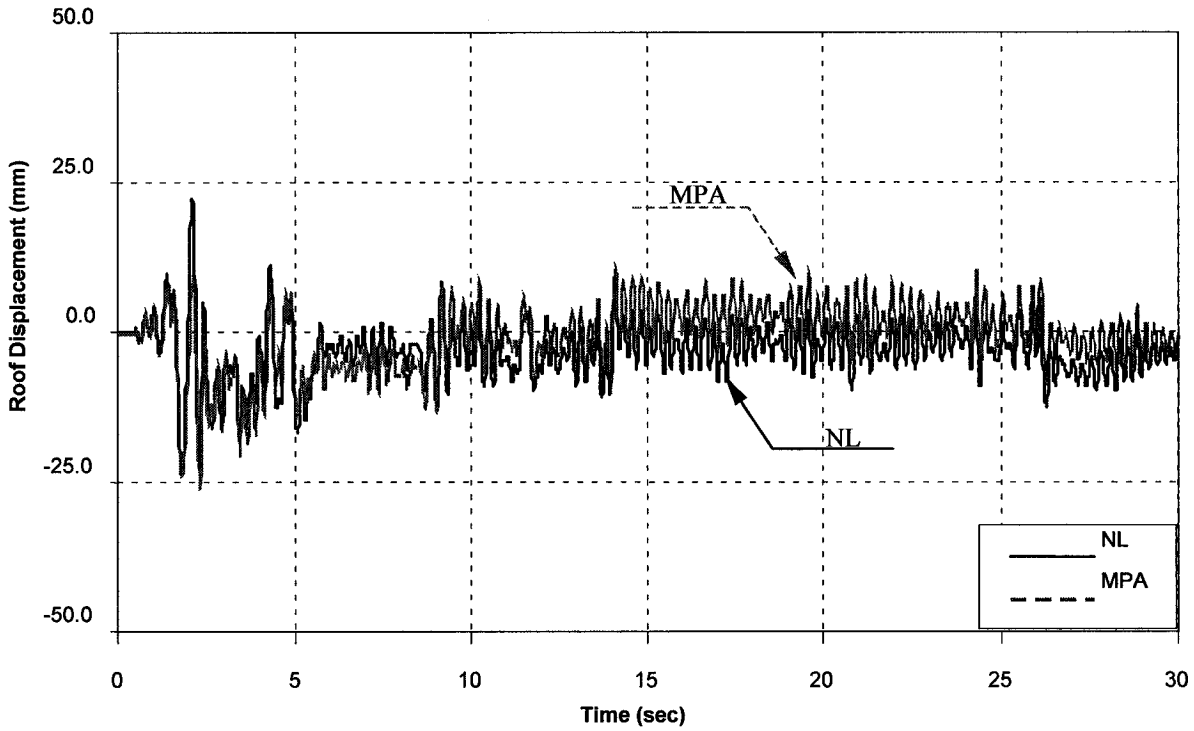

Figure 3.13. Comparison of Roof Displacement of One-story FDBF Analyzed by MPA and Nonlinear RHA to 2.0 EL-Centro Ground Motion

CHAPTER 4

MULTISTORY MOMENT RESISTING FRAMES (MRF)

4.1 THEORY OF MPA FOR MULTISTORY STRUCTURES

4.1.1 Linear MDF System

For a linear MDF system subjected to ground motion, the governing equation of motion is

$$[m]\cdot\{\ddot{u}(t)\}+[c]\cdot\{\dot{u}(t)\}+[k]\cdot\{u(t)\}=-[m]\cdot\{1\}\cdot\ddot{u}_g(t) \tag{4.1}$$

where $[m]$ is the mass matrix; $[c]$ is the damping matrix; $\{\ddot{u}(t)\},\{\dot{u}(t)\},\{u(t)\}$ are the relative acceleration vector, velocity vector and displacement vector, respectively; $\ddot{u}_g(t)$ denotes the ground acceleration history and $\{1\}$ is the unity vector.

According to orthogonal property of modes that only the nth mode contributes to its response, the floor displacement vector of the nth mode is defined by [Chopra and Goel, 2001]

$$\{u_n(t)\}=\{\phi_n\}q_n(t) \tag{4.2}$$

where $\{\phi_n\}$ is the mode shape, $q_n(t)$ is the modal coordinate, i.e., none of the modes other than the nth mode contribute to the response of the nth mode.

Substituting equation (4.2) into equation (4.1), pre-multiplying by $\{\phi_n\}^T$, then converting it by dividing by $\{\phi_n\}^T[m]\{\phi_n\}$, equation (4.1) is changed to

$$\ddot{q}_n(t)+2\zeta_n\omega_n\dot{q}_n(t)+\omega_n^2q_n(t)=-\Gamma_n\ddot{u}_g(t) \qquad n=1,2,....N \tag{4.3}$$

where ζ_n, ω_n are the damping ratio and the natural vibration frequency for the nth mode.

The modal participation factor Γ_n and the effective modal mass M_n^* are expressed as

$$L_n = \{\phi_n\}^T [m]\{1\}, \qquad M_n = \{\phi_n\}^T [m]\{\phi_n\} \tag{4.4}$$

$$\Gamma_n = \frac{L_n}{M_n}, \qquad M_n^* = \Gamma_n \cdot L_n \tag{4.5}$$

For the nth-mode elastic SDF system, with the same vibration properties, ζ_n and ω_n, the equation of motion is changed to be

$$\ddot{D}_n(t) + 2\zeta_n \omega_n \dot{D}_n(t) + \omega_n^2 D_n(t) = -\ddot{u}_g(t) \qquad n = 1,2,....N \tag{4.6}$$

Comparing Equation (4.3) and Equation (4.6) gives

$$q_n(t) = \Gamma_n D_n(t) \tag{4.7}$$

Substituting Equation (4.7) into Equation (4.2) also gives

$$\{u_n(t)\} = \Gamma_n \{\phi_n\} D_n(t) \tag{4.8}$$

By the above equation, the floor displacements of the nth mode of the MDF system can easily be obtained by analyzing the nth mode elastic SDF system. And similarly, other response of the system, such as the story drift, internal element forces, etc., can be calculated as well.

4.1.2 Non-linear MDF System

For a nonlinear MDF system, Equation (4.1) is change to be

$$[m]\cdot\{\ddot{u}(t)\} + [c]\cdot\{\dot{u}(t)\} + \{f_s(u(t))\} = -[m]\cdot\{1\}\cdot\ddot{u}_g(t) \tag{4.9}$$

where $\{f_s(u)\}$ denotes the lateral force vector with nonlinear relationship to the lateral displacement $u(t)$, and Equation (4.3) becomes

$$\ddot{q}_n(t) + 2\zeta_n \omega_n \dot{q}_n(t) + \frac{F_{sn}}{M_n} = -\Gamma_n \ddot{u}_g(t) \qquad n = 1,2,....N \tag{4.10}$$

The only difference between Equation (4.10) and Equation (4.3) is the resisting lateral force F_{sn}

$$F_{sn} = F_{sn}(q_n) = \{\phi_n\}^T \{f_s(u(t))\} \tag{4.11}$$

Equation (4.6) is changed to be

$$\ddot{D}_n(t) + 2\zeta_n \omega_n \dot{D}_n(t) + \frac{F_{sn}}{L_n} = -\ddot{u}_g(t) \qquad n = 1,2,....N \tag{4.12}$$

Equation (4.12) is the equation of motion of the *n*th-mode inelastic SDF system, $\frac{F_{sn}}{L_n}$ is defined as one of the properties of the nth mode inelastic SDF system. The equation can be solved by any commercial structural analysis software; or the peak value of the deformation, D_{no}, can be simply estimated by hand or in a spreadsheet using the capacity spectrum method (CSM) [ATC, 1996] which was described in section 1.3.2. In this investigation, the capacity spectrum method is preferred because it is the most direct application of the concepts and it is not necessary for any structural analysis software. In ATC-40, the issue to determine the peak value of the deformation of the equivalent SDF system, D_{no}, is changed to be the problem to develop the demand performance point for the system for given earthquake ground motion, i.e., the peak value of the deformation is equal to the spectral displacement at the demand performance point,

$$D_{no} = d_{np} \tag{4.13}$$

where d_{np} is the spectral displacement of the demand performance point for nth-mode.

4.2 SYSTEM DESCRITION

The single-bay, 10 story moment resisting steel frame chosen for this investigation is from Workman [Workman, 1969] and shown in Fig.4.1, the frame dimensions and properties of the elements are summarized as below.

Beams

The beams of the frame are steel wide-flange sections with yield strength F_y=*250 MPa.* The sections of the beams are *W460x113*, *W460x89*, *W460x74* at the 1st level, the 2nd –5th level and the 6th –10th level, respectively.

Columns

The columns of the frame are steel wide-flange sections with yield strength F_y=*250 MPa.* The sections of the columns are *W360x262, W360x179, W360x147, W360x110, W360x79, W360x51* in the 1st floor, the 2nd –3rd floor, the 4th –5th floor, the6th –7th floor, the 8th –9th floor and the10th (roof) floor, respectively.

Restraints

The two columns in 1st floor are fixed, that is the only restraint of the system.

Dimensions

The bay width of the frame is *6,100 mm*, all the heights of the floors are *3,600 mm* and all measurements are centerline.

Seismic Mass

The same value of the seismic mass, m_i=*60,000 kg*, is assigned at each floor level of the structure. The properties of the selected structure illustrated in Figure 4.1 are summarized in Table 4.1.

4.3 NONLINEAR RESPONSE HISTORY ANALYSIS (NL-RHA)

For the 10-story MRF shown in Fig.4.1, the structural responses determined by DRAIN-2DX [Allahabadi and Powell, 1988], such as the history response of the roof displacement, the top story drift and the plastic hinge location, are shown in Figures 4.2, 4.3 and 4.4, respectively. It is assumed that the system is subjected to the north-south component of the El-Centro (1940) ground motion with the scale factor of 1.5.

4.4 MODAL PUSHOVER ANALYSIS (MPA)

The step-by-step MPA procedure presented in section 1.3.2 [Chopra and Goel, 2001] is implemented for the 10-story MRF in this section. In additional, the procedure A of CSM in ATC-40 [ATC, 1996] is applied as an aid procedure for calculating the seismic performance point, the roof displacement of the system.

Structural Dynamic Characteristics

The prerequisites for MPA procedure are the structural dynamic characteristics, such as the natural frequencies ω_n, the modes ϕ_n, the modal participation factor Γ_n, and the effective modal mass M_n^* for linear-elastic vibration of the structure. The structural dynamic characteristics for the selected 10-story MRF are computed by DRAIN-2DX [Allahabadi and Powell, 1988], and summarized in Table 4.2, where the modal participation factor Γ_n, and the effective modal mass M_n^* are calculated by Equations (4.4), (4.5). Figure 4.5 illustrates the first three modes and frequencies of the system.

Modal Pushover Capacity Curves and Capacity Spectrum

The pushover capacity curve for the *n*th-mode, a plot of base shear versus roof displacement, can be developed by pushing the structure to an assumed target displacement with the lateral force distribution for the *n*th-mode.

The lateral force distributions of the first three modes are shown in Figure 4.6 determined by

$$\{s_n^*\} = [m] \cdot \{\phi_n\} \tag{4.14}$$

For the lateral force distributions mentioned above, the system is pushed to the assumed target roof displacements *540mm, 180mm* and *90mm* for the first three modes, respectively and the coresponding modal pushover capacity curves are shown in Figure 4.7.

The capacity spectrums for the first three modes, a plot of spectral acceleration versus spectral displacement, which are converted from capacity curves by Equation (4.15), are shown in Figure 4.8,

$$S_{ai} = \frac{V_i}{M_n^*} \quad , \qquad S_{di} = \frac{u_i}{\Gamma_n \cdot \phi_{no}} \tag{4.15}$$

where S_{di}, S_{ai} are the horizontal axis and vertical axis of any point i in the capacity spectrum, V_i and u_i are the horizontal axis and vertical axis of any point i in the capacity curve, respectively. The modal participation factor Γ_n, and the effective modal mass M_n^* are calculated by Equations (4.4), (4.5). ϕ_{no} is the roof level amplitude of the nth-mode.

Modal Roof Displacement Determined by CSM

The following steps are involved for estimating the seismic performance point for the first mode using procedure A of CSM in ATC-40 [ATC, 1996]:

1. Develop the 5 percent damped (elastic) response spectrum appropriate for the site.

   1.1. Develop the elastic traditional spectrum, with S_a versus T, by equation (1.1). For the ground motion considered in this investigation (1.5 X El-Centro ground motion, 1940, N-S component), the site properties are: Z=0.3 for seismic zone 3, E=1.5 for the maximum earthquake ground motion, and N=1.0 for no near-fault effects. ZEN is equal to 0.45. For the normal soil profile type S_B, the seismic coefficients C_A and C_V are computed by (Appendices B-1 and B-2)

$$C_A = 1.0 \cdot (ZEN), \quad C_V = 1.0 \cdot (ZEN) \tag{4.16}$$

For this case, $C_A = 0.45$, $C_V = 0.45$. The traditional elastic spectrum is shown in Figure 4.9.

1.2. Transform the elastic traditional spectrum to the elastic response spectrum *(ζ=5%)* with S_a versus S_d, by equations (1.3) and (1.4). The elastic response spectrum *(ζ=5%)*, with S_a versus S_d, is shown in Figure 4.10.

2. Develop the capacity curve by pushing the structure to a target roof displacement. The modal pushover capacity curves are shown in Figure 4.7.
3. The converted capacity spectrums for the first three modes are shown in Figure 4.8.
4. Plot the capacity spectrum for the mode1 on the same chart as the elastic response spectrum *(ζ=5)* as shown in Figure 4.11
5. Select a trial performance point, a_{pi}, d_{pi} as shown in Figure 4.11.The first choice of the trial performance point can be arbitrary. It could be the intersection of the capacity spectrum and the elastic response spectrum, or the end point of the capacity spectrum, or even any point on the capacity spectrum. Here, the end point of the capacity spectrum is selected as the first trial performance point, $a_{p1} = 0.837g$, $d_{p1} = 398mm$. Develop the bilinear curve representing the portion of the capacity spectrum from the beginning point (0,0) to the trial performance point, using the rule of equal area, i.e., the area under the bilinear curve is equal to that under the capacity spectrum. The bilinear curve is also shown in Figure 4.11.

6. Calculate the effective viscous damping $\hat{\zeta}_{eq}$ by equation (1.6), where a_y, d_y, a_{pi}, d_{pi} are the coordinates of the yield point and the trial point i on the bilinear curve, κ is the value for damping modification factor shown in Appendix B-3 [Table 8-1, ATC, 1996].
7. Calculate the spectral reduction factors SR_A and SR_V by equations (1.7) and (1.8). The demand spectrum is developed by equation (1.9).
8. Draw the demand spectrum on the same plot as the capacity spectrum as shown in Figure 4.12.
9. Compare the intersection point of the demand spectrum and the capacity spectrum with the initial trial performance point. If the error of the displacement between these two points is less than *5%*, i.e., the demand spectrum intersects the capacity spectrum within acceptable tolerance, a_{pi}, d_{pi}, can be considered as the demand performance point, a_p, d_p.
10. If the demand spectrum does not intersect the capacity spectrum within acceptable tolerance, then select the intersection point as a new trial performance point and return to step 4, until the demand spectrum intersects the capacity spectrum within acceptable tolerance. Figure 4.13 illustrates the family of demand spectrums for various effective damping and Table 4.3 lists the trials to find the demand performance point, a_{np}, d_{np}, for the 1st mode. Here, the seismic performance point for the first mode is, $a_{1p} = 0.0796g$ and $d_{1p} = 307mm$.

Recall from equation (4.13) that the peak value of the deformation of the equivalent SDF system, D_{no}, is equal to the spectral displacement at the demand performance point, d_{np}, for the 1st mode

$$D_{1o} = d_{1p} = 307mm$$

and the peak value of the roof displacement for mode 1 can be obtained by Equation (4.8) as

$$u_{1o} = \Gamma_1 \phi_{1o} D_{1o} = 1.3557 \times 1.0 \times 307 = 416mm$$

where $\phi_{1o} = 1.0$ is the roof level amplitude of the 1st mode.

Similarly, the peak value of the roof displacement for mode 2 and mode 3 can be estimated by this same procedure. For this system,

$$u_{2o} = 67mm, \quad u_{3o} = 22mm$$

Comparison with NL-RHA

At the roof displacements, $u_1 = 416mm$, $u_2 = 67mm$, $u_3 = 22mm$, the values of floor displacements and story drifts for MPA are determined by Equation (4.8). The peak values of floor displacements (as % of the building height=36.6m) are shown in Table 4.4 and the peak amplitudes of story drift ratios (as % of story height=3.66m) are shown in Table 4.5. Table 4.6 illustrates the hinge rotations calculated by subtracting the yield rotation from the total hinge rotations.

By the SRSS combination rule, the total responses of the floor displacements, story drifts and hinge rotations for 1 mode, two modes and 3 modes are also included in Tables 4.4, 4.5 and 4.6, respectively.

The comparison of floor displacement ratios estimated by MPA and NL-RHA is illustrated in Figure 4.14 and also summarized in Tables 4.4. The comparison of story drift ratios estimated by MPA and NL-RHA is illustrated in Figure 4.15.and also shown in Tables 4.5. Figure 4.16 illustrates the comparison of plastic hinge locations estimated by MPA and NL-RHA. It is noticed that the locations of plastic hinges from MPA for two and three modes are exactly the same as that for the first mode because the system is still elastic during the second and third modal pushover procedure for 1.5x El Centro ground motion.

The comparisons demonstrate that, for a moment resisting frame (MRF), the MPA procedure is able in estimating floor displacements, story drifts and most locations of the plastic hinges for the structure subjected to a strong ground motion, such as 1.5 x El Centro ground motion. But it cannot provide enough accuracy for estimating the hinge plastic rotations.

4.5 FEMA-273 PUSHOVER ANALYSIS

4.5.1 Force Distributions for FEMA-273 Pushover Analysis

In FEMA-273, three force distributions are used in developing the pushover curves, which are defined as uniform distribution, equivalent lateral force (ELF) distribution and SRSS distribution. The calculations of the FEMA-273 force distributions are described in detail in Appendix C in [Chopra and Goel, 2001].

Uniform Distribution

The uniform distribution means that the lateral force at a floor is equal to the mass at that floor. For this example, the uniform distribution is summarized in Table 4.7 and computed by

$$s_j^* = \frac{m_j}{\sum_i m_i} \tag{4.17}$$

in which m_j is the mass at the jth floor and $\sum_i m_i$ denotes the total value of mass for the system.

ELF Distribution

The equivalent lateral force (ELF) distribution is determined by

$$s_j^* = \frac{m_j h_j^k}{\sum_i m_i h_i^k} \tag{4.18}$$

where m_j is the mass at the jth floor, and h_j is the height of the jth floor above the ground, and the exponent k is related to the fundamental period T_1 (sec) and determined by

$$\begin{cases} k = 1 & T_1 \le 0.5 \\ k = 1 + \frac{1}{2}(T_1 - 0.5) & 0.5 < T_1 < 2.5 \\ k = 2 & T_1 \ge 2.5 \end{cases} \tag{4.19}$$

For the selected 10-story MRF, $T_1 = 3.27\,\text{sec}$ and $k = 2.0$. The equivalent lateral force (ELF) distribution is summarized in Table 4.8.

SRSS Force Distribution

For SRSS distribution, the lateral forces at the floor levels are determined from the story shears V_j combined by SRSS rule

$$V_j = \sqrt{\sum_n (V_{jn})^2} \tag{4.20}$$

Here, n denotes the n modes which shears would be combined. The story shear, V_{jn}, depend on the lateral force for the nth-mode, f_{jn}, calculated by

$$V_{jn} = \sum_{i=j}^{N} f_{in} \tag{4.21}$$

$$f_{jn} = \Gamma_n m_j \phi_{jn} A_n \tag{4.22}$$

in which the capital N is considered as the total floors of the system, Γ_n is the modal participation factor from Equation (4.5), m_j is the mass at the jth floor, ϕ_{jn} is the mode shape of the nth-mode, and A_n is the pseudo-acceleration of the nth-mode SDF elastic system determined by

$$A_n = \omega_n{}^2 D_{no} \tag{4.23}$$

The SRSS lateral force distribution of the 10-story MRF for first three modes is calculated and summarized in Table 4.9.

The above three force distributions for FEMA-273 are illustrated in Figure 4.17.

4.5.2 FEMA-273 Pushover Analysis

With the force distributions mentioned in the previous section, the 10-story MRF is pushed to a target displacement, which is the combined the peak value of roof

displacements for the first three modes by SRSS rule, i.e., $u_t = \sqrt{u_{1o}^2 + u_{2o}^2 + u_{3o}^2} = 422mm$. The pushover curves, plots of base shear versus roof displacement, are shown in Figure 4.18. At the target displacement, the peak values of floor displacements (as % of the building height=*36.6m*) are shown in Table 4.10 and the peak amplitudes of story drift ratios (as % of story height=*3.66m*) are shown in Table 4.11. Table 4.12 illustrates the hinge rotations calculated by subtracting the yield rotation from the total hinge rotations for FEMA-273 pushover analysis.

4.5.3 Comparison of MPA and FEMA-273 with NL-RHA

For 1.5x El Centro ground motion, the comparison of floor displacement ratios estimated by FEMA-273 pushover analysis with three force distributions, MPA with 3 modes, and NL-RHA is illustrated in Figure 4.19 and also shown in Tables 4.10. The comparison of story drift ratios estimated by the three different procedures is illustrated in Figure 4.20.and also shown in Tables 4.11.Tables 4.12 show the comparison of plastic hinge rotations estimated by FEMA-273, MPA and NL-RHA.

The errors of floor displacement ratios for the FEMA-273 uniform force distribution are between *3.63%* and *26.20%*, *-36.27%* and *11.69%* for ELF force distribution, *-27.46%* and *7.71%* for SRSS force distribution, respectively. They are not better than that from MPA which errors are between *–14.98%* and *13.28%.*

Similarly, for the story drift ratios, the errors for the FEMA-273 uniform force distribution are between *–64.34%* and *24.46%, -46.09%* and *11.01%* for ELF force

distribution, and *–29.05%* and *–0.54%* for SRSS force distribution, respectively. For comparison, the errors for MPA are between *–23.14%* and *12.24%*.

And for the plastic slips of the friction bracing, the errors for the FEMA-273 uniform force distribution are between *–100%* and *80%*, *-100%* and *-20%* for ELF force distribution, *–100%* and *-28%* for SRSS force distribution, respectively. The errors for MPA are between *–100%* and *–5.26%*.

It is concluded that the FEMA-273 uniform, ELF and SRSS force distributions underestimate the seismic response of the MRF system by more than MPA procedure for the floor displacements and story drifts. For the plastic hinge rotations, all of the procedures cannot provide acceptable estimations.

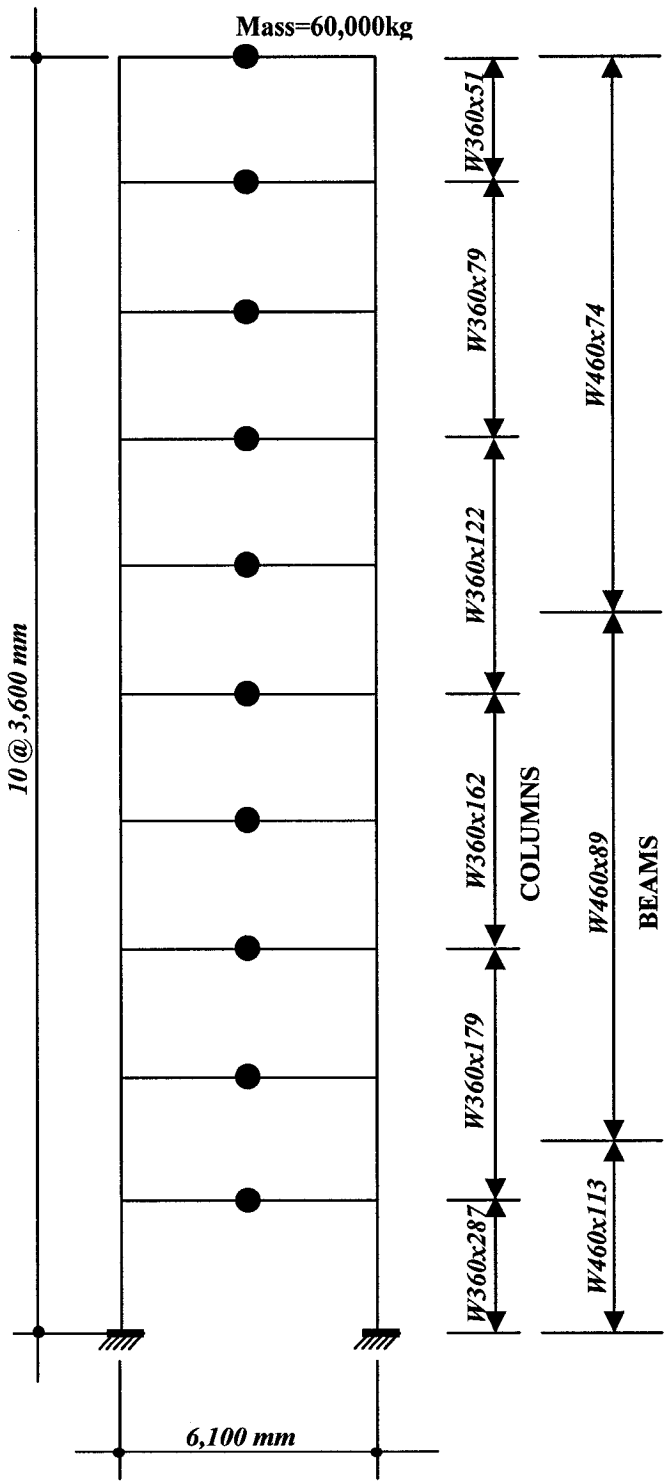

Table 4.1. System Description	
Beams (250MPa)	
1st level	W460x113
2nd -5th level	W460x89
6th -10th level	W460x74
Columns (250MPa)	
1st floor	W360x262
2nd -3rd floor	W360x179
4th -5th floor	W360x147
6th -7th floor	W360x110
8th -9th floor	W360x79
10th floor	W360x51
Restraints	
Columns fixed at ground floor	
Seismic Mass	
1st -10th level	60,000 Kg

Figure 4.1. 1-Bay, 10-Story MRF System

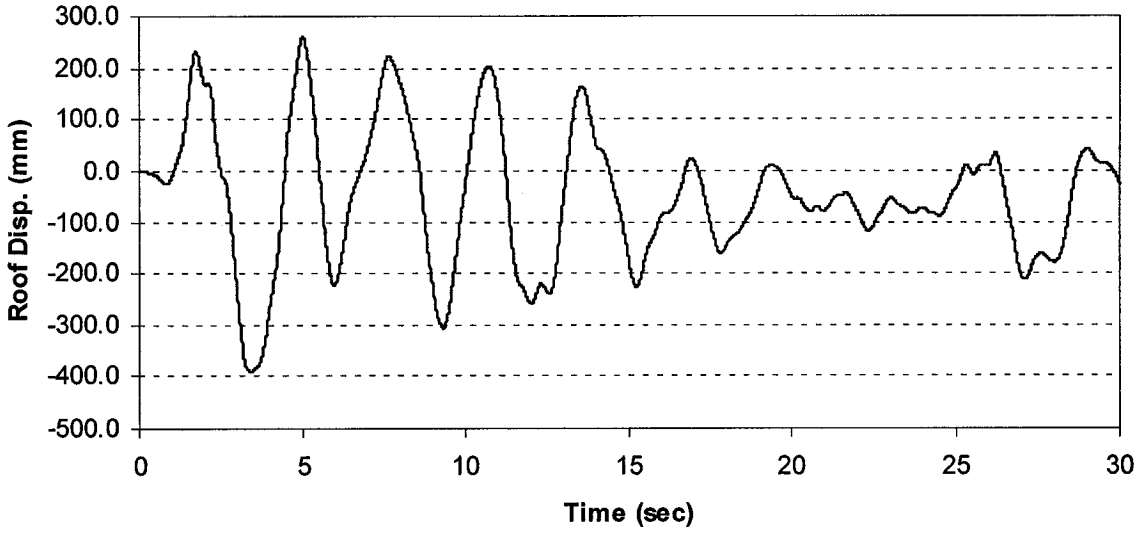

Figure 4.2. Roof Displacement History Response of 10-Story MRF System to 1.5 El-Centro Ground Motion

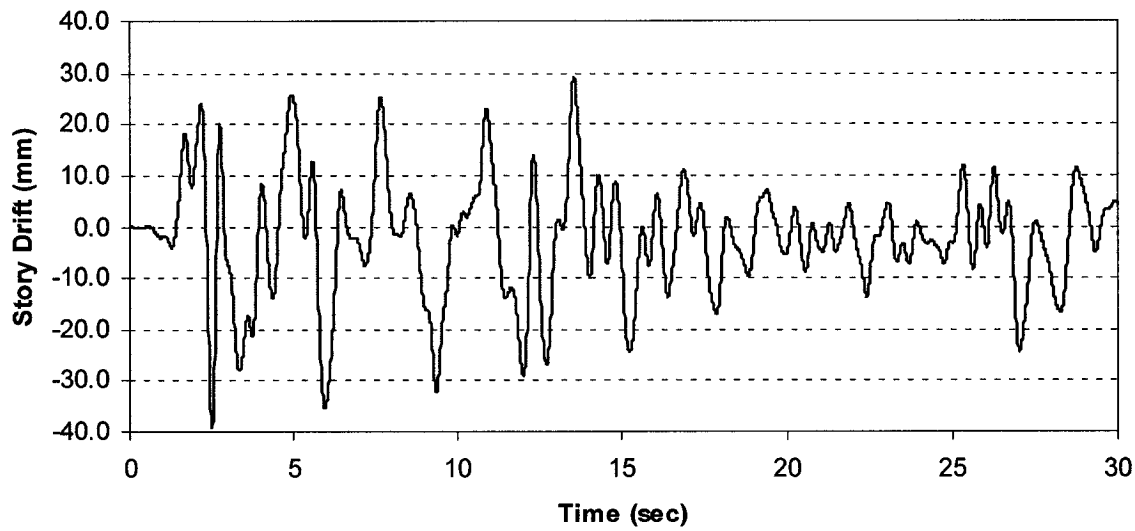

Figure 4.3. Top Story Drift History Response of 10-Story MRF System to 1.5 El-Centro Ground Motion

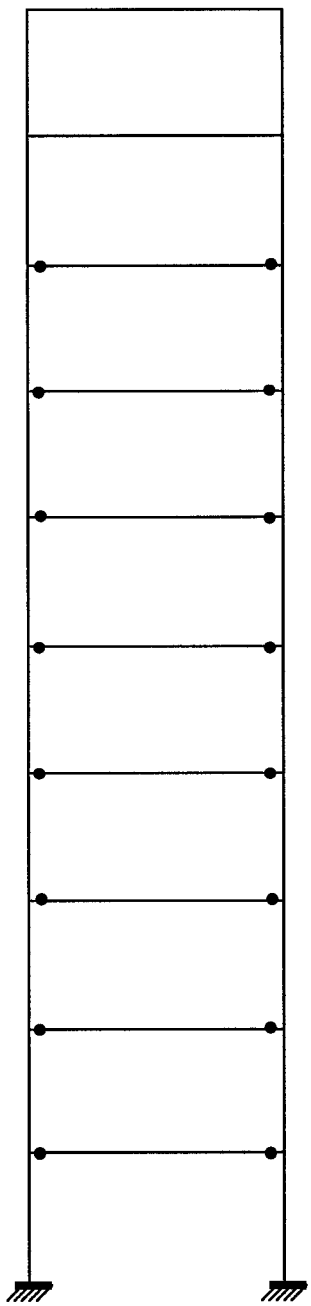

Table 4.2. Modal Properties for 10-story MRF

Mode		1	2	3
Period, T_n (sec)		3.270	1.118	0.626
Frequency, ω_n (rad/sec)		1.925	5.622	10.035
Participation factor, Γ_n		1.356	0.537	0.303
Effective mass, M_n^* (k kg)		447.0	73.4	25.5
Mode shape at story levels (normalized)	10 (Roof)	1.000	1.000	1.000
	9	0.939	0.626	0.060
	8	0.856	0.153	-0.738
	7	0.746	-0.344	-0.975
	6	0.628	-0.697	-0.573
	5	0.503	-0.881	0.130
	4	0.383	-0.872	0.682
	3	0.259	-0.704	0.890
	2	0.140	-0.426	0.680
	1	0.042	-0.136	0.245
	0 (Base)	0.000	0.000	0.000

Figure 4.4. Plastic Hinge Locations of 10-Story MRF System to 1.5 El-Centro Ground Motion

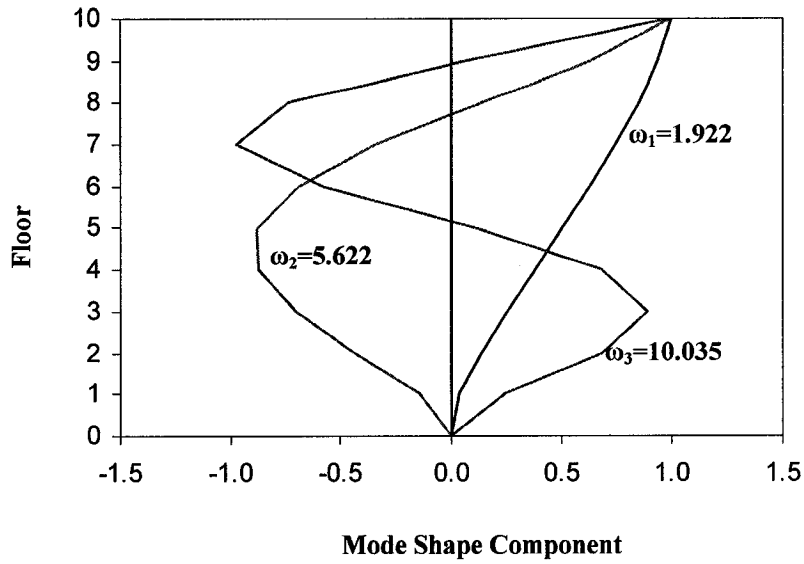

Figure 4.5. First Three Natural-vibration Frequencies and Modes of 10-story MRF

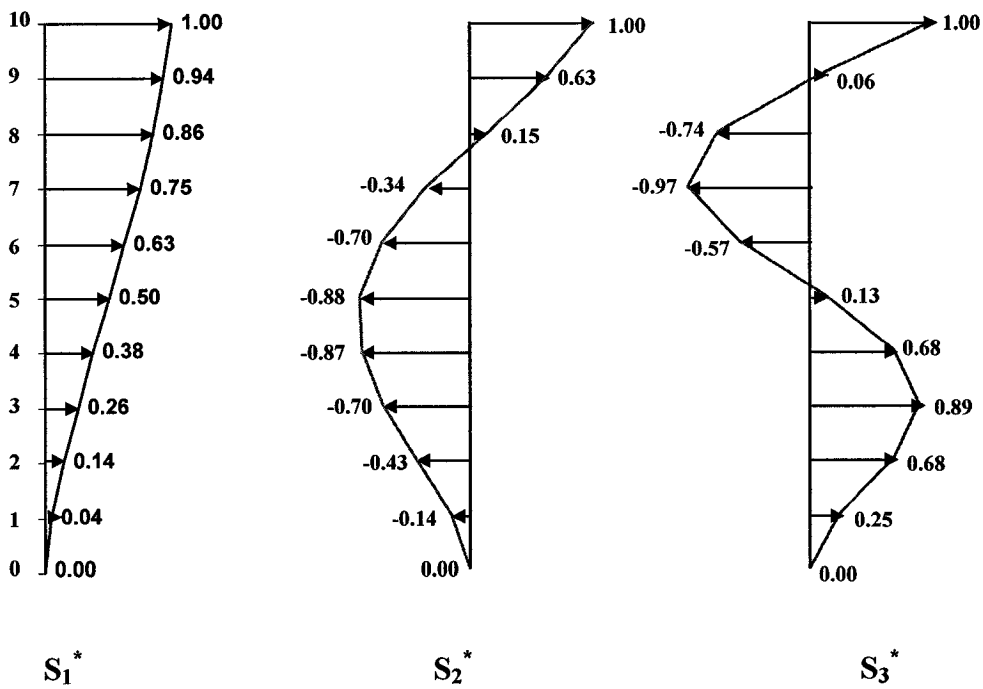

Figure 4.6. Lateral Force Distributions $\{s_n^*\} = [m] \cdot \{\phi_n\}$, n=1, 2, 3

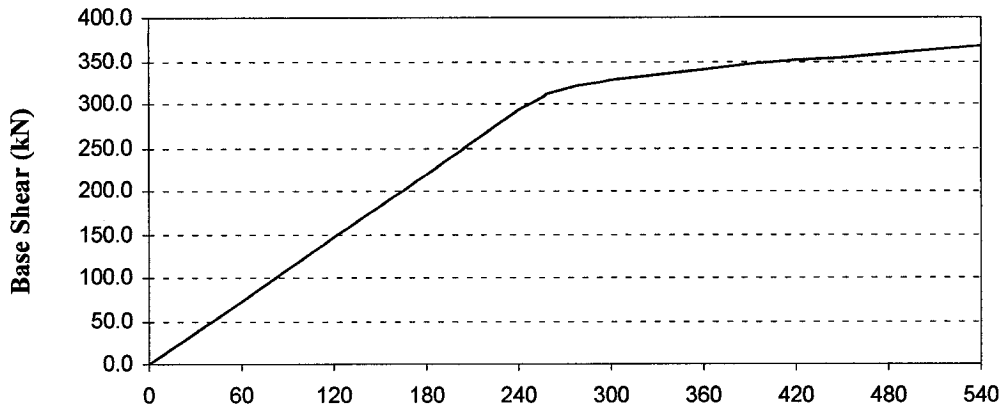

(a) Roof Displacement (mm)

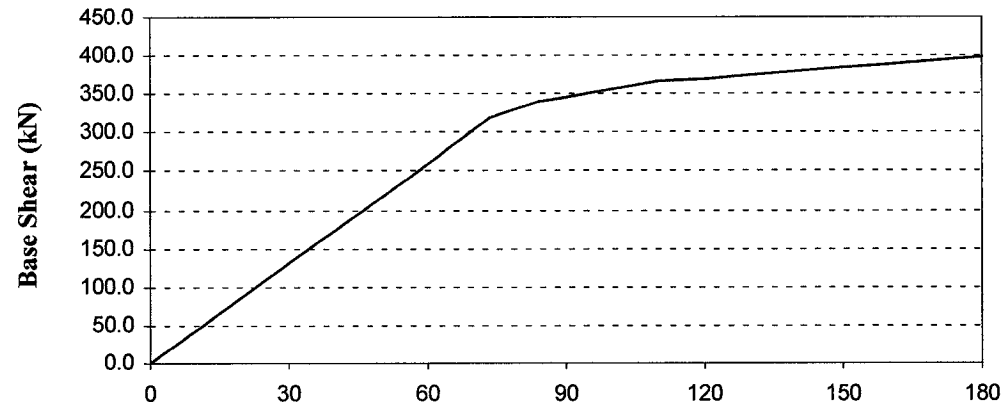

(b) Roof Displacement (mm)

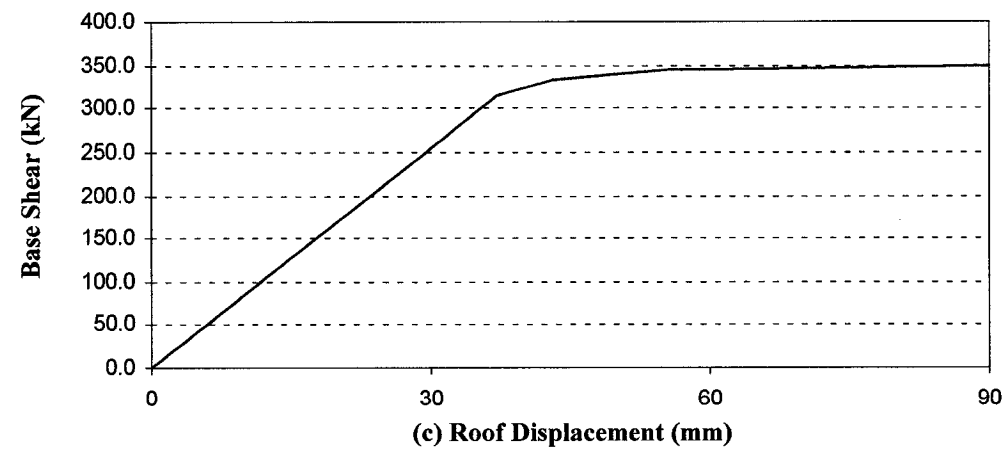

(c) Roof Displacement (mm)

Figure 4.7. Modal Pushover Capacity Curve for 10-story MRF: (a) "Mode" 1, (b) "Mode" 2, (c) "Mode" 3

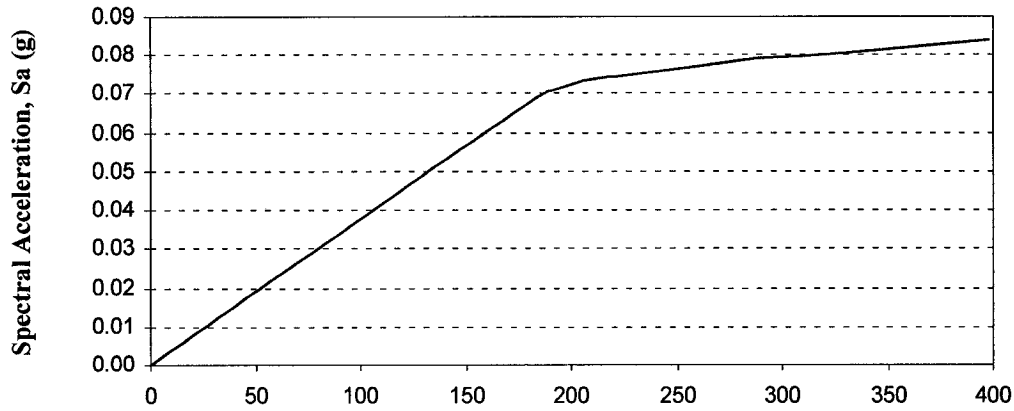

(a) Spectral Displacement, S_d (mm)

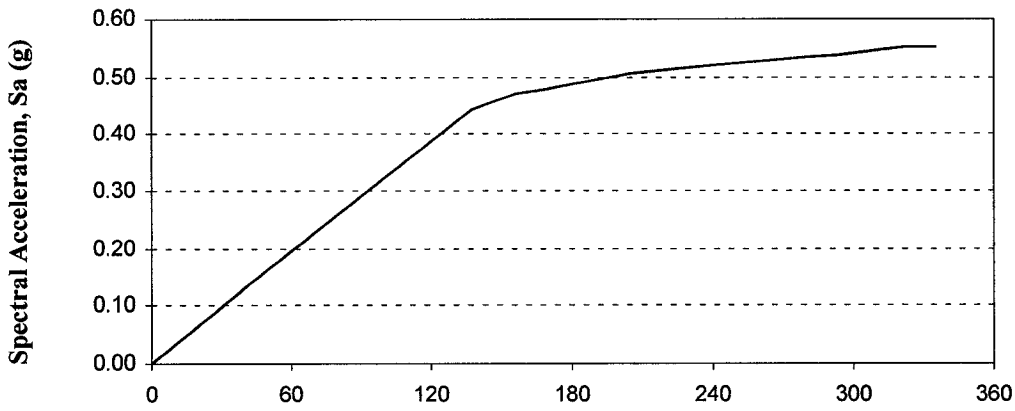

(b) Spectral Displacement, S_d (mm)

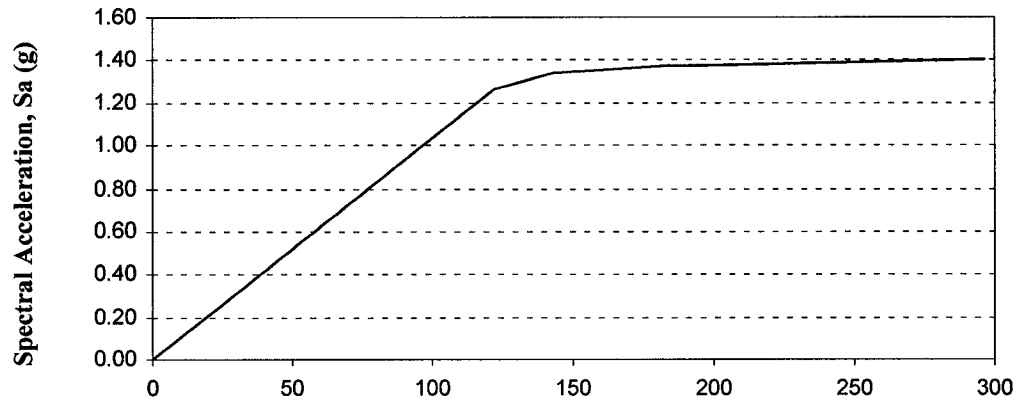

(c) Spectral Displacement, S_d (mm)

Figure 4.8. Capacity Spectrum Curves for 10-story MRF: (a) "Mode" 1, (b) "Mode" 2, (c) "Mode" 3

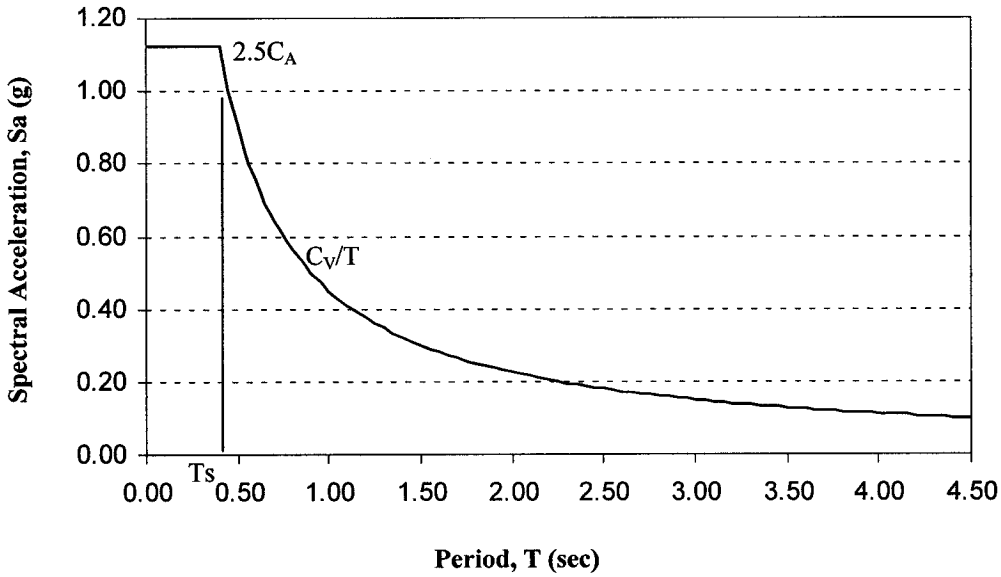

Figure 4.9. Traditional Spectrum

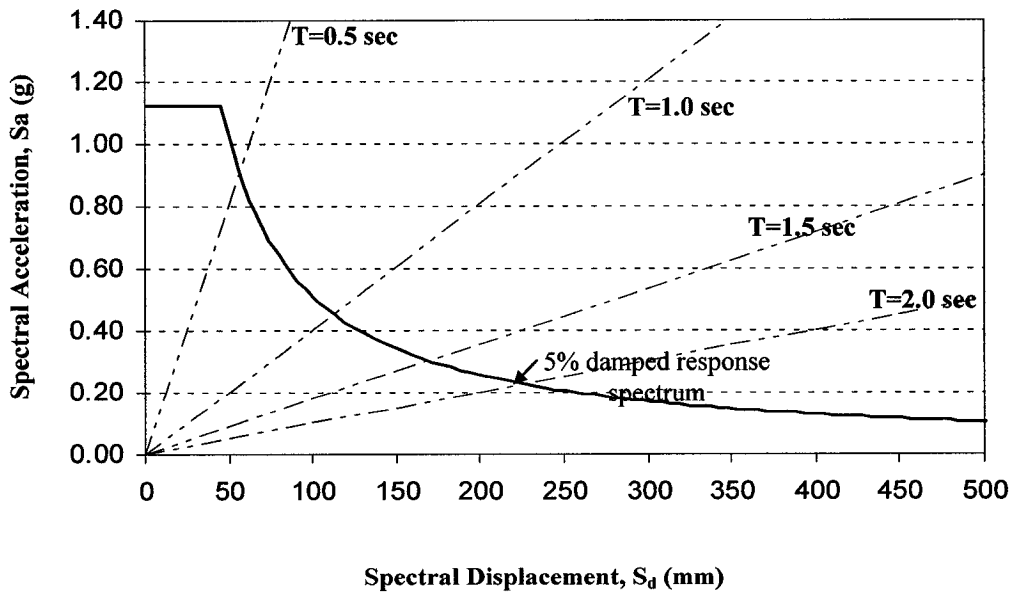

Figure 4.10. Elastic Response Spectrum (ζ=5%)

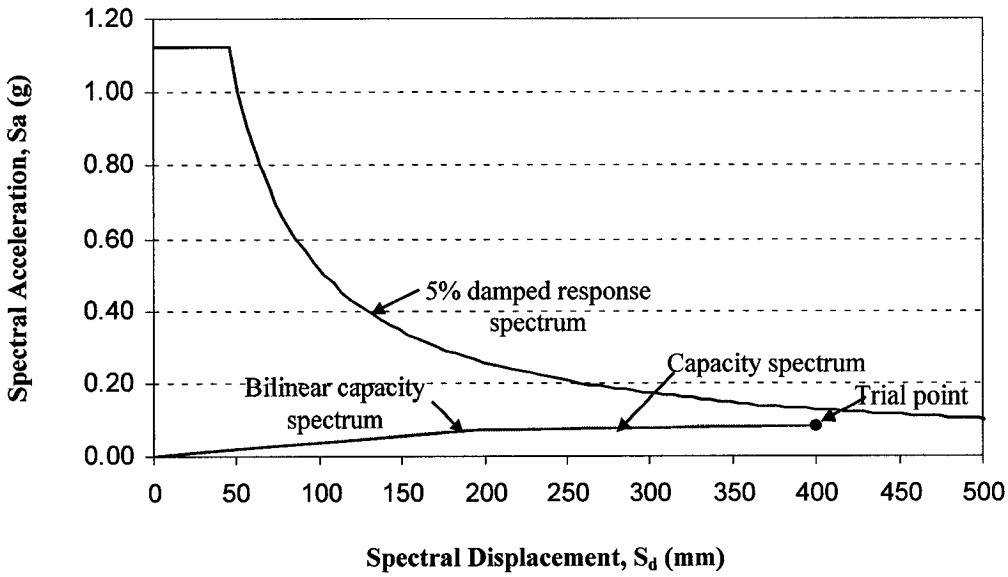

Figure 4.11. Capacity Spectrum Procedure A after Step 4 for Mode 1

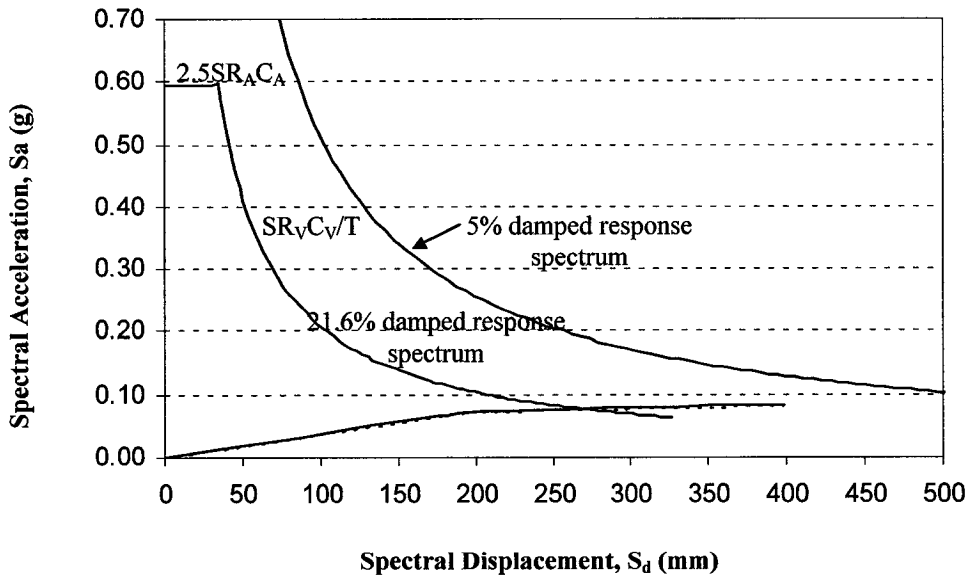

Figure 4.12. Capacity Spectrum Procedure A after Step 5 for Mode 1

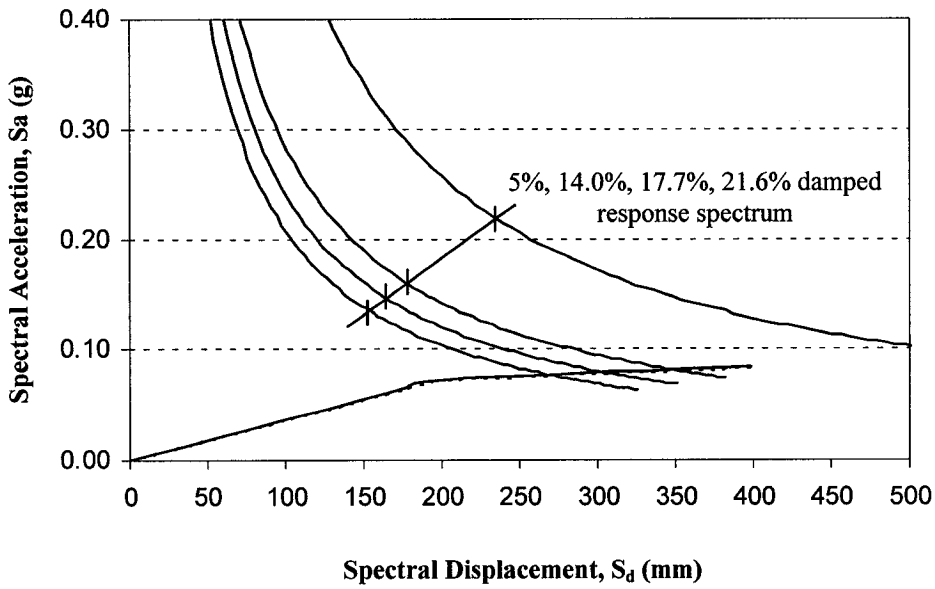

Figure 4.13. Capacity Spectrum Procedure A after Step 7 for Mode 1

Table 4.3. Trial for Demand Performance Point for Mode 1

Trial	a_y (g)	d_y(mm)	a_{pi} (g)	d_{pi}(mm)	Error (%)	$\hat{\zeta}_{eq}$ (%)	SR_A	SR_V	T_s
0						5.0	0.998	1.000	0.401
1	0.0738	196	0.0837	398		21.6	0.528	0.636	0.482
2	0.0722	192	0.0774	266	-33.2	14.0	0.668	0.744	0.446
3	0.0732	194	0.0808	332	24.8	18.7	0.574	0.672	0.468
4	0.0727	193	0.0791	299	-9.9	16.7	0.612	0.701	0.458
5	0.0730	194	0.0800	316	5.5	17.8	0.591	0.685	0.463
Final			0.0796	307	-2.7				

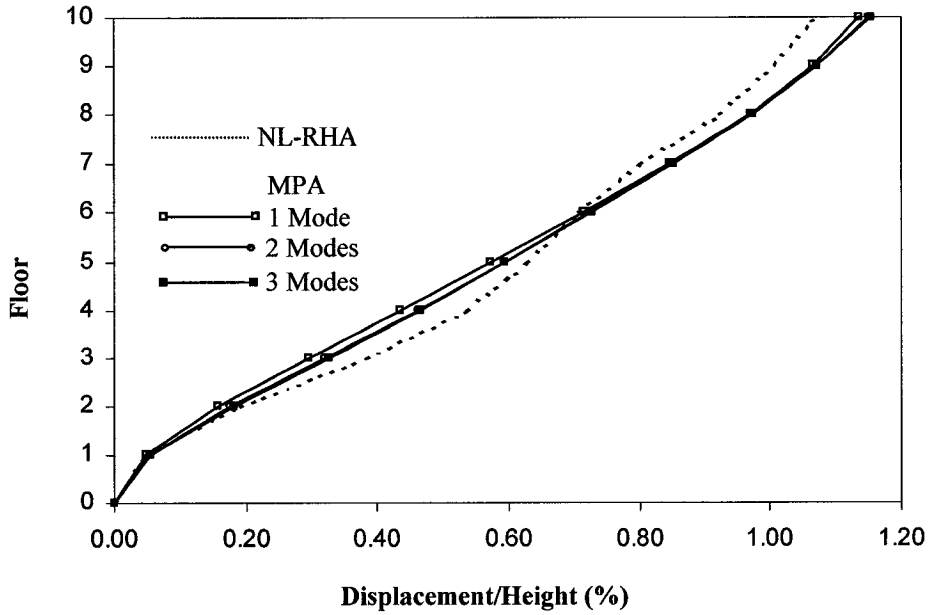

Figure 4.14. Comparison of Floor Displacement Ratios Determined by MPA and NL-RHA

Table 4.4. Peak Values of Floor Displacements (as % of building height=36.6m) from MPA for 1.5x El Centro Ground Motion

	Displacement/Height (%)							Error (%)		
	Modal Response			Combined (MPA)						
Floor	Mode #1	Mode #2	Mode #3	1 Mode	2 Modes	3 Modes	NL--RHA	1 Mode	2 Modes	3 Modes
0	0.000	0.000	0.000	0.000	0.000	0.000	0.000	0.00	0.00	0.00
1	0.047	-0.025	-0.015	0.047	0.054	0.056	0.049	-3.38	9.22	13.28
2	0.159	-0.078	-0.041	0.159	0.177	0.181	0.193	-17.80	-8.40	-5.98
3	0.294	-0.129	-0.053	0.294	0.321	0.326	0.383	-23.18	-16.14	-14.98
4	0.435	-0.160	-0.041	0.435	0.463	0.465	0.539	-19.27	-14.01	-13.68
5	0.572	-0.161	-0.008	0.572	0.594	0.594	0.630	-9.22	-5.69	-5.68
6	0.714	-0.128	0.034	0.714	0.726	0.726	0.710	0.61	2.20	2.32
7	0.848	-0.063	0.059	0.848	0.850	0.852	0.804	5.45	5.75	6.00
8	0.973	0.028	0.044	0.973	0.973	0.974	0.926	5.03	5.07	5.18
9	1.067	0.115	-0.004	1.067	1.074	1.074	1.005	6.22	6.83	6.83
10	1.137	0.183	-0.060	1.137	1.151	1.153	1.072	6.03	7.39	7.54

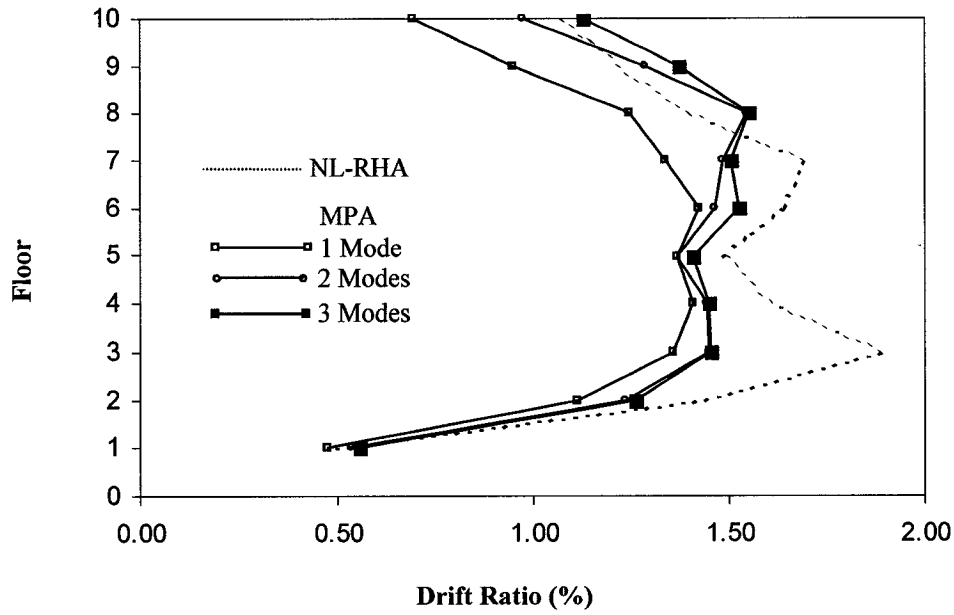

Figure 4.15. Comparison of Drift Ratios Determined by MPA and NL-RHA

Table 4.5. Peak Values of Story Drift Ratio (as % of story height=3.66m) from MPA for 1.5x El Centro Ground Motion

	Drift Ratio (%)							Error (%)		
	Modal Response			Combined (MPA)						
Floor	Mode #1	Mode #2	Mode #3	1 Mode	2 Modes	3 Modes	NL--RHA	1 Mode	2 Modes	3 Modes
1	0.473	-0.250	-0.147	0.473	0.535	0.555	0.495	-4.35	8.12	12.14
2	1.113	-0.530	-0.262	1.113	1.233	1.260	1.437	-22.54	-14.20	-12.29
3	1.356	-0.509	-0.126	1.356	1.448	1.453	1.891	-28.31	-23.43	-23.14
4	1.409	-0.307	0.125	1.409	1.442	1.448	1.607	-12.31	-10.25	-9.92
5	1.368	-0.016	0.332	1.368	1.368	1.407	1.489	-8.15	-8.14	-5.48
6	1.424	0.336	0.423	1.424	1.463	1.523	1.637	-12.99	-10.60	-6.95
7	1.335	0.647	0.242	1.335	1.484	1.503	1.694	-21.17	-12.42	-11.26
8	1.247	0.910	-0.142	1.247	1.544	1.551	1.399	-10.86	10.37	10.84
9	0.949	0.865	-0.480	0.949	1.284	1.370	1.221	-22.28	5.14	12.24
10	0.691	0.685	-0.565	0.691	0.973	1.126	1.074	-35.62	-9.36	4.80

Table4.6. Peak Values of Hinge Plastic Rotations from MPA for 1.5x El Centro Ground Motion

	Plastic Hinge Rotation (rad)							Error (%)		
	Modal Response			Combined (MPA)						
Floor	Mode #1	Mode #2	Mode #3	1 Mode	2 Modes	3 Modes	NL--RHA	1 Mode	2 Modes	3 Modes
1	0.0000	0.0000	0.0000	0.0000	0.0000	0.0000	0.0010	-100.00	-100.00	-100.00
2	0.0057	0.0000	0.0000	0.0057	0.0057	0.0057	0.0070	-18.57	-18.57	-18.57
3	0.0087	0.0000	0.0000	0.0087	0.0087	0.0087	0.0092	-5.43	-5.43	-5.43
4	0.0090	0.0000	0.0000	0.0090	0.0090	0.0090	0.0095	-5.26	-5.26	-5.26
5	0.0073	0.0000	0.0000	0.0073	0.0073	0.0073	0.0100	-27.00	-27.00	-27.00
6	0.0048	0.0000	0.0000	0.0048	0.0048	0.0048	0.0108	-55.56	-55.56	-55.56
7	0.0008	0.0000	0.0000	0.0008	0.0008	0.0008	0.0073	-89.04	-89.04	-89.04
8	0.0000	0.0000	0.0000	0.0000	0.0000	0.0000	0.0035	-100.00	-100.00	-100.00
9	0.0000	0.0000	0.0000	0.0000	0.0000	0.0000	0.0004	-100.00	-100.00	-100.00
10	0.0000	0.0000	0.0000	0.0000	0.0000	0.0000	0.0000	0.00	0.00	0.00

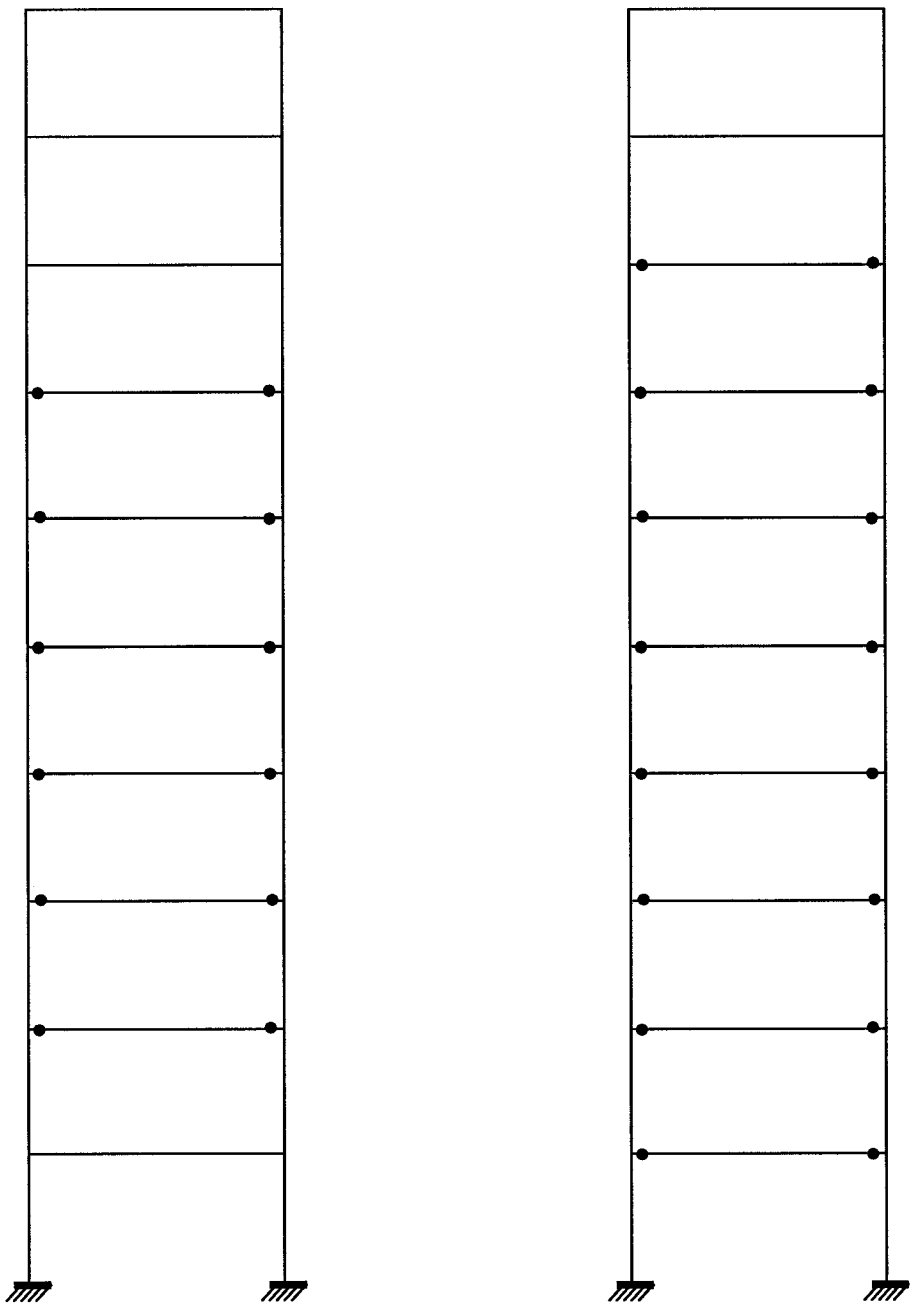

Figure 4.16. Comparison of Plastic Hinge Locations Estimated by MPA and NL-RHA

Table 4.7. FEMA-273 Uniform Force Distribution

Floor, j	Mass, m_j (kg)	$s_j^* = \frac{m_j}{\sum_{i=1}^{n} m_i}$
1	60,000	0.100
2	60,000	0.100
3	60,000	0.100
4	60,000	0.100
5	60,000	0.100
6	60,000	0.100
7	60,000	0.100
8	60,000	0.100
9	60,000	0.100
10	60,000	0.100

Table 4.8. FEMA-273 ELF Distribution

Floor, j	Mass, m_j (kg)	h_j (m)	$m_j h_j^k$ (kg-m^k)	$s_j^* = \frac{m_j h_j^k}{\sum_{i=1}^{n} m_i h_i^k}$
1	60,000	3.66	803,736	0.003
2	60,000	7.32	3,214,944	0.010
3	60,000	10.98	7,233,624	0.023
4	60,000	14.64	12,859,776	0.042
5	60,000	18.30	20,093,400	0.065
6	60,000	21.96	28,934,496	0.094
7	60,000	25.62	39,383,064	0.127
8	60,000	29.28	51,439,104	0.166
9	60,000	32.94	65,102,616	0.210
10	60,000	36.60	80,373,600	0.260

* $k = 2.0$

Table 4.9. FEMA-273 SRSS Distribution

	Lateral Forces			Story Shears				Lateral Forces	
Floor, j	f_{j1} (kN)	f_{j2} (kN)	f_{j3} (kN)	V_{j1} (kN)	V_{j2} (kN)	V_{j3} (kN)	V_j (kN)	f_j (kN)	$s_j^* = \frac{f_j}{\sum_{i=1}^{n} f_i}$
1	3.84	17.34	32.79	506.68	290.12	187.55	613.24	20.62	0.034
2	12.87	54.19	91.00	502.84	272.78	154.76	592.63	52.34	0.085
3	23.87	89.54	119.01	489.97	218.59	63.76	540.29	53.51	0.087
4	35.30	110.90	91.24	466.10	129.04	-55.25	486.78	31.39	0.051
5	46.39	112.02	17.44	430.81	18.14	-146.49	455.39	27.07	0.044
6	57.95	88.68	-76.60	384.41	-93.88	-163.93	428.32	44.22	0.072
7	68.78	43.75	-130.40	326.47	-182.56	-87.33	384.10	38.45	0.063
8	78.89	-19.52	-98.75	257.69	-226.31	43.07	345.66	37.68	0.061
9	86.59	-79.59	8.04	178.80	-206.80	141.82	307.97	101.62	0.166
10	92.20	-127.21	133.78	92.20	-127.21	133.78	206.35	206.35	0.336

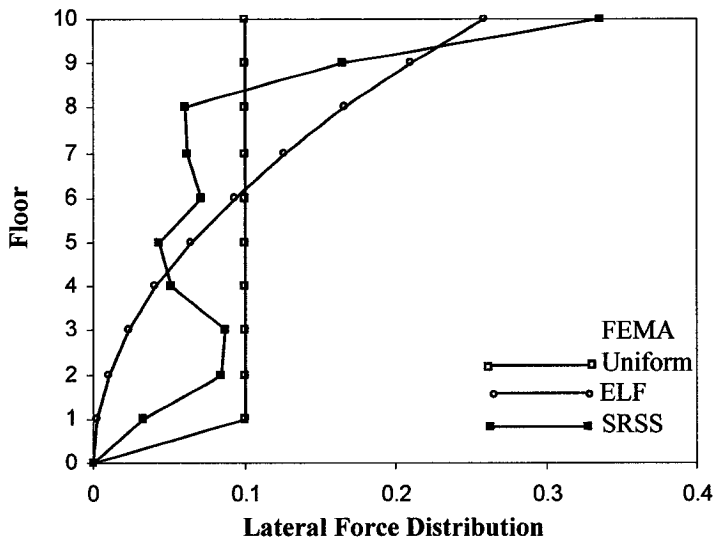

Figure 4.17. FEMA-273 Lateral Force Distributions

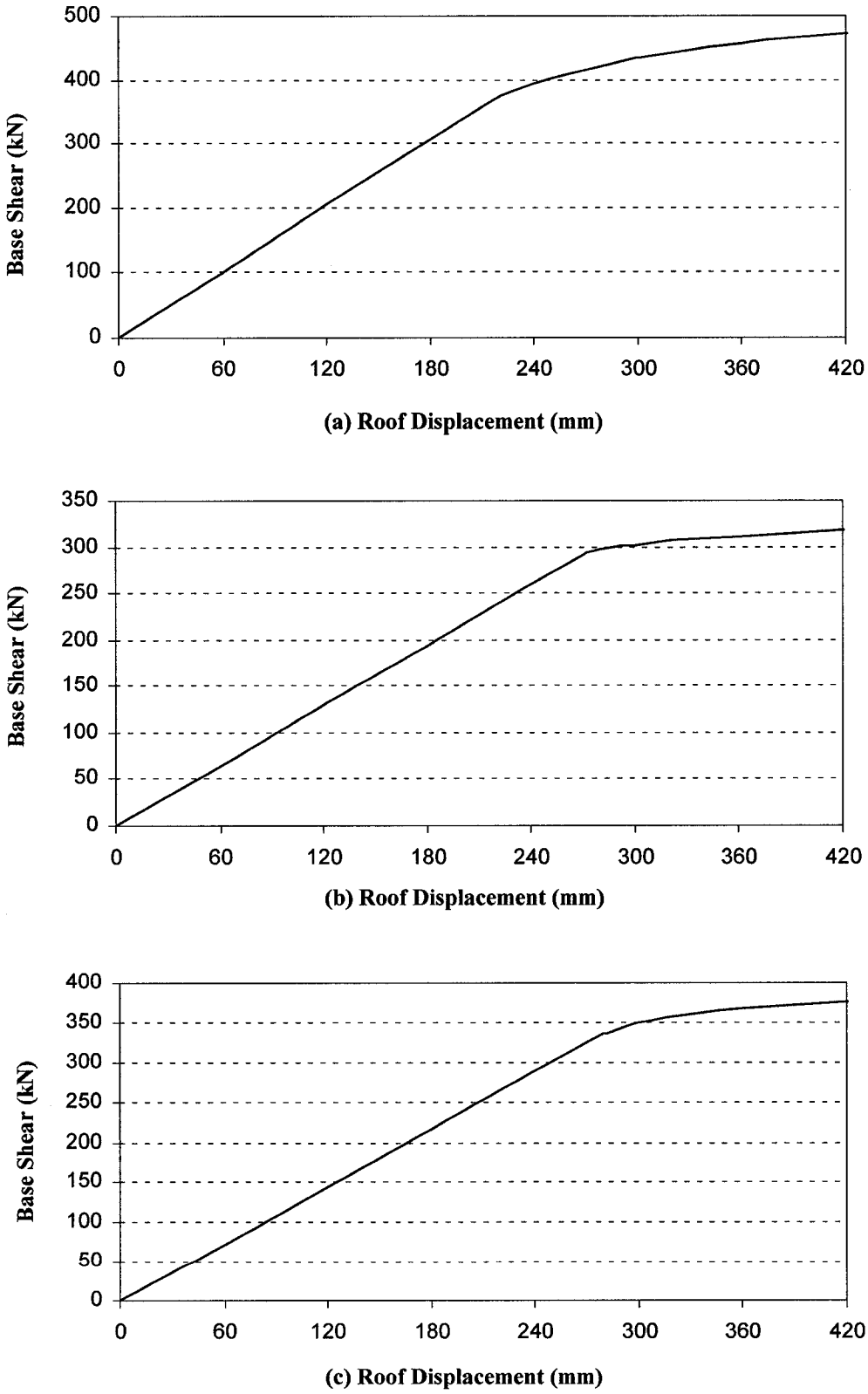

Figure 4.18. FEMA-273 Pushover Curves: (a) Uniform Force, (b) ELF, (c) SRSS Force Distribution

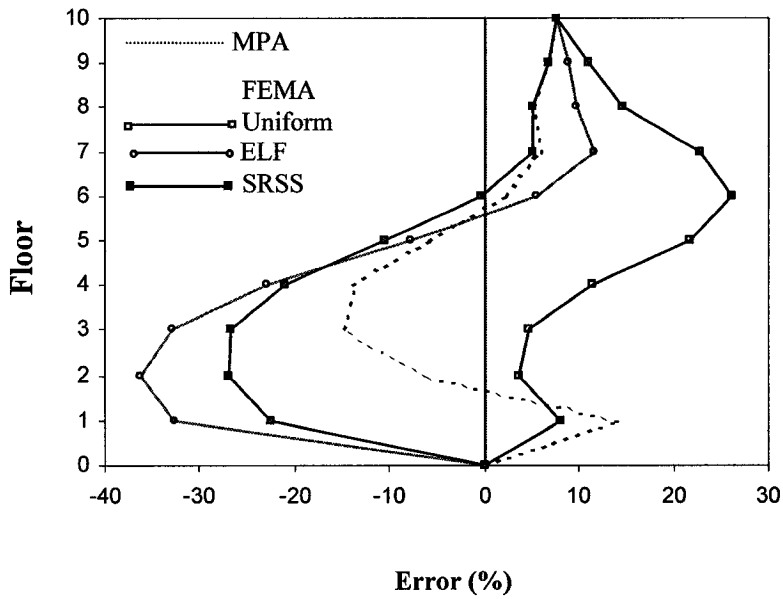

Figure 4.19. Errors in Floor Displacement Ratios Estimated by FEMA-273 and MPA

Table 4.10. Peak Values of Floor Displacement Ratios (as % of building height=36.60 m) from FEMA and MPA for 1.5 El-Centro Ground Motion

Floor	Displacement/Height (%)					Error (%)			
	FEMA			MPA 3 modes	NL-RHA	FEMA			MPA 3 modes
	Uniform	ELF	SRSS			Uniform	ELF	SRSS	
0	0	0	0	0	0	0	0	0	0
1	0.053	0.033	0.038	0.056	0.049	8.16	-32.65	-22.45	13.28
2	0.200	0.123	0.140	0.181	0.193	3.63	-36.27	-27.46	-5.98
3	0.401	0.257	0.282	0.326	0.383	4.70	-32.90	-26.37	-14.98
4	0.601	0.416	0.435	0.465	0.539	11.50	-22.82	-19.29	-13.68
5	0.767	0.581	0.583	0.594	0.630	21.75	-7.78	-7.46	-5.68
6	0.896	0.749	0.731	0.726	0.710	26.20	5.49	2.96	2.32
7	0.988	0.898	0.866	0.852	0.804	22.89	11.69	7.71	6.00
8	1.062	1.016	0.984	0.974	0.926	14.69	9.72	6.26	5.18
9	1.115	1.095	1.077	1.074	1.005	10.95	8.96	7.16	6.83
10	1.153	1.153	1.153	1.153	1.072	7.56	7.56	7.56	7.54

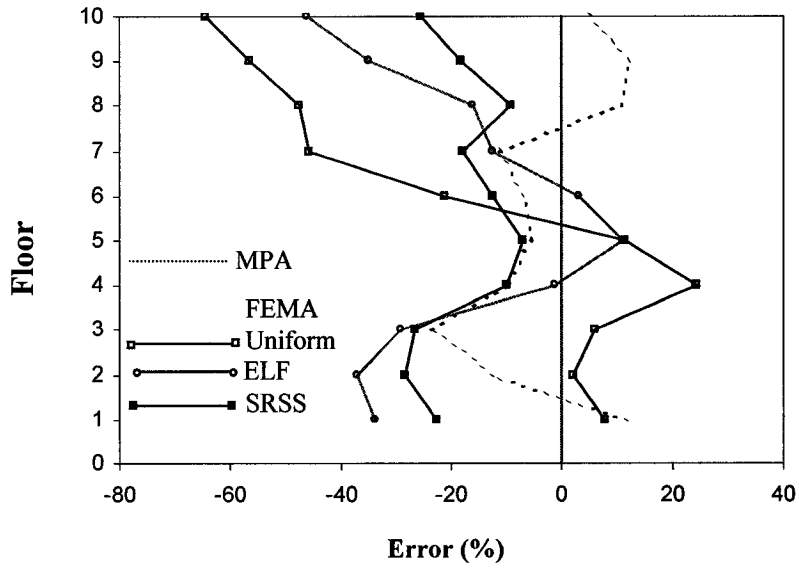

Figure 4.20. Errors in Floor Story Drift Ratios Estimated by FEMA-273 and MPA

Table 4.11. Peak Values of Story Drifts Ratios (as % of story height) from FEMA and MPA for 1.5 El-Centro Ground Motion

Floor	Drifts Ratio (%)					Error (%)			
	FEMA			MPA 3 modes	NL-RHA	FEMA			MPA 3 modes
	Uniform	ELF	SRSS			Uniform	ELF	SRSS	
1	0.533	0.328	0.377	0.555	0.495	7.68	-33.74	-23.84	12.14
2	1.464	0.907	1.025	1.260	1.437	1.88	-36.88	-28.67	-12.29
3	2.008	1.339	1.418	1.453	1.891	6.19	-29.19	-25.01	-23.14
4	2.000	1.585	1.525	1.448	1.607	24.46	-1.37	-5.10	-9.92
5	1.661	1.653	1.481	1.407	1.489	11.55	11.01	-0.54	-5.48
6	1.292	1.686	1.489	1.523	1.637	-21.08	2.99	-9.04	-6.95
7	0.923	1.486	1.347	1.503	1.694	-45.51	-12.28	-20.48	-11.26
8	0.735	1.175	1.175	1.551	1.399	-47.46	-16.01	-16.01	10.84
9	0.530	0.795	0.929	1.370	1.221	-56.59	-34.89	-23.91	12.24
10	0.383	0.579	0.762	1.126	1.074	-64.34	-46.09	-29.05	4.80

Table 4.12. Peak Values of Plastic Hinge Rotations from FEMA and MPA for 1.5 El-Centro Ground Motion

Floor	Plastic Hinge Rotation (rad)					Error (%)			
	FEMA			MPA 3 modes	NL-RHA	FEMA			MPA 3 modes
	Uniform	ELF	SRSS			Uniform	ELF	SRSS	
1	0.0018	0.0000	0.0000	0.0000	0.0010	80.00	-100.00	-100.00	-100.00
2	0.0104	0.0035	0.0048	0.0056	0.0070	48.57	-50.00	-31.43	-18.57
3	0.0124	0.0064	0.0066	0.0086	0.0092	34.78	-30.43	-28.26	-5.43
4	0.0099	0.0076	0.0063	0.0088	0.0095	4.21	-20.00	-33.68	-5.26
5	0.0058	0.0075	0.0055	0.0071	0.0100	-42.00	-25.00	-45.00	-27.00
6	0.0016	0.0068	0.0050	0.0046	0.0108	-85.19	-37.04	-53.70	-55.56
7	0.0000	0.0036	0.0027	0.0007	0.0073	-100.00	-50.68	-63.01	-89.04
8	0.0000	0.0000	0.0000	0.0000	0.0035	-100.00	-100.00	-100.00	-100.00
9	0.0000	0.0000	0.0000	0.0000	0.0004	-100.00	-100.00	-100.00	-100.00
10	0.0000	0.0000	0.0000	0.0000	0.0000	0.00	0.00	0.00	0.00

CHAPTER 5

MULTISTORY FRICTION DAMPED BRACED FRAME (FDBF)

5.1 SYSTEM DESCRIPTION

The single-bay, 10-story Friction Damped Braced Frame (FDBF) shown in Figure 5.1 is compose of two systems. The main structure is the moment resisting steel frame which is the same as shown in Fig.4.1and the second part is the bracing system with a friction damped brace in each story. The optimum of these friction damped braces is described in the next section.

5.2 OPTIMUM SLIP LOAD AND STIFFNESS OF BRACES

Slip Load of Braces

By the approach presented in the thesis of [Baktash, 1989], the slip load is optimized when the maximum amount of energy is dissipated by the brace. It was demonstrated that the friction damped bracing system provides maximum energy dissipation when the shear resisted by the brace is equal to that of the frame without bracing

$$V_b = V_f \tag{5.1}$$

For the weak beam/ strong column single-bay, 10-story FDB-Frame shown in Figure 5.1, the shear resisted by the frame is

$$V_b = V_f = \frac{2M_{pb}}{h} \tag{5.2}$$

where M_{pb} is the yield moment for the beam.

By the geometric relation, the slip load of the braces P_s is

$$P_s = \frac{V_b}{\cos\varphi} = \frac{2M_{pb}}{h\cos\varphi} \tag{5.3}$$

where φ is the angle between the brace and the beam at each floor.

For the FDBF system shown in Figure 5.1, $\varphi = 31^\circ, h = 3660mm$, $M_{pb} = 650kN \cdot m$ for 1st floor, $M_{pb} = 500kN \cdot m$ for 2nd to 5th floor, $M_{pb} = 410kN \cdot m$ for 6th to 10th floor, giving the slip loads, $P_s = 415kN$ for 1st story, $P_s = 320kN$ for 2nd to 5th story, $P_s = 260kN$ for 6th to 10th story.

Stiffness of the Braces

The braces of the FDBF are chosen the same as in the thesis of [Baktash, 1989], i.e., for 1st to 2nd story, the brace is $2L150\times150\times13, 2L150\times150\times10$ for 3rd to 6th story, $2L125\times125\times13$ for 7th to 10th story, respectively. After dynamic analysis by DRAIN-2DX [Allahabadi and Powell, 1988], the comparison of the stiffness of FDBF with MRF is obtained as

$$\frac{K_{FDBF}}{K_{MRF}} = \frac{\omega_F^2}{\omega_M^2} \tag{5.4}$$

where K_{FDBF}, K_{MRF} are the stiffnesses of the FDBF and MRF, ω_F, ω_M are chosen as the first natural frequencies of the FDBF and MRF, respectively. Here, the ratio of $\frac{\omega_F^2}{\omega_M^2}$ is equal to *4.97*.

Recall the Equation (3.16), the stiffness ratio of the brace to the frame is,

$\lambda = \frac{K_b}{K_f} = \frac{4.97-1}{1} = 3.97$. That is acceptable.

5.3 NONLINEAR RESPONSE HISTORY ANALYSIS (NL-RHA)

Assuming the 10-story FDBF shown in Figure 5.1 is subjected to the north-south component of the El-Centro (1940) ground motion with the scaling factor of 1.5, the structural responses computed by DRAIN-2DX [Allahabadi and Powell, 1988] are shown in Figures 5.2, 5.3. Figure 5.2 also illustrates the comparison of roof displacement response of 10-story FDBF with that of MRF system, For MRF system, the peak roof displacement, $u_M^r = 392.4mm$, but for FDBF system, $u_F^r = 210.6mm$, i.e., the roof displacement of FDBF system is only about *54%* of that of MRF system. Similarly, the top story drift of FDBF system is only about *33%* of that of MRF system, the comparison is shown in Figure 5.3. Figure 5.4 illustrates the plastic slip locations of the friction bracing for FDBF system. It is noted that there are no plastic hinges formed in the beams or columns, the main element of the system.

It is obvious that the FDBF system has better seismic performance than the MRF system, in terms of roof displacements, story drifts and plastic hinges.

5.4 MODAL PUSHOVER ANALYSIS (MPA)

Pushover Capacity Curve and Spectrum

Recalling the procedure of MPA in section 1.3.2, the structural dynamic characteristics for the FDBF shown in Figure 5.1, are determined by DRAIN-2DX [Allahabadi and

Powell, 1988], and summarized in Table 5.1.The first three natural-vibration frequencies and modes of the system are illustrated in Figure 5.5. Pushing the structure to assumed target displacements with the lateral force distributions shown in Figure 5.6, the pushover capacity curves for the first three modes, a plot of base shear versus roof displacement, are shown in Figure 5.7.

Accordingly, the capacity spectrums for the first three modes, a plot of spectral acceleration versus spectral displacement, which are converted from capacity curves by Equation (4.15), are illustrated in Figure 5.8,

Modal Roof Displacement

Similar to the MRF system, the modal roof displacements for the first three modes are determined by estimating the seismic performance points using procedure A in ATC-40 [ATC, 1996].

The capacity spectrum for the mode1of FDBF system is plotted on the same chart as the elastic response spectrum (ζ=5%, shown in figure 4.10) as shown in Figure 5.9. And the idealized bilinear capacity spectrum, based on the end of the curve considered as the first trial point, is illustrated on the same diagram.

For the first idealized bilinear capacity spectrum as shown in Figure 5.9, the effective damping ratio for the first trial point can be determined by

$$\hat{\zeta}_{eq} = \frac{63.7\kappa(a_y d_{pi} - d_y a_{pi})}{a_{pi} d_{pi}} + 5 \qquad (5.5)$$

where $\hat{\zeta}_{eq}$ is the effective viscous damping ratio and κ is the value for damping modification factor from Table 8-1 [ATC, 1996] and shown in Appendix B-3. Here, β_{eff} =*22.1%*. Then the first demand spectrum for the damping ratio of *22.1%* is developed by Equations (1.7), (1.8) and (1.9) and illustrated in Figure 5.10.

Comparing the intersection point of the demand spectrum and the capacity spectrum with the initial trial performance point, if the error of the displacement between these two point is less than 5%, i.e., the demand spectrum intersects the capacity spectrum within acceptable tolerance, then the trial performance point, a_{pi}, d_{pi}, can be considered as the demand performance point, a_p, d_p. If the demand spectrum does not intersect the capacity spectrum within acceptable tolerance, then select the intersection point as the next trial performance point and return to try it again, until the demand spectrum intersects the capacity spectrum within acceptable tolerance. Figure 5.11 illustrates the family of demand spectrums and Table 5.2 lists the trials to find the demand performance point, a_p, d_p. For the FDBF system as shown in Figure 5.1, the seismic performance point for the first mode is $a_{1p} = 0.1421g$ and $d_{1p} = 160.0mm$.

Recall from Equation (4.13) that the peak value of the deformation of the equivalent SDF system, D_{no}, is equal to the spectral displacement at the demand performance point, d_{np}

$$D_{1o} = d_{1p} = 160.0mm$$

and the peak value of the roof displacement for mode 1 and be obtained by Equation (4.8) as

$$u_{1o} = \Gamma_1 \phi_{1o} D_{1o} = 1.468 \times 1.0 \times 160.0 = 229.7mm$$

Similarly, the peak value of the roof displacement for mode 2 and mode 3 of the FDBF system can be estimated by this same procedure. For this system

$$u_{2o} = 31.1mm,\ u_{3o} = 4.7mm$$

At the roof displacements, $u_{1o} = 229.7mm, u_{2o} = 31.1mm, u_{3o} = 4.7mm$, the values of floor displacements and story drifts for MPA are determined by Equation (4.8). The peak values of floor displacements (as % of the building height=36.6m) for the first three modes of the FDBF system are summarized in Table 5.3 and illustrated in Figure 5.12. Similarly, the story drift ratios (as % of story height=3.66m) for the first three modes of FDBF system are shown in Figure 5.13 and summarized in Table 5.4.

Comparison of Results Determined by MPA with NL-RHA

By the SRSS combination rule, the total responses of the floor displacement ratios and story drift ratios for 1 mode, 2 modes and 3 modes are also included in Tables 5.3 and 5.4 and Figures 5.12 and 5.13, respectively.

Comparing the results determined by MPA, with that by NL-RHA procedure, the errors of the floor displacements for the combined 3 modes are between *-25.79 %* and *10.24 %.* The accuracy of the MPA results is considered acceptable.

Similarly, the comparisons of the story drift ratios estimated by MPA and NL-RHA show that the errors of the story drift ratios for the combined 3 modes are between *-33.20 %* and *157.58 %,* which is too poor to be acceptable. But the result is to be expected,

because one of the basic assumptions which assume that the mode shape vector remains constant throughout the time history response is not correct, especially after the first plastic hinge/slip has been formed. This kind of limitation of MPA procedure leads to produce an Improved Modal Pushover Analysis (IMPA) procedure.

5.5 IMPROVED MODEL PUSHOVER ANALYSIS (IMPA)

Difference between MPA and IMPA

The Improved Modal Pushover Analysis (IMPA) procedure implements similar steps as the MPA procedure in developing the pushover capacity curves and capacity spectrum of the system, and estimating the modal roof displacements using the capacity spectrum method (CSM) in ATC-40 [ATC, 1996]. After the modal roof displacements are obtained, the values of floor displacements for IMPA are not simply determined by Equation (4.8), $\{u_n\} = \Gamma_n \{\phi_n\} D_{no}$, i.e., the modal floor displacements are not linear to the mode shape of the system. In IMPA procedure, the structure is pushed again to the obtained roof displacements with the lateral force distributions the same as shown in Figure 5.6, and the response of each floor is considered as the floor displacement of the system. Simultaneously, the story drifts are calculated.

For this example, at the roof displacements, $u_{1o} = 229.7mm, u_{2o} = 31.1mm, u_{3o} = 4.7mm$, the values of floor displacements and story drifts for IMPA are calculated by one more pushover analysis. The peak values of floor displacements (as % of the building height=36.6m) for the first three modes of the FDBF system are summarized in Table 5.5 and illustrated in Figure 5.14. Similarly, the story drift ratios (as % of story

height=3.66m) for the first three modes of the FDBF system are shown in Figure 5.15 and summarized in Table 5.6. Respectively, Figure 5.16 and Table 5.7 illustrate the peak values of the plastic slip of the friction bracing estimated by IMPA procedure for the FDBF system.

Comparison of Results Determined by IMPA with NL-RHA

By the SRSS combination rule, the total responses of the floor displacement ratios, story drift ratios and plastic extensions of friction damped bracing for 1 mode, two modes and 3 modes determined by IMPA are summarized in Tables 5.5, 5.6 and 5.7.

The comparison of floor displacement ratios estimated by IMPA and NL-RHA is also illustrated in Figure 5.14. For response consisting of combined 3 modes, the errors for IMPA to the NL-RHA results are between *-15.47 %* and *9.34 %.* Thus, the accuracy of IMPA results is better than that of MPA which was compared with NL-RHA in the previous section.

The comparisons of story drift ratios estimated by IMPA and NL-RHA is shown in Figure 5.15. For response consisting of combined 3 modes, the errors for IMPA to the NL-RHA results are between *-14.51 %* and 32.90%, *i.e.* the IMPA procedure can provide much better estimates than the MPA procedure in estimating the story drifts of FDBF systems.

The comparison of the plastic slips of the friction damped bracing estimated by IMPA and NL-RHA is illustrated in Figure 5.16. For response of combined 3 modes, the errors for IMPA to the NL-RHA results are between *-34.47 %* and *39.32 %*. The accuracy of IMPA results is also acceptable.

5.6 FEMA-273 PUSHOVER ANALYSIS

Force Distributions for FEMA-273 Pushover Analysis

The three force distributions for the FDBF system for FEMA-273 pushover analysis, the uniform force distribution, the equivalent lateral force (ELF) distribution and the SRSS distribution, are summarized in Table 5.8, Table 5.9 and Table 5.10, respectively. All are illustrated in Figure 5.17. The uniform force distribution for FDBF system is same as that for MRF system as shown in Table 4.7 because this force distribution depends only on the distribution of mass to each floor. Compared with the MRF system, the equivalent lateral force (ELF) distribution and the SRSS distribution for the FDBF system have changed because of the difference in the dynamic properties between the FDBF and the MRF system.

FEMA-273 Pushover Analysis for FDBF

Similar to the MRF, the target roof displacement for FDBF for FEMA-273 pushover analysis is determined by combining the peak value of roof displacements of the first three modes by SRSS rule, i.e., $u_t = \sqrt{u_{1o}^2 + u_{2o}^2 + u_{3o}^2} = 231mm$. The pushover curves for the three force distributions are developed and illustrated in Figure 5.18. At the target displacement, $u_t = 231mm$, the peak values of floor displacements (as % of the building

height=36.6m) are shown in Table 5.11, and the peak amplitudes of story drift ratios (as % of story height=3.66m) are shown in Table 5.12, respectively; and Table 5.13 illustrates the peak values of plastic slip of the friction damped bracing calculated by subtracting the yield slip from the total slip for FEMA-273 pushover analysis.

5.7 COMPARISON OF RESPONSE BY IMPA, FEMA-273 WITH NL-RHA

The comparison of floor displacement ratios estimated by FEMA-273 pushover analysis with three force distributions, IMPA combined with 3 modes, and NL-RHA procedure is illustrated in Figure 5.19 and also summarized in Tables 5.11. The errors for the FEMA-273 uniform force distribution are between *10.14%* and *38.48%*, *-30.09%* to *10.14%* for ELF force distribution, and *–11.60%* to *10.14%* for SRSS force distribution. The errors of the floor displacement ratios by IMPA are between *-15.47 %* and *9.34 %.*, so that, the FEMA-273 pushover analysis with the SRSS force distribution and IMPA are acceptable for estimating the floor displacement for FDBF system.

Similarly, for the story drift ratios summarized in Table 5.12 and Figure 5.20, the errors for the FEMA-273 uniform force distribution are between *–34.66%* and *45.58%*, *-30.50%* and *16.32%* for ELF force distribution, and *–12.12%* to *69.21%* for SRSS force distribution. In contrast, the errors of the story drift ratios by IMPA are between *-14.51 %* and 32.90%, thus, IMPA can provide better results than FEMA-273 pushover analysis in estimating the story drifts of the FDBF systems.

For the plastic slip of the friction bracing shown in Table 5.13 and Figure 5.21, the errors for the FEMA-273 uniform force distribution are between *–100%* and *60.28%*, *-44.16%* and *21.71%* for ELF force distribution, and *–20.24%* and *232%* for SRSS force distribution. For IMPA, the errors of the plastic slip of the friction bracing are between *-34.47 %* and *39.32 %.*. Although they are quite poor, the results of IMPA are still more accurate than that determined by all the FEMA-273 pushover analysis procedures.

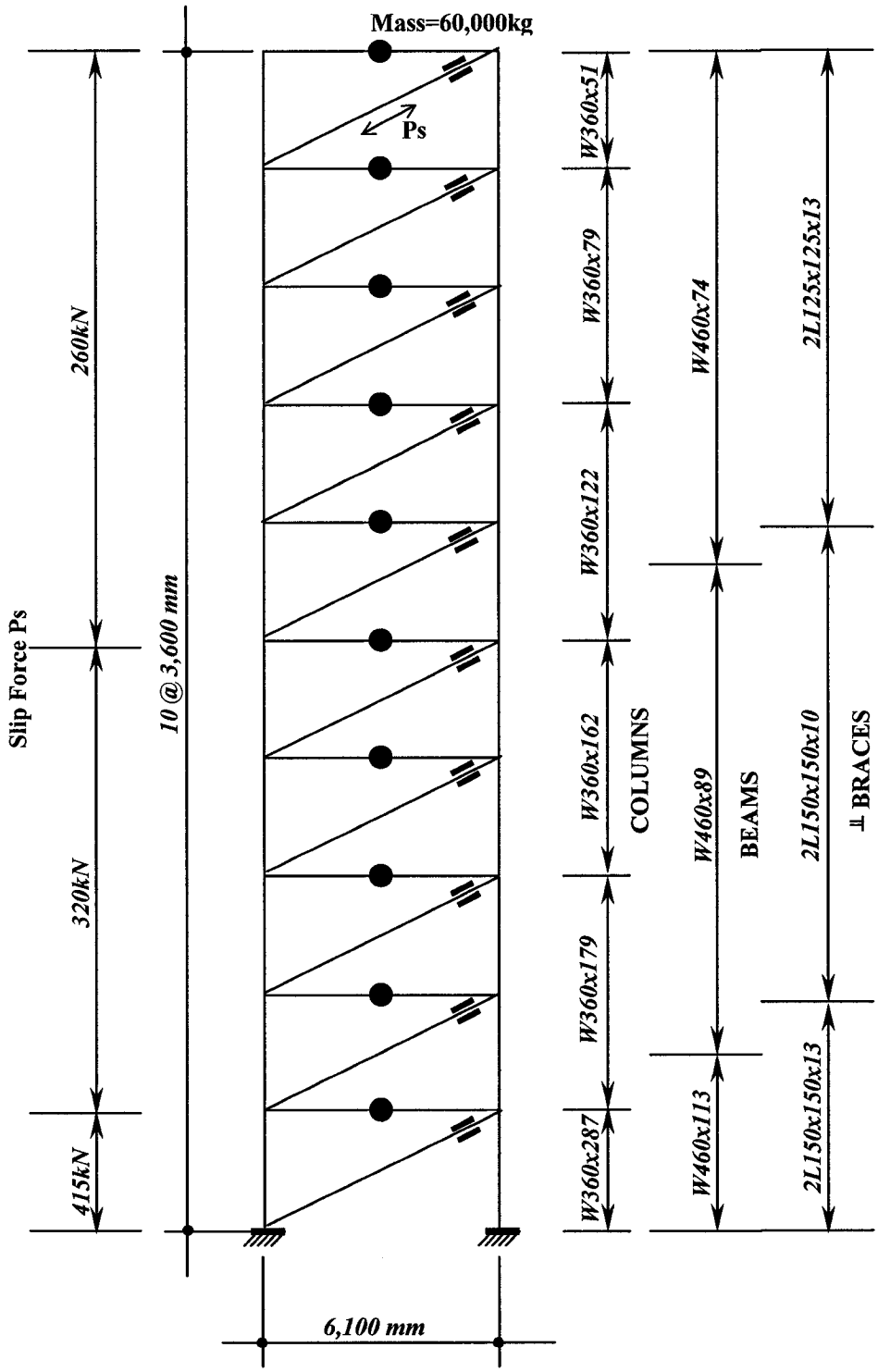

Figure 5.1. 1-Bay, 10-Story FDBF System

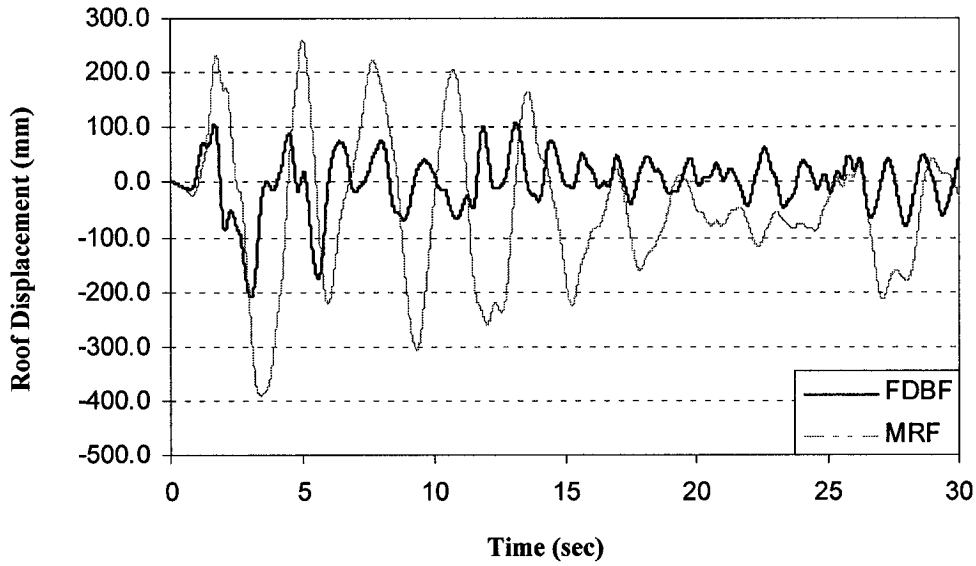

Figure 5.2. Comparison of Roof Displacement History Response of 10-Story FDBF with MRF to 1.5 El-Centro Ground Motion

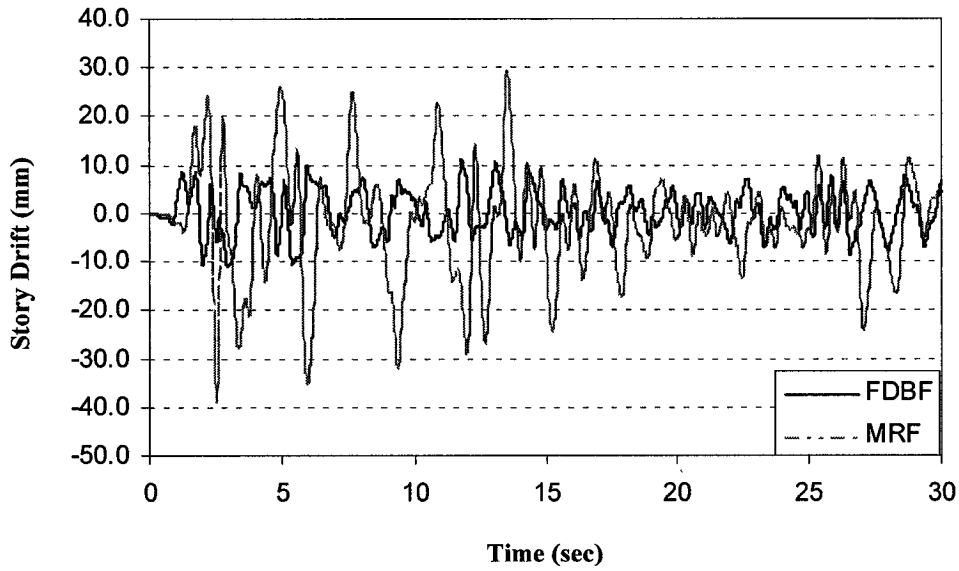

Figure 5.3. Comparison of Top Story Drift History Response of 10-Story FDBF with MRF System to 1.5 El-Centro Ground Motion

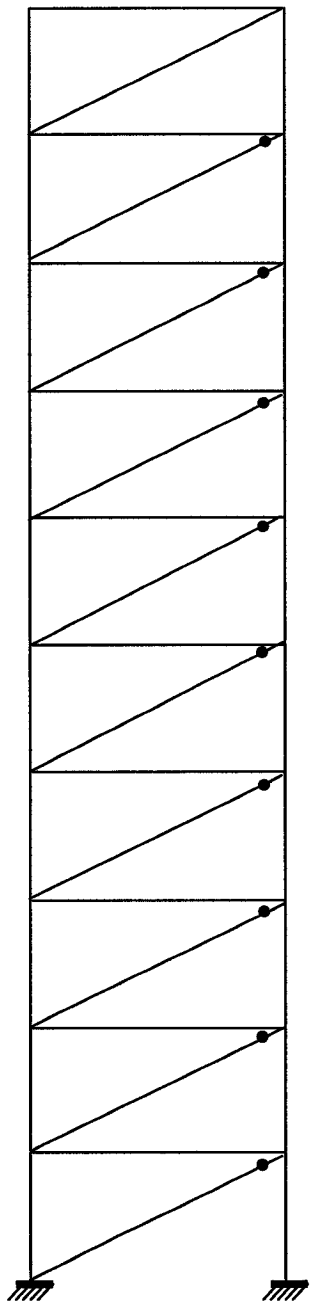

Table 5.1. Modal Properties for 10-story FDBF

Mode		1	2	3
Period, T_n (sec)		1.468	0.429	0.225
Frequency, ω_n (rad/sec)		4.281	14.636	27.960
Participation factor, Γ_n		1.436	0.621	0.317
Effective mass, M_n^* (k kg)		421.7	110.4	30.7
Mode shape at story levels (normalized)	10 (Roof)	1.000	1.000	1.000
	9	0.891	0.555	0.152
	8	0.774	0.062	-0.680
	7	0.653	-0.398	-1.054
	6	0.531	-0.745	-0.794
	5	0.411	-0.936	-0.076
	4	0.299	-0.950	0.670
	3	0.195	-0.801	1.087
	2	0.104	-0.524	0.971
	1	0.038	-0.226	0.480
	0 (Base)	0.000	0.000	0.000

Figure 5.4. Plastic Slip Location of Friction Braces for 10-story FDBF System to 1.5 El-Centro Ground Motion

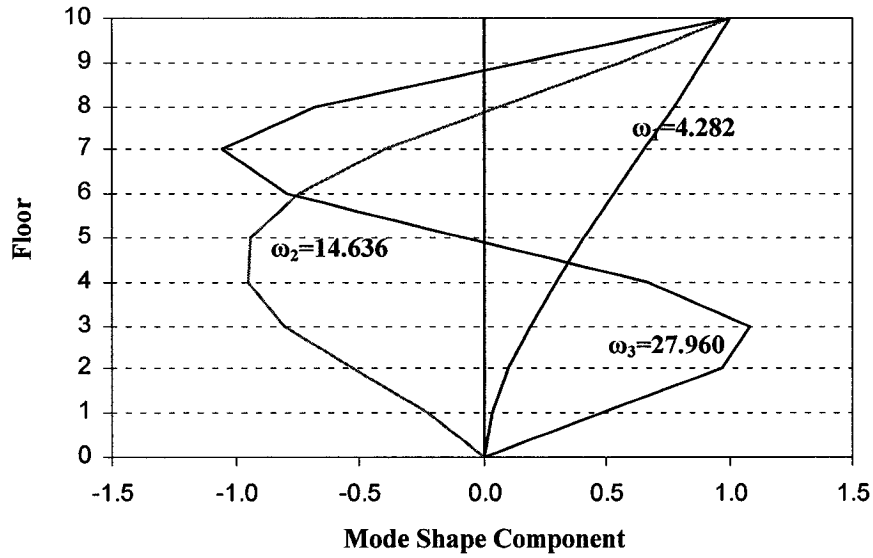

Figure 5.5. First three natural-vibration frequencies and modes of 10-story FDBF

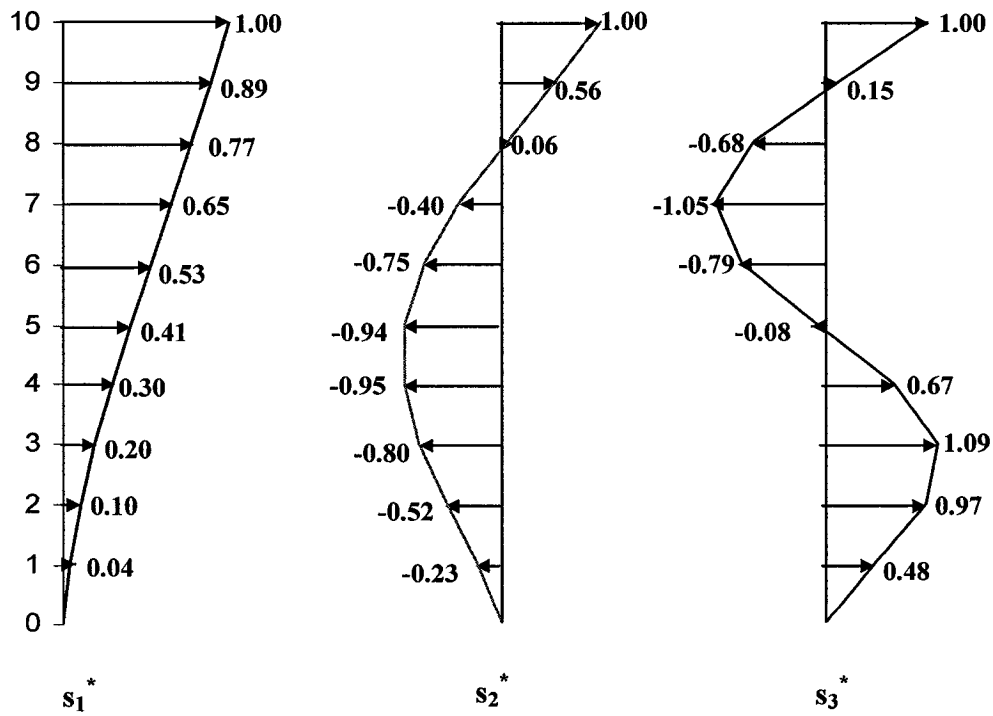

Figure 5.6. Lateral Force Distributions $\{s_n^*\} = [m] \cdot \{\phi_n\}$, n=1, 2, 3

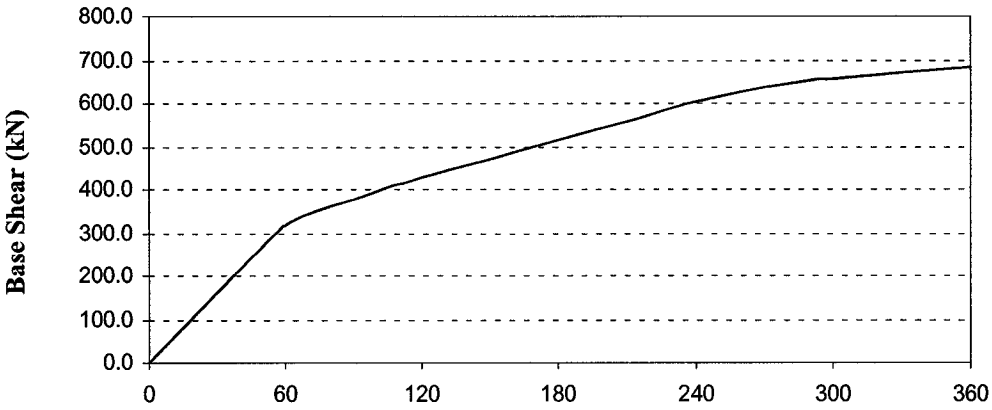

(a) Roof Displacement (mm)

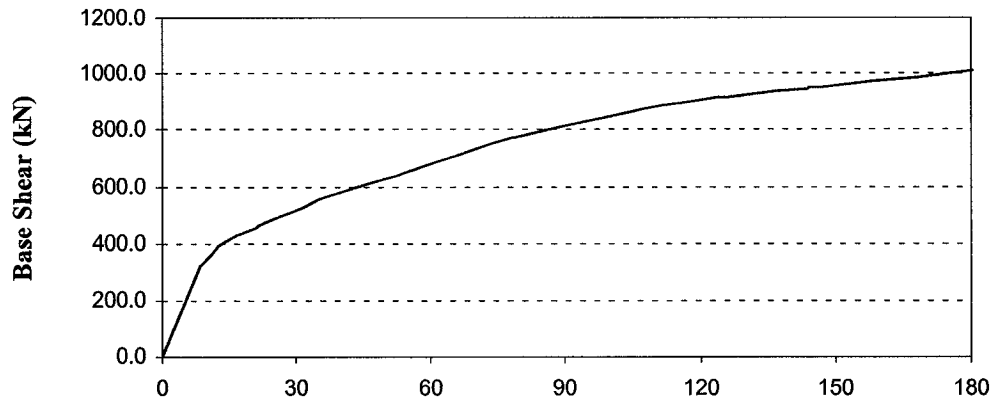

(b) Roof Displacement (mm)

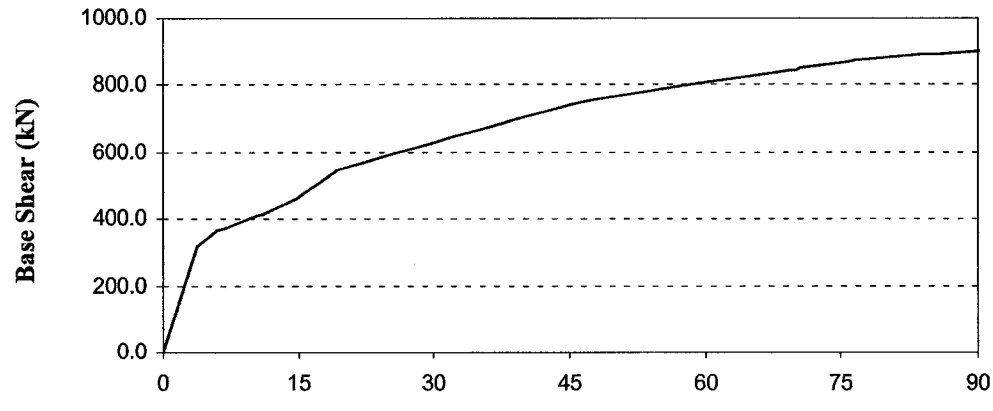

(c) Roof Displacement (mm)

Figure 5.7. Modal Pushover Capacity Curve for 10-story FDBF: (a) "Mode" 1, (b) "Mode" 2, (c) "Mode" 3

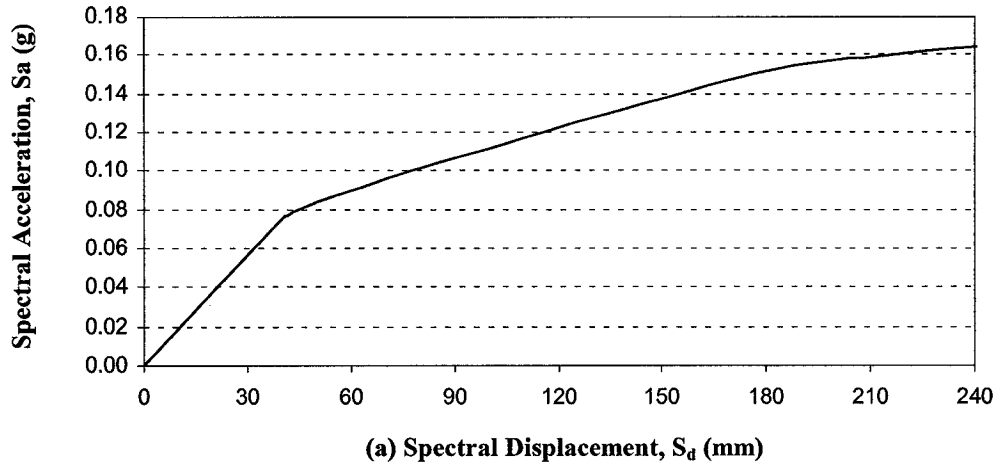

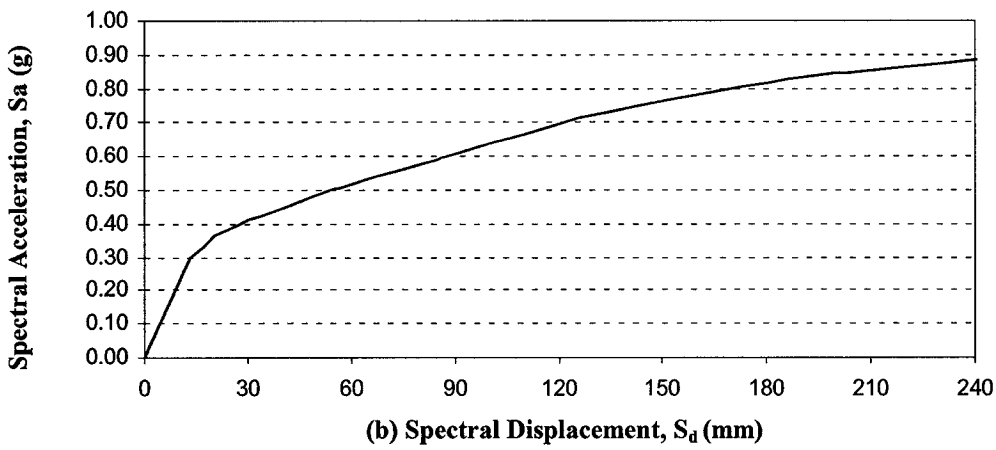

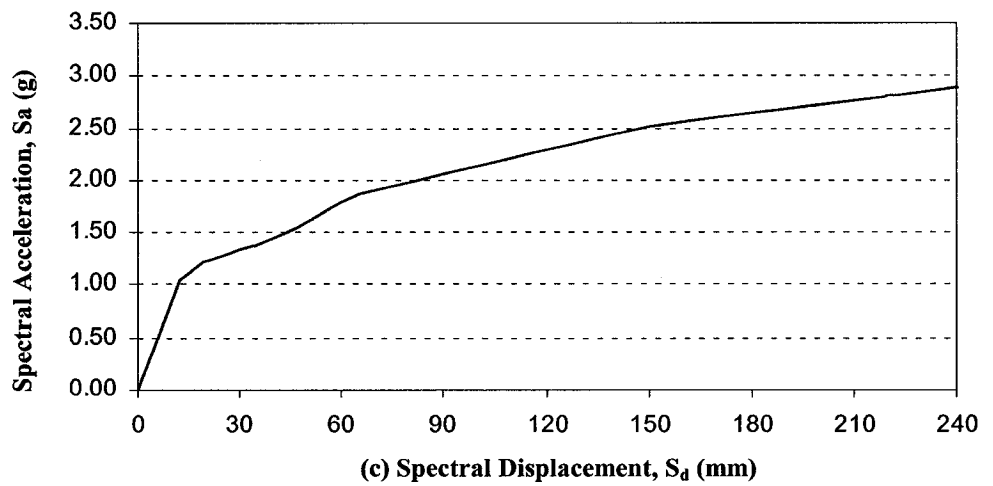

Figure 5.8. Capacity Spectrum Curves for 10-story FDBF: (a) "Mode" 1, (b) "Mode" 2, (c) "Mode" 3

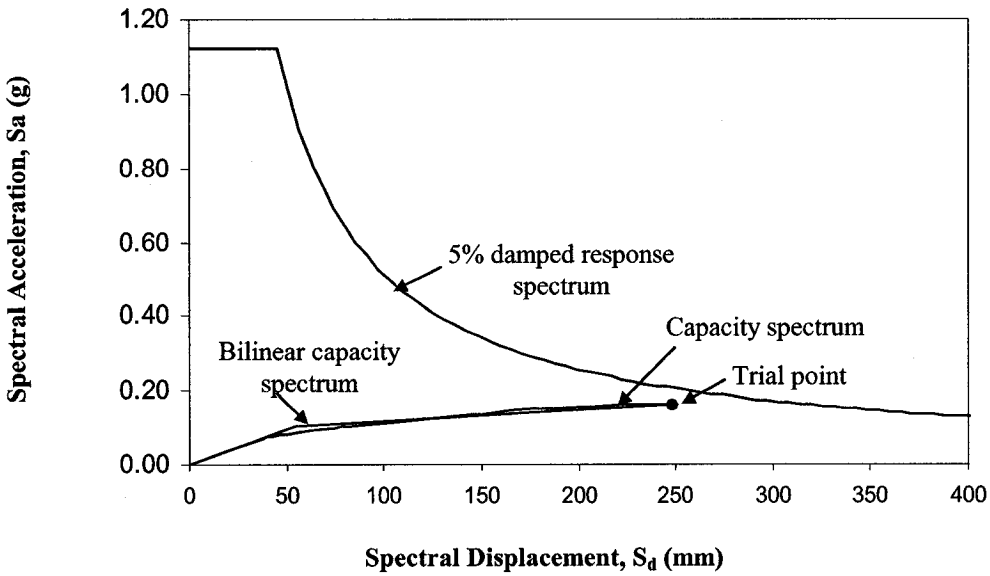

Figure 5.9. Capacity Spectrum Procedure A After Step 4 for FDBF Mode 1

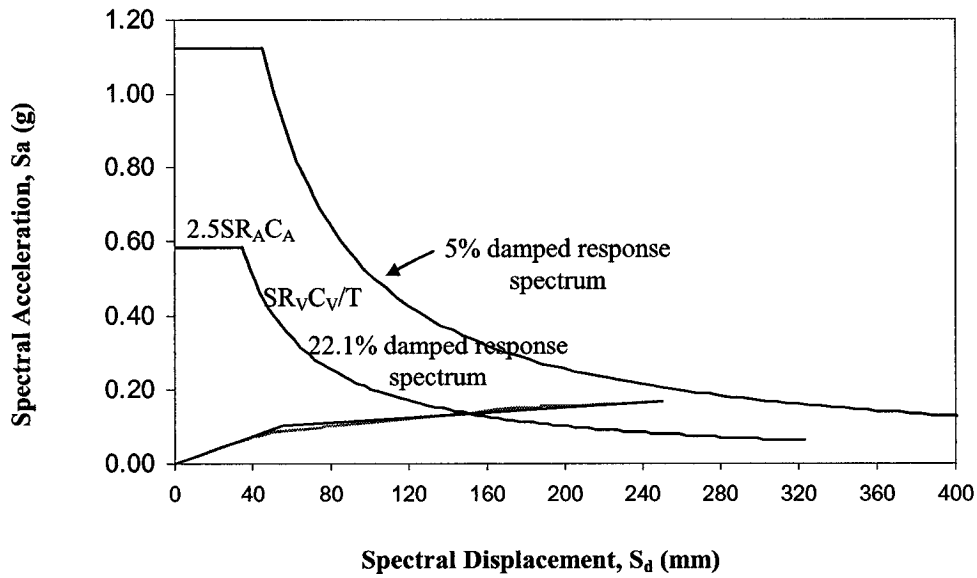

Figure 5.10. Capacity Spectrum Procedure A After Step 5 for FDBF Mode 1

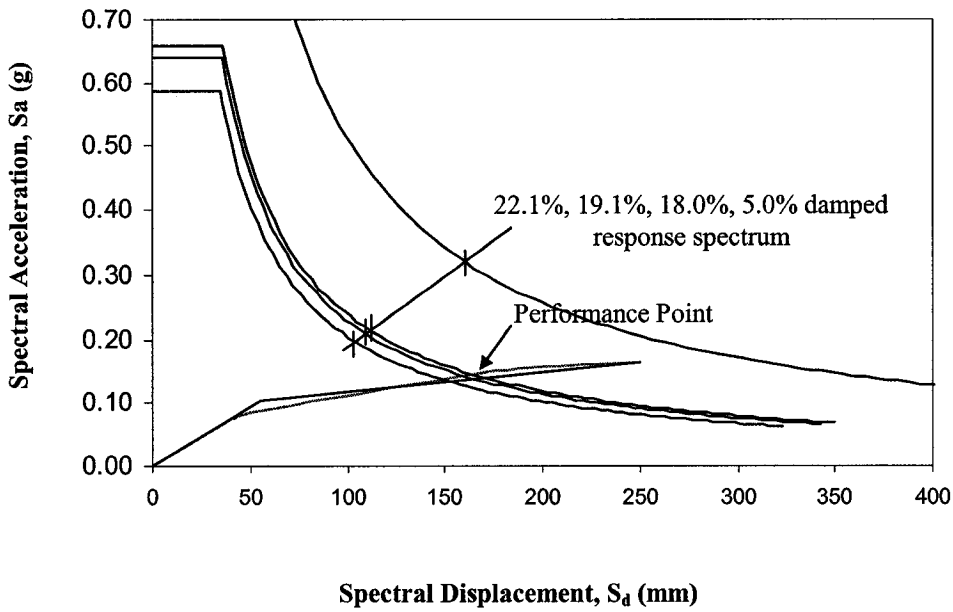

Figure 5.11. Capacity Spectrum Procedure A After Step 7 for FDBF Mode 1

Table 5.2. Trial for Demand Performance Point for Mode 1

Trial	a_y (g)	d_y (mm)	a_{pi} (g)	d_{pi} (mm)	Error (%)	$\hat{\zeta}_{eq}$ (%)	SR_A	SR_V	Ts
0						5.0	0.998	1.000	0.401
1	0.1025	54.9	0.1652	250.7		22.1	0.521	0.630	0.484
2	0.0820	43.9	0.1376	150.8	-39.8	18.0	0.587	0.682	0.465
3	0.0897	48.0	0.1445	165.0	9.4	19.1	0.568	0.667	0.470
Final			0.1421	160.0	-3.0				

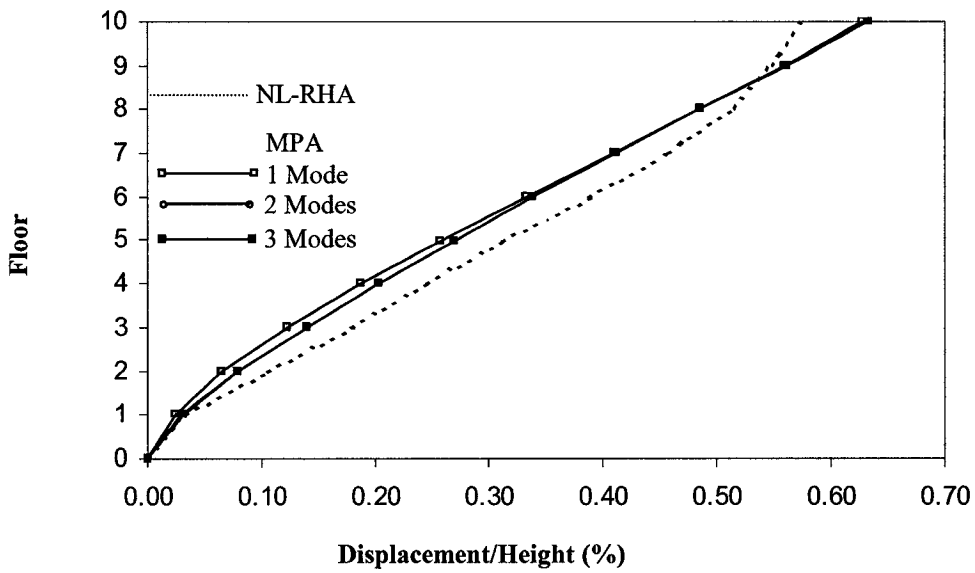

Figure 5.12. Comparison of Floor Displacement Ratios Determined by MPA and NL-RHA for FDBF

Table 5.3. Peak Values of Floor Displacement Ratios (as % of building height=36.6m) from MPA for 1.5x El Centro Ground Motion

Floor	Displacement/Height (%)							Error (%)		
	Modal Response			Combined (MPA)			NL--RHA			
	Mode #1	Mode #2	Mode #3	1 Mode	2 Modes	3 Modes		1 Mode	2 Modes	3 Modes
0	0.000	0.000	0.000	0.000	0.000	0.000	0.000	0.00	0.00	0.00
1	0.024	-0.019	0.006	0.024	0.031	0.031	0.034	-29.41	-9.97	-8.26
2	0.065	-0.044	0.012	0.065	0.078	0.079	0.107	-39.25	-26.64	-25.79
3	0.122	-0.068	0.014	0.122	0.140	0.140	0.180	-32.22	-22.40	-22.02
4	0.187	-0.081	0.009	0.187	0.204	0.204	0.248	-24.60	-17.83	-17.75
5	0.258	-0.080	-0.001	0.258	0.270	0.270	0.314	-17.83	-13.98	-13.97
6	0.333	-0.063	-0.010	0.333	0.339	0.339	0.390	-14.62	-13.10	-13.06
7	0.410	-0.034	-0.014	0.410	0.411	0.412	0.459	-10.68	-10.37	-10.32
8	0.486	0.006	-0.009	0.486	0.486	0.486	0.514	-5.45	-5.44	-5.42
9	0.559	0.047	0.002	0.559	0.561	0.561	0.547	2.19	2.55	2.56
10	0.628	0.085	0.013	0.628	0.634	0.634	0.575	9.22	10.21	10.24

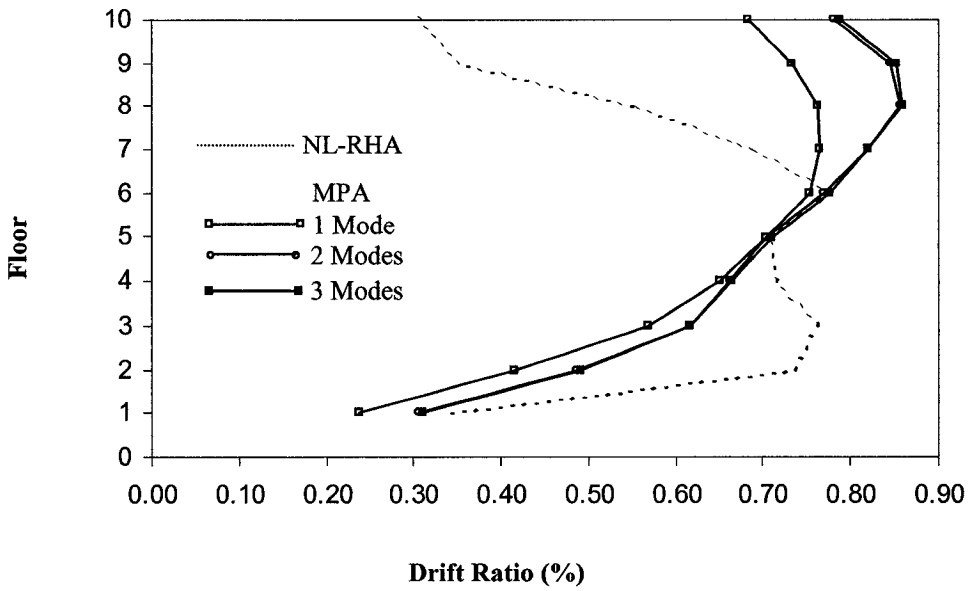

Figure 5.13. Comparison of Drift Ratios Determined by MPA and NL-RHA for FDBF

Table 5.4 Peak Values of Story Drift Ratios (as % of story height) from MPA for 1.5x El Centro Ground Motion

Floor	Drift Ratio (%)							Error (%)		
	Modal Response			Combined (MPA)			NL--RHA			
	Mode #1	Mode #2	Mode #3	1 Mode	2 Modes	3 Modes		1 Mode	2 Modes	3 Modes
1	0.237	-0.192	0.062	0.237	0.305	0.311	0.342	-30.70	-10.81	-8.99
2	0.416	-0.253	0.063	0.416	0.487	0.491	0.735	-43.40	-33.76	-33.20
3	0.569	-0.235	0.015	0.569	0.616	0.616	0.762	-25.33	-19.21	-19.19
4	0.651	-0.127	-0.054	0.651	0.663	0.665	0.716	-9.08	-7.36	-7.06
5	0.704	0.012	-0.096	0.704	0.704	0.711	0.708	-0.56	-0.55	0.37
6	0.753	0.162	-0.092	0.753	0.770	0.776	0.776	-2.96	-0.74	-0.04
7	0.765	0.295	-0.033	0.765	0.820	0.821	0.689	11.03	19.00	19.10
8	0.763	0.391	0.048	0.763	0.857	0.859	0.552	38.22	55.32	55.56
9	0.733	0.420	0.107	0.733	0.845	0.852	0.352	108.24	140.00	141.92
10	0.683	0.378	0.109	0.683	0.781	0.788	0.306	123.20	155.11	157.58

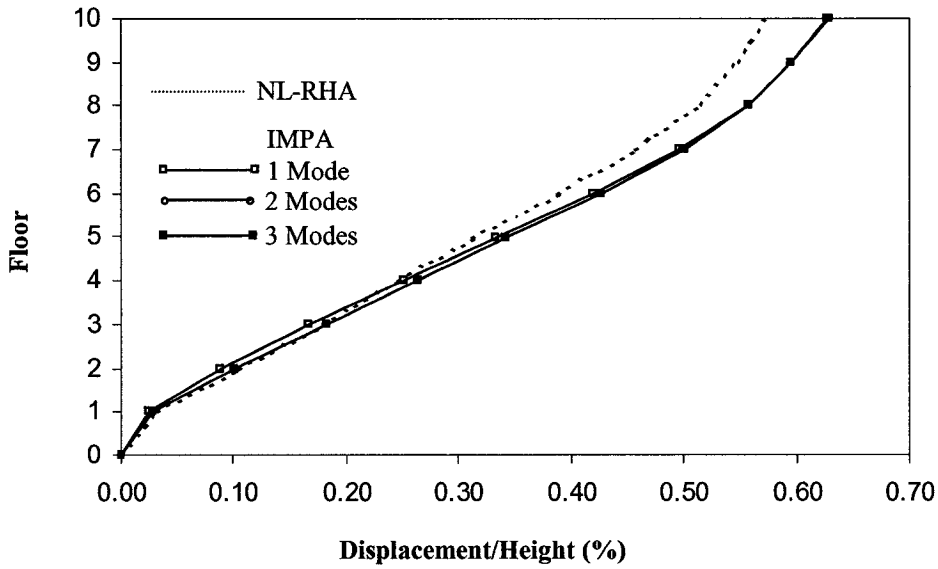

Figure 5.14. Comparison of Floor Displacement Ratios Determined by IMPA and NL-RHA for FDBF

Table 5.5. Peak Values of Floor Displacement Ratios (as % of building height=36.6m) from IMPA for 1.5x El Centro Ground Motion

Floor	Displacement/Height (%)							Error (%)		
	Modal Response			Combined (IMPA)			NL--RHA			
	Mode #1	Mode #2	Mode #3	1 Mode	2 Modes	3 Modes		1 Mode	2 Modes	3 Modes
0	0.000	0.000	0.000	0.000	0.000	0.000	0.000	0	0	0
1	0.024	0.015	-0.005	0.024	0.028	0.029	0.034	-29.41	-16.76	-15.47
2	0.088	0.049	-0.011	0.088	0.101	0.101	0.107	-17.76	-5.87	-5.31
3	0.167	0.074	-0.012	0.167	0.183	0.183	0.180	-7.22	1.48	1.70
4	0.251	0.081	-0.007	0.251	0.264	0.264	0.248	1.21	6.35	6.39
5	0.333	0.080	0.001	0.333	0.342	0.342	0.314	6.05	9.07	9.07
6	0.420	0.073	0.011	0.420	0.426	0.426	0.390	7.69	9.31	9.34
7	0.497	0.060	0.014	0.497	0.501	0.501	0.459	8.28	9.07	9.11
8	0.558	0.033	0.010	0.558	0.559	0.559	0.514	8.56	8.75	8.77
9	0.595	-0.013	-0.002	0.595	0.595	0.595	0.547	8.78	8.80	8.80
10	0.628	-0.023	-0.010	0.628	0.628	0.629	0.575	9.22	9.29	9.30

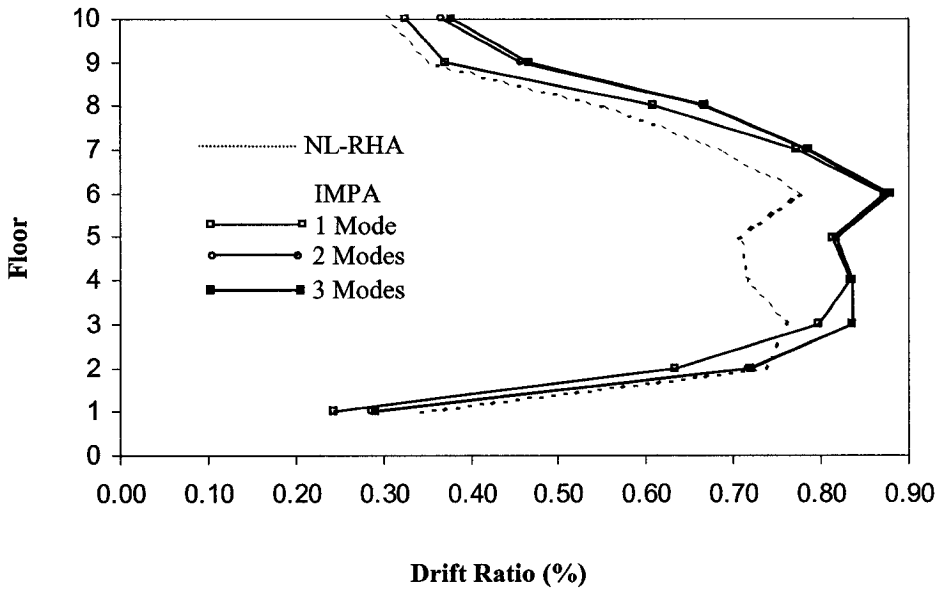

Figure 5.15. Comparison of Drift Ratios Determined by IMPA and NL-RHA for FDBF

Table 5.6. Peak Values of Story Drift Ratios (as % of story height) from IMPA for 1.5x El Centro Ground Motion

Floor	Drift Ratio (%)							Error (%)		
	Modal Response			Combined (IMPA)			NL--RHA			
	Mode #1	Mode #2	Mode #3	1 Mode	2 Modes	3 Modes		1 Mode	2 Modes	3 Modes
1	0.243	0.153	-0.055	0.243	0.287	0.292	0.342	-28.95	-16.04	-14.51
2	0.634	0.336	-0.055	0.634	0.718	0.720	0.735	-13.74	-2.38	-2.09
3	0.798	0.251	-0.014	0.798	0.837	0.837	0.762	4.72	9.78	9.80
4	0.833	0.063	0.046	0.833	0.835	0.837	0.716	16.34	16.67	16.85
5	0.814	-0.005	0.085	0.814	0.814	0.818	0.708	14.97	14.97	15.60
6	0.872	0.071	0.098	0.872	0.875	0.880	0.776	12.37	12.74	13.45
7	0.773	-0.134	0.030	0.773	0.785	0.785	0.689	12.19	13.86	13.95
8	0.609	-0.268	-0.041	0.609	0.665	0.667	0.552	10.33	20.54	20.77
9	0.372	-0.268	-0.093	0.372	0.458	0.468	0.352	5.68	30.25	32.90
10	0.325	-0.169	-0.096	0.325	0.366	0.379	0.306	6.21	19.71	23.75

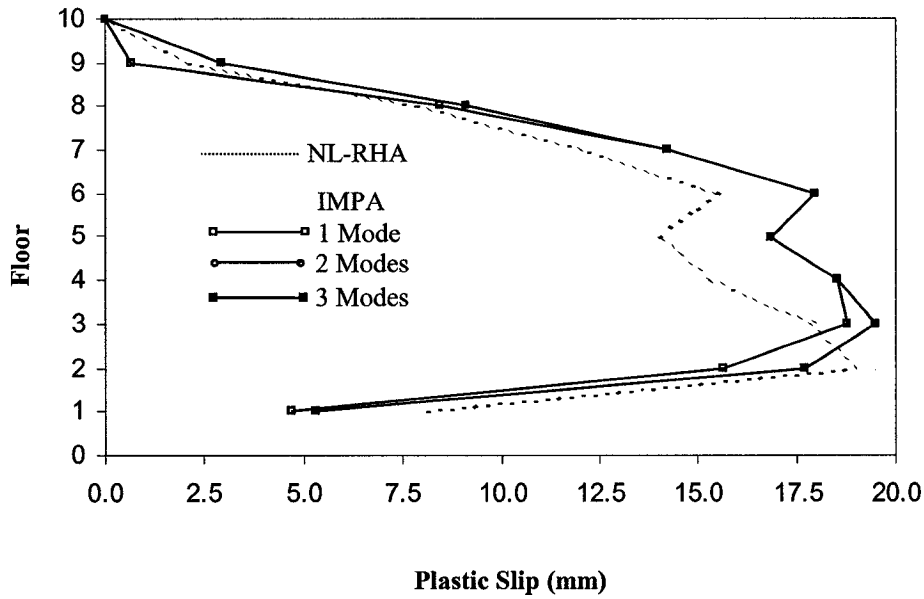

Figure 5.16. Comparison of Plastic Slips of Braces Determined by IMPA and NL-RHA for FDBF

Table 5.7. Peak Values of Plastic Slips of Braces Determined by IMPA for 1.5x El Centro Ground Motion

Floor	Plastic Slip (mm)							Error (%)		
	Modal Response			Combined (IMPA)			NL--RHA			
	Mode #1	Mode #2	Mode #3	1 Mode	2 Modes	3 Modes		1 Mode	2 Modes	3 Modes
1	4.7	2.4	0.0	4.7	5.3	5.3	8.1	-41.82	-34.47	-34.47
2	15.6	8.3	0.0	15.6	17.7	17.7	19.0	-17.67	-6.85	-6.85
3	18.8	5.3	0.0	18.8	19.5	19.5	17.9	4.86	8.94	8.94
4	18.5	0.0	0.0	18.5	18.5	18.5	15.3	21.07	21.07	21.07
5	16.8	0.0	0.0	16.8	16.8	16.8	14.1	19.47	19.47	19.47
6	18.0	0.0	0.7	18.0	18.0	18.0	15.5	15.97	15.97	16.05
7	14.2	0.0	0.0	14.2	14.2	14.2	12.1	17.38	17.38	17.38
8	8.5	-3.3	0.0	8.5	9.1	9.1	7.9	7.32	15.37	15.37
9	0.7	-2.9	0.0	0.7	2.9	2.9	2.1	-68.86	39.32	39.32
10	0.0	0.0	0.0	0.0	0.0	0.0	0.0	0.00	0.00	0.00

Table 5.8. FEMA-273 Uniform Force Distribution

Floor, j	Mass, m_j (kg)	$s_j^* = \frac{m_j}{\sum_{i=1}^{n} m_i}$
1	60,000	0.100
2	60,000	0.100
3	60,000	0.100
4	60,000	0.100
5	60,000	0.100
6	60,000	0.100
7	60,000	0.100
8	60,000	0.100
9	60,000	0.100
10	60,000	0.100

Table 5.9. FEMA-273 ELF Distribution

Floor, j	Mass, m_j (kg)	h_j (m)	$m_j h_j^k$ (kg-m^k)	$s_j^* = \frac{m_j h_j^k}{\sum_{i=1}^{n} m_i h_i^k}$
1	60,000	3.66	411,488	0.007
2	60,000	7.32	1,151,027	0.020
3	60,000	10.98	2,100,899	0.037
4	60,000	14.64	3,219,691	0.057
5	60,000	18.30	4,483,619	0.079
6	60,000	21.96	5,876,702	0.103
7	60,000	25.62	7,387,248	0.130
8	60,000	29.28	9,006,224	0.158
9	60,000	32.94	10,726,377	0.188
10	60,000	36.60	12,541,722	0.220

* $k = 1.484$

Table 5.10. FEMA-273 SRSS Distribution

	Lateral Forces			Story Shears				Lateral Forces	
Floor, j	f_{j1} (kN)	f_{j2} (kN)	f_{j3} (kN)	V_{j1} (kN)	V_{j2} (kN)	V_{j3} (kN)	V_j (kN)	f_j (kN)	$s_j^* = \frac{f_j}{\sum_{i=1}^{n} f_i}$
1	9.56	90.15	98.42	1236.84	1182.32	360.05	1748.51	84.93	0.049
2	26.31	208.98	199.01	1227.28	1092.16	261.63	1663.57	171.51	0.098
3	49.23	319.56	222.68	1200.97	883.18	62.62	1492.07	199.86	0.114
4	75.45	379.31	137.22	1151.74	563.62	-160.06	1292.21	160.50	0.092
5	103.81	373.50	-15.60	1076.29	184.31	-297.28	1131.70	101.72	0.058
6	134.11	297.21	-162.48	972.48	-189.19	-281.68	1029.98	53.42	0.031
7	164.91	158.88	-215.90	838.38	-486.41	-119.19	976.56	38.85	0.022
8	195.64	-24.58	-139.32	673.46	-645.28	96.71	937.71	119.60	0.068
9	225.16	-221.62	31.12	477.82	-620.71	236.03	818.11	303.23	0.173
10	252.66	-399.09	204.91	252.66	-399.09	204.91	514.88	514.88	0.294

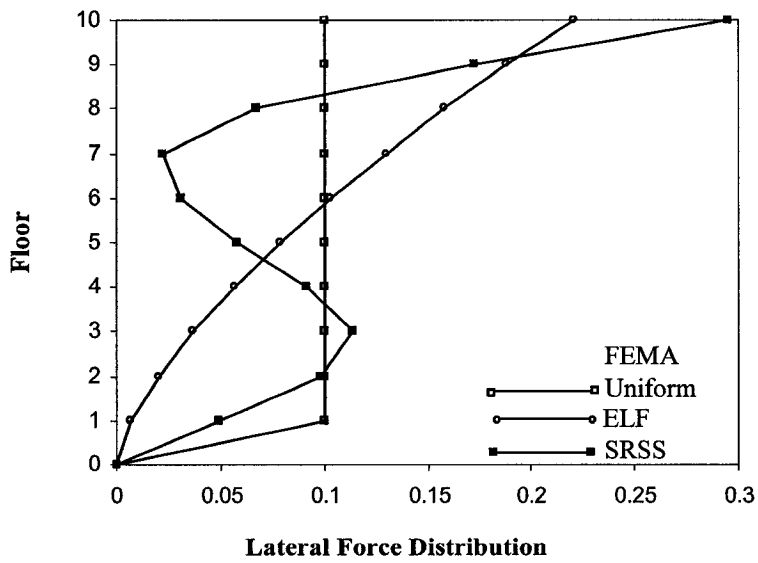

Figure 5.17. FEMA-273 Lateral Force Distributions for FDBF System

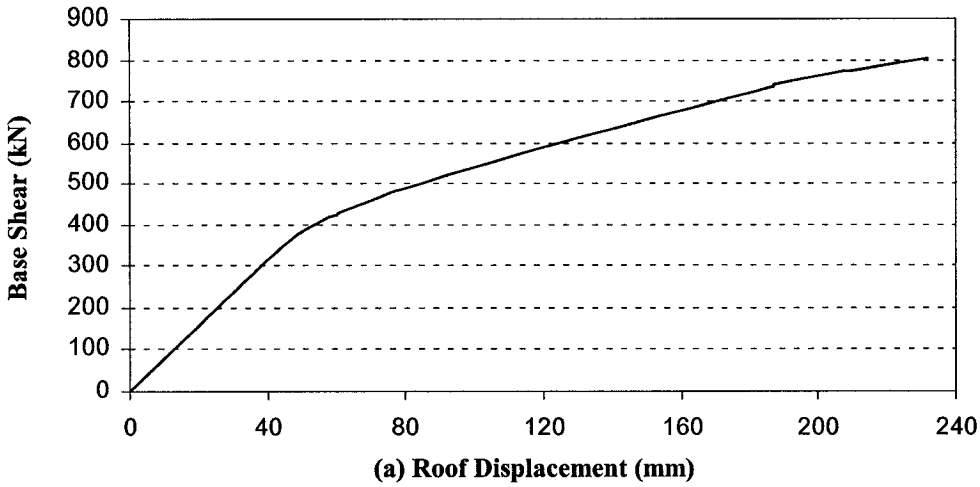

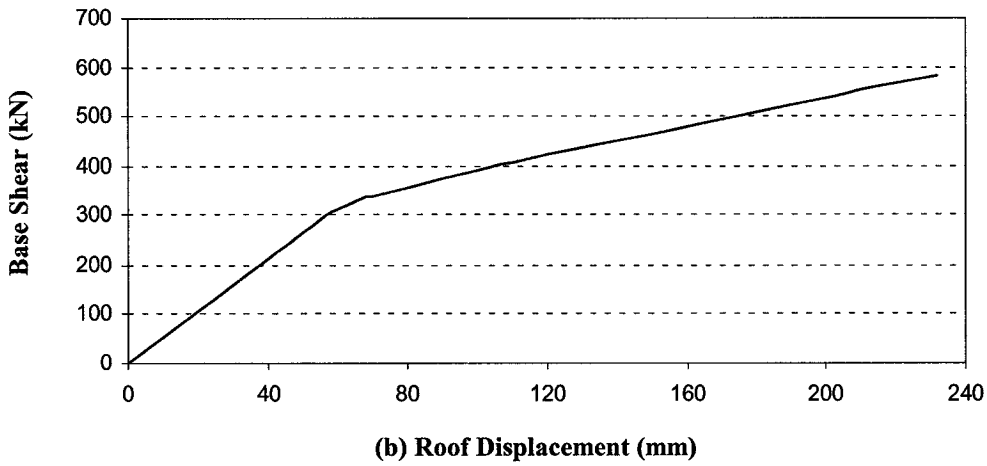

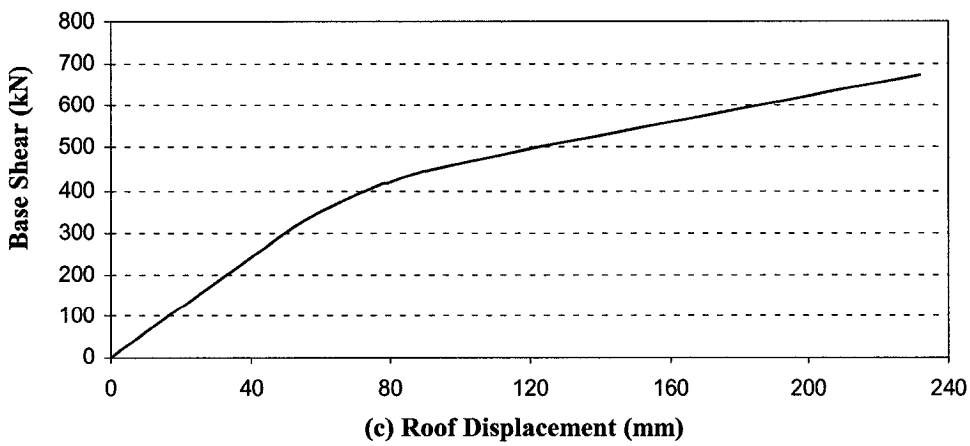

Figure 5.18. FEMA-273 Pushover Curves for FDBF: (a), Uniform Force, (b), ELF, (c), SRSS Force Distribution

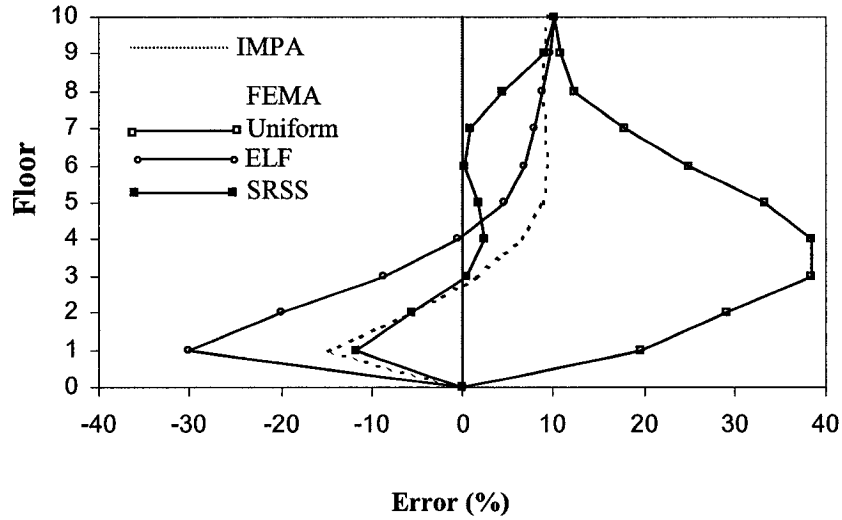

Figure 5.19. Errors in Floor Displacement Ratios Estimated by FEMA-273 and IMPA for FDBF

Table 5.11. Peak Values of Floor Displacement Ratios (as % of building height=36.60 m) from FEMA and IMPA for 1.5 El-Centro Ground Motion

Floor	Displacement/Height (%)					Error (%)			
	FEMA			IMPA 3 modes	NL-RHA	FEMA			IMPA 3 modes
	Uniform	ELF	SRSS			Uniform	ELF	SRSS	
0	0.000	0.000	0.000	0.000	0.000	0.00	0.00	0.00	0.00
1	0.041	0.024	0.030	0.029	0.034	19.74	-30.09	-11.60	-15.47
2	0.138	0.086	0.101	0.101	0.107	29.21	-19.82	-5.52	-5.31
3	0.249	0.164	0.181	0.183	0.180	38.43	-8.62	0.49	1.70
4	0.343	0.247	0.254	0.264	0.248	38.48	-0.41	2.35	6.39
5	0.419	0.328	0.319	0.342	0.314	33.31	4.59	1.72	9.07
6	0.488	0.416	0.391	0.426	0.390	25.05	6.77	0.25	9.34
7	0.541	0.496	0.463	0.501	0.459	17.86	7.98	0.90	9.11
8	0.577	0.560	0.537	0.559	0.514	12.27	8.92	4.40	8.77
9	0.606	0.600	0.596	0.595	0.547	10.79	9.69	8.99	8.80
10	0.633	0.633	0.633	0.629	0.575	10.14	10.14	10.14	9.30

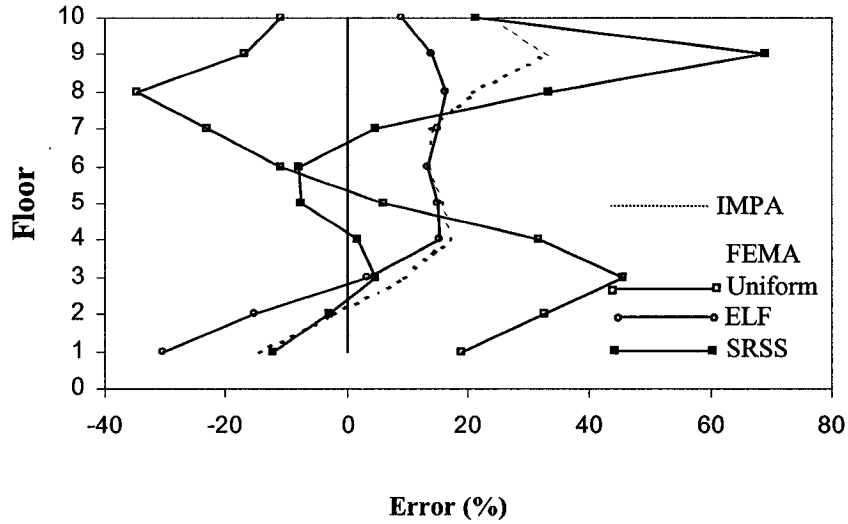

Figure 5.20. Errors in Story Drift Ratios Estimated by FEMA-273 and IMPA for FDBF

Table 5.12. Peak Values of Story Drifts Ratios (as % of story height) from FEMA and IMPA for 1.5 El-Centro Ground Motion

Floor	Drift Ratio (%)					Error (%)			
	FEMA			IMPA 3 modes	NL-RHA	FEMA			IMPA 3 modes
	Uniform	ELF	SRSS			Uniform	ELF	SRSS	
1	0.407	0.238	0.301	0.292	0.342	19.04	-30.50	-12.12	-14.51
2	0.975	0.623	0.713	0.720	0.735	32.71	-15.24	-2.98	-2.09
3	1.109	0.787	0.798	0.837	0.762	45.58	3.27	4.70	9.80
4	0.943	0.825	0.730	0.837	0.716	31.65	15.24	1.89	16.85
5	0.751	0.814	0.656	0.818	0.708	6.13	15.00	-7.38	15.60
6	0.691	0.880	0.716	0.880	0.776	-10.92	13.37	-7.75	13.45
7	0.530	0.792	0.721	0.785	0.689	-23.07	15.00	4.69	13.95
8	0.361	0.642	0.735	0.667	0.552	-34.66	16.32	33.15	20.77
9	0.292	0.402	0.596	0.468	0.352	-16.95	14.10	69.21	32.90
10	0.273	0.333	0.372	0.379	0.306	-10.71	8.93	21.43	23.75

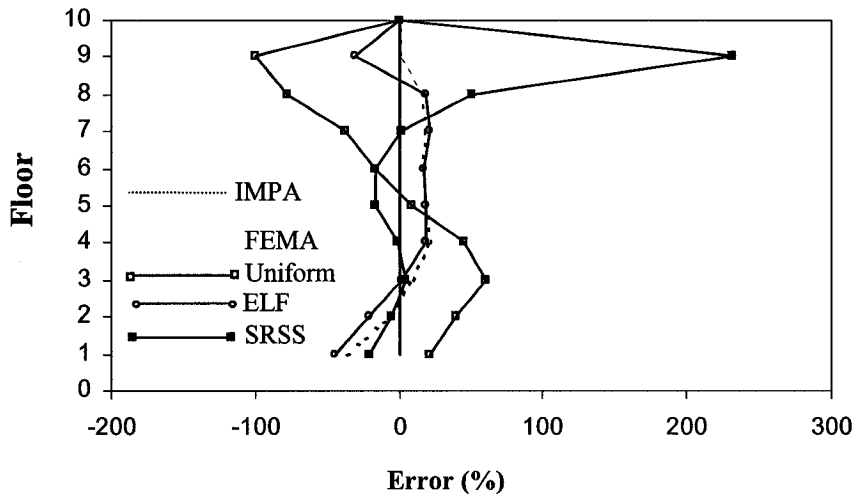

Figure 5.21. Errors in Plastic Slips of Braces Determined by FEMA-273 and IMPA to 1.5 El-Centro Ground Motion for FDBF

Table 5.13. Peak Values of Plastic Slips of Braces Determined by FEMA and IMPA for 1.5 El-Centro Ground Motion

Floor	Plastic Slip (mm)					Error (%)			
	FEMA			IMPA 3 modes	NL-RHA	FEMA			IMPA 3 modes
	Uniform	ELF	SRSS			Uniform	ELF	SRSS	
1	9.8	4.5	6.5	5.3	8.1	21.09	-44.16	-20.24	-34.47
2	26.4	15.2	18.0	17.7	19.0	39.11	-19.77	-5.01	-6.85
3	28.7	18.4	18.7	19.5	17.9	60.28	2.55	4.44	8.94
4	22.3	18.2	15.2	18.5	15.3	45.71	19.13	-0.38	21.07
5	15.4	16.8	11.8	16.8	14.1	9.18	18.80	-16.36	19.47
6	13.1	18.2	13.0	18.0	15.5	-15.61	17.25	-16.11	16.05
7	7.6	14.7	12.4	14.2	12.1	-37.60	21.71	2.20	17.38
8	1.8	9.3	11.9	9.1	7.9	-76.99	18.25	51.04	15.37
9	0.0	1.5	7.0	2.9	2.1	-100.00	-29.94	232.19	39.32
10	0.0	0.0	0.0	0.0	0.0	0.00	0.00	0.00	0.00

CHAPTER 6

CONCLUSIONS

6.1 CONCLUSIONS

Focusing on case studies, this investigation was aimed at applying the Modal Pushover Analysis (MPA) procedure for determining the performance evaluation of Friction Damped Braced Frame (FDBF) Systems and checking the accuracy by comparing MPA with Nonlinear Response History Analysis (NL-RHA) and FEMA-273 Pushover Analysis for FDBF systems. For the limitations posed by the assumption of MPA procedure, an Improvement Modal Pushover Analysis procedure (IMPA) was introduced and developed to provide better estimate of story drifts than MPA procedure.

In Chapter 3, the basic concepts of single-degree-of-freedom (SDF) system were introduced because, according to MPA procedure, all the multi-degree-of-freedom (MDF) systems would finally transfer to the equivalent SDF system. The north-south component of El Centro (1940) ground excitation was used for the analysis for all structures in this research. An approach to optimize the slip load and stiffness of the brace for the one-story FDBF was presented. For the selected one-story FDBF system, the MPA procedure was implemented and shown to provide good estimation for the seismic response.

In Chapter 4, the theory of MPA procedure for multi-story structures was presented and implemented in detail for a selected multi-story MRF system. In particularly in this

investigation, the peak value of the roof displacement for pushover analysis was estimated by the capacity spectrum method (CSM) which is described in detail in ATC-40 [ATC, 1996] because it is the most direct application of the concepts and it is not necessary for any structural analysis software to be used. Thus, the issue to determine the peak value of the deformation of the equivalent SDF system in MPA is changed to be the problem to develop the demand performance point for the system for given earthquake ground motion in ATC-40, i.e., the peak value of the deformation is equal to the spectral displacement at the demand performance point, $D_{no} = d_{np}$.

In Chapter 5, a multi-story FDBF system was optimized for the maximum amount of energy dissipated by the braces to protect the main elements of the structures from yielding. The system was also analyzed by MPA, FEMA-273 and NL-RHA methods. In order to obtain more accurate prediction of seismic performance of the FDBF system, an improved modal pushover analysis (IMPA) procedure was proposed in this chapter.

The research has led to the following conclusions which are based on only El-Centro ground motion:

1. Comparing the time history responses of the one-story FDBF with MRF, the peak value of the roof displacement of FDBF is just only 32% of that of MRF. It is obvious that the friction damped brace in the FDBF is effective in controlling the deformation of the system.
2. Because the beam and the columns of the selected one-story MRF were designed to yield simultaneously, the pushover curve of the system is exactly the bilinear curve,

so that the roof displacement of the system determined by MPA is almost the same as that computed by NL-RHA procedure.

3. For the one-story FDBF with fiction damping, the pushover curve is changed to be a tri-linear curve, the peak value of roof displacements estimated by MPA is 11.0% more than that by NL-RHA procedure, which is acceptable.
4. Similarly for the multi-story structures, the roof displacement of the 10-story FDBF is only about *54%* of that of MRF system. The top story drift of FDBF system is only about *33%* of that of MRF system. It is noted that there are no hinges formed in the beams and columns, the main elements of the system. It is obvious that the multi-story FDBF system has better seismic performance than the MRF system, in terms of the roof displacements, story drifts and plastic hinges.
5. Comparing the seismic response of the 10-story MRF determined by MPA with NL-RHA procedure, the errors of floor displacements are between *-14.98%* and *13.28%*, the errors of story drifts are between *-23.14%* and *12.29%*, and the errors of plastic hinge rotations are between -100% and 0.0%. It is demonstrated for a moment resisting frame (MRF), the MPA procedure is acceptable in estimating floor displacements, story drifts and most locations of the plastic hinges for the structure, but it cannot provide enough accuracy for estimating the hinge plastic rotations.
6. The seismic performances for the MRF system estimated by FEMA-273 pushover analysis with three force distributions, MPA combined with 3 modes, and NL-RHA procedure are compared in Figures and Tables. The peak errors of the displacements determined by the FEMA-273 three force distributions to NL-RHA procedure are *26.20%, -36.27%* and *–27.46%*, all of them poorer than that by MPA procedure of -

14.98%; the peak errors of the story drifts is *–64.34%, -46.09%* and *–29.05%*, all of them poorer than that by MPA procedure of *-23.14%*; and the peak error of the plastic hinge rotations for all FEMA-273 three force distributions is *100%*, the same as by MPA procedure of *100%*. It is evident that for a multi-story MRF, the MPA is more accurate than FEMA-273 pushover analysis in estimating floor displacements, story drifts and hinge locations, but both of them are not accurate enough for estimating the hinge plastic rotations.

7. Comparing the seismic response of the 10-story FDBF determined by MPA with NL-RHA procedure, the errors of floor displacements for the combined 3 modes are between *-25.79%* and *10.24%*, but the errors of story drifts are between *-33.20 %* and *157.58 %*. It is concluded that for a FDBF system, the MPA procedure is probably acceptable in estimating floor displacements, but for the story drifts of the structure, the accuracy of the MPA is too poor to be acceptable.
8. As an improved modal pushover analysis procedure, the IMPA can provide better estimates than MPA for determining the seismic performance of the FDBF system. The differences of the roof displacement for the combined 3 modes between IMPA and NL-RHA are between *-15.47%* and *9.34%*, the differences of the story drifts of that two procedures are between *-14.51%* and *32.90%*, and the differences of the plastic slips of friction bracing determined by IMPA and NL-RHA are between -34.47% and 39.32%.
9. The comparisons of response of the FDBF system by IMPA and FEMA-273 with NL-RHA are illustrated in Figures and Tables in Chapter 5. The peak difference of floor displacement ratios estimated by the FEMA-273 three force distributions from

NL-RHA is *38.48%, -30.09%* and *–11.60%*, two of them poorer than that for IMPA procedure of *-15.47%*. Thus, both the FEMA-273 pushover analysis with the SRSS force distribution and IMPA are acceptable for estimating the floor displacements for FDBF systems.

10. Compared to the NL-RHA, the peak error of story drift ratios of the FDBF for the FEMA-273 three force distributions is *45.58%, -30.50%* and *69.21%*, two of them larger than that for IMPA procedure of *32.90%*. It is suggested to use the FEMA-273 pushover analysis with the ELF force distribution and the IMPA procedure for estimating the story drifts for FDBF systems.
11. The comparison of peak values of plastic slips of friction damped bracing determined by FEMA-273 pushover analysis with three force distributions, IMPA combined with 3 modes, and NL-RHA procedure shows that IMPA procedure can provide better estimates than the FEMA-273 pushover analysis procedure, because the peak errors of plastic slips for all the FEMA-273 three force distributions are poorer than that for IMPA procedure.

6.2 RECOMMENDATIONS FOR FUTURE WORK

From the previous discussions, pushover analysis procedures consist of three parts: lateral force distributions, target displacement and pushover results. Even for IMPA, the results for FDBFs are not so satisfied. So that, there is still much work to do in the future, such as to define a more appropriate static lateral force distribution, to find a better way to calculate the target displacement and finally to get the more rigorous seismic performance of FDBF systems.

REFERENCES

1. Adam, C. and Ziegler, F. (1996), 'Dynamic response of substructures in friction damped braced frames', *Proc. 11th World Conference on Earthquake Engineering*, Acapulco, Mexico, June 23 - 28, 1996, CD-Rom, Paper 256: 8p.
2. Allahabadi, R. and Powell, G.H. (1988), 'DRAIN-2DX user guide', *Report No.UCB/EERC-88/06,* Earthquake Engineering Research Center, University of California, Berkeley, Calif.
3. Applied Technology Council (1996), 'ATC-40, Seismic Evaluation and Retrofit of Concrete Buildings', Vol. 1, California Seismic Safety Commission, etc.
4. Baktash, P. (1989), 'Friction damped braced frames', Ph. D. Thesis, Concordia University, Montreal
5. Building Seismic Safety Council (1997), 'NEHRP Guidelines for the Seismic Rehabilitation of Buildings, FEMA-273', Federal Emergency Management Agency, Washington, D.C.
6. Chopra, A. K. and Goel, R. K. (1999), 'Capacity-demand-diagram methods for estimating seismic deformation of inelastic structures: SDF systems', *PEER 1999/02,* Pacific Earthquake Engineering Research Center, Berkeley, California, USA
7. Chopra, A. K. and Goel, R. K (1999), 'Capacity-demand-diagram methods based on inelastic design spectrum', Earthquake spectra, Earthquake Engineering Research Institute, 15(4), 637-656.

8. Chopra, A. K. (2001). 'Dynamics of Structures: Theory and Applications to Earthquake Engineering', Prentice Hall: New Jersey
9. Chopra, A. K. and Goel, R. K. (2001), 'A modal pushover analysis procedure to estimate seismic demand for buildings: theory and preliminary evaluation', *PEER, 2001/03*, Pacific Earthquake Engineering Research Center, Berkeley, California, USA
10. Dowdell, D. J. and Cherry, S. (1996), 'On Passive and Semi-active Friction Damping for Seismic Response Control of Structures', *Proc. 11th World Conference on Earthquake Engineering*, Acapulco, Mexico, June 23 - 28, 1996, CD-Rom, Paper 957: 8p.
11. Kelly, T. and Chambers, J. D. (2000), 'Analysis Procedures for Performanced Based Design', *Proc. 12th World Conference on Earthquake Engineering*, Auckland, 30 Jan.-4 Feb. 2000, CD-Rom, Paper 2400: 8p.
12. Kilar, V., and Fajfar, P. (1997), 'Simple Push-over Analysis of Asymmetric Buildings', Earthquake Engineering and Structural Dynamics, Vol. 26, 233-249 (1997)
13. Kim, S. Eeri, M. and D'Amore, E. (1999), 'Push-over Analysis Procedure in Earthquake Engineering', Earthquake Spectra, Volume 15, No.3, 417-434 (1999)
14. Kuramoto, H., Teshigawara, M., Okuzono, T., Koshika, N., Takayama, M. and Hori, T. (2000), 'Predicting the earthquake response of building using equivalent SDF system', *Proc. 12th World Conference on Earthquake Engineering*, Auckland, 30 Jan.-4 Feb. 2000, CD-Rom, Paper 1039: 8p.

15. Lee, H. S. and Kang, K. Y. (2000), 'Correlation of experimental and analytical response of a 1:12 scale 10-story RC frame having non-seismic details', *Proc. 12th World Conference on Earthquake Engineering*, Auckland, 30 Jan.-4 Feb. 2000, CD-Rom, Paper 0598: 8p.

16. Lin, X., Moss, P. J. and Carr, A. J. (2000), 'Seismic analysis and design of building structures with supplemental lead dampers', *Proc. 12th World Conference on Earthquake Engineering*, Auckland, 30 Jan.-4 Feb. 2000, CD-Rom, Paper 1417: 8p.

17. Magenes, G. (2000), 'A method for pushover analysis in seismic assessment of masonry building', *Proc. 12th World Conference on Earthquake Engineering*, Auckland, 30 Jan.-4 Feb. 2000, CD-Rom, Paper 1866: 8p.

18. Martin, L. and Pekau, O. A. (1996), 'Plan-wise Distribution of Slip Load in Friction Damped Eccentric Structures', *Proc. 11th World Conference on Earthquake Engineering*, Acapulco, Mexico, June 23 - 28, 1996, CD-Rom, Paper 554: 8p.

19. Moghadam, A.S. and Tso, W.K. (1996), 'Damage Assessment of Eccentric Multistory Buildings Using 3-D Pushover Analysis', *Proc. 11th World Conference on Earthquake Engineering*, Acapulco, Mexico, June 23 - 28, 1996, CD-Rom, Paper 997: 8p.

20. Moghadam, A.S. and Tso, W.K. (2000), 'Pushover Analysis for Asymmetric and Set-back Multi-story Buildings', *Proc. 12th World Conference on Earthquake Engineering*, Auckland, 30 Jan.-4 Feb. 2000, CD-Rom, Paper 1093: 8p.

21. Nagao, T., Mukai, H. and Nishikawa, D. (2000), 'Case studies on performance based seismic design using capacity spectrum method' *Proc. 12th World Conference on Earthquake Engineering*, Auckland, 30 Jan.-4 Feb. 2000, CD-Rom, Paper 0694: 8p.

22. Pall, A. S., and Marsh, C. (1982), 'Response of friction damped braced frames', Journal Structure Division ASCE, Vol. 108: 1313-1323

23. Pall, A.S., Pall, R., 1993, "Friction-Dampers Used for Seismic Control of New and Existing Buildings in Canada", Proceedings, ATC 17-1, Seminar on Seismic Base Isolation, Passive Energy Dissipation and Active Control, San Francisco, Vol. 2, PP. 675-686

24. Pall, A. S. and Pall, R. (1996), 'Friction-dampers for seismic control of buildings—a Canadian experience', *Proc. 11th World Conference on Earthquake Engineering*, Acapulco, Mexico, June 23 - 28, 1996, CD-Rom, Paper 497: 8p.

25. Pekau, O. A. and Guimond, R. (1991), 'Controlling seismic response of eccentric structure by friction dampers', Earthquake Engineering and Structural Dynamics, Vol. 20, 505-521

26. Peter, K. and Badoux, M. (2000), 'Application of the Capacity Method to R.C. Building with Bearing Walls', *Proc. 12th World Conference on Earthquake Engineering*, Auckland, 30 Jan.-4 Feb. 2000, CD-Rom, Paper 0609: 8p.

27. Rao, R., Gergely, P. and White, R. N. (1996), 'A simplified design method for retrofit of gravity load design RC frames with friction dampers', *Proc. 11th World Conference on Earthquake Engineering*, Acapulco, Mexico, June 23 - 28, 1996, CD-Rom, Paper 1691: 8p.

28. Saiidi, M. and Sozen, M. A. (1981), 'Simple nonlinear seismic analysis of R/C structures', Journal of the Structural Division, *Proceedings* of the American Society of Civil Engineers, V. 107, N. ST5, May 1981, pp. 937-962.

29. Sheu, M. S., Chen, Y. H. and Liu, P. M. (2000). 'Dynamic Pushover Curve for Building Structures Under 3-Directional Earthquake Input', *Proc. 12th World Conference on Earthquake Engineering*, Auckland, 30 Jan.-4 Feb. 2000, CD-Rom, Paper 0384: 8p.

30. Skokan, M. J. and Hart, G. C. (2000), 'Reliability of nonlinear static methods for the seismic performance prediction of steel frame buildings', *Proc. 12th World Conference on Earthquake Engineering*, Auckland, 30 Jan.-4 Feb. 2000, CD-Rom, Paper 1972: 8p.

31. Tso, W. K., and Moghadam, A. S. (1996). 'Damage Assessment of Eccentric Multistory Buildings Using 3-D Pushover Analysis' *Proc. 11th World Conference on Earthquake Engineering*, Acapulco, Mexico, June 23 - 28, 1996, CD-Rom, Paper 997: 8p.

32. SAP2000 (1999). 'Getting Started, Basic Analysis Reference, Tutorial Manuals', Integrated Finite Element Analysis and Design of Structures, Computers and Structures, Inc., Berkeley, California, USA.

33. SAP2000 (1999). 'Concrete Design Manual, Steel Design Manual', Integrated Finite Element Analysis and Design of Structures, Computers and Structures, Inc., Berkeley, California, USA.

34. SAP2000 (1999). 'Analysis Reference', Integrated Finite Element Analysis and Design of Structures, Computers and Structures, Inc., Berkeley, California, USA.

35. Yang, P. and Wang, Y. (2000), 'A study on improvement of pushover analysis', *Proc. 12th World Conference on Earthquake Engineering*, Auckland, 30 Jan.-4 Feb. 2000, CD-Rom, Paper 1940: 8p.

APPENDIX A

A 5-BAY & 9-STORY FDBF SYSTEM

A.1 SYSTEM DESCRIPTION

A.1.1 Main Structure-MRF

The main structure of the 5-bay & 9-story FDBF is similar and simplified to the 9-story MRF that was designed by Brandow & Johnston Associates [Chopra and Goel, 2001] that is described in Table A.1 and shown in Figure A.1. The simplified 5-bay & 9-story FDBF which will be analyzed in this investigation is illustrated in Table A.2 and shown in Figure A.2.

A.1.2 Optimum Slip Load and Stiffness of Braces

Slip Load of Braces

Similarly to the single bay FDBF system in section 5.2, the friction damped braces for the multi-bay FDBF system can provide maximum energy dissipation only when the shear force resisted by the brace at each floor is equal to that of the frame without bracing

$$V_b = V_f \tag{A.1}$$

The free-body diagram of forces of the MRF system is illustrated in Figure A.2. For the weak beam/ strong column structure, the shear resisted by the frame is

$$V_f = \sum_{i=1}^{6} V_{fi} = \frac{\sum_{i=1}^{5} M_{pbi}}{h} = \frac{10 M_{pb}}{h} \tag{A.2}$$

where M_{pb} is the yield moment for the beams.

By the geometric relation, the slip loads P_s of the braces are

$$P_s = \frac{V_b}{\cos\varphi} = \frac{10M_{pb}}{h\cos\varphi} \tag{A.3}$$

where φ is the angle between the brace and the beam.

At optimum, the cross sections of the braces for this case are: for 1st floor, $A_b = 0.120m^2$, for 2nd -6th floor, $A_b = 0.114m^2$, for 7th floor, $A_b = 0.070m^2$, for 8th-9th floor, $A_b = 0.056m^2$, respectively. These sections of the braces are just chosen for analysis but they are too large to be acceptable in practical engineering.

Stiffness of the Braces

After dynamic analysis by DRAIN-2DX [Allahabadi and Powell, 1988], the comparison of the stiffness of FDBF with MRF is obtained from Equation (5.4)

$$\frac{K_{FDBF}}{K_{MRF}} = \frac{\omega_F^2}{\omega_M^2}$$

where K_{FDBF}, K_{MRF}, are the stiffnesses of FDBF and MRF, ω_F and ω_M are the first natural frequencies of FDBF and MRF, respectively. Here, the ratio of $\frac{\omega_F^2}{\omega_M^2}$ is equal to *2.86.*

Recalling Equation (3.16), the stiffness ratio of the brace to the frame is $\lambda = \frac{K_b}{K_f} = \frac{2.86-1}{1} = 1.86$. The reason that $\lambda << 4.0 \sim 5.0$ is because, in the 5-bay MRF system, there is only one bay with bracing.

A.2 NONLINEAR RESPONSE HISTORY ANALYSIS (NL-RHA)

Figure A.4 illustrates the comparison of roof displacement response of the 9-story FDBF with that of the MRF system, computed by DRAIN-2DX [Allahabadi and Powell, 1988]. For the MRF system subjected to the north-south component of the El-Centro (1940) ground motion with the scaled factor of *1.5*, the peak roof displacement, $u_M^r = 459.0mm$, but for FDBF system, $u_F^r = 180.0mm$, i.e., the roof displacement of the FDBF system is only about *39%* of that of the MRF system. Similarly, the top story drift of the FDBF system is only about *55%* of that of the MRF system. The comparison is shown in Figure A.5.

It is demonstrated again that the FDBF system has better seismic performance than the MRF system in controlling the roof displacements and story drifts.

A.3 MODAL PUSHOVER ANALYSIS (MPA)

Pushover Capacity Curve and Spectrum

The modal properties for the 5-bay & 9-story FDBF are summary in Table A.3. The force distributions of the first three modes are summarized in Table A.4 and the modal pushover capacity curves and spectrums are illustrated in Figure A.6 and Figure A.7, respectively.

By the capacity spectrum method from ATC-40 [ATC, 1996], the peak value of the deformation for the equivalent SDF systems of the first three modes are obtained, $D_{1o} = 135mm$ for mode 1, $D_{2o} = 47.4mm$ for mode 2 and $D_{3o} = 22.1mm$ for mode 3,

respectively. The procedures for developing the peak values of the deformation for mode 1 are illustrated and summary in Figures A.8, A.9, A.10 and Table A.5. According to Equation (4.8), the peak roof displacements of the first three modes for the MPA procedure are determined as $u_{1o} = 189.3mm$ for mode 1, $u_{2o} = 27.5mm$ for mode 2 and $u_{3o} = 6.4mm$ for mode 3, respectively.

At the roof displacements, $u_{1o} = 189.3mm, u_{2o} = 27.5mm, u_{3o} = 6.4mm$, the values of floor displacements and story drifts for MPA are determined by Equation (4.8). The peak values of floor displacement ratios (as % of the building height=*37.17m*) for the first three modes of the FDBF system are summarized in Table A.6 and illustrated in Figure A.11. Similarly, the story drift ratios (as % of story height) for the first three modes of FDBF system are shown in Figure A.12 and summarized in Table 8.7.

Comparison of Results Determined by MPA with NL-RHA

By SRSS combination rule, the responses of the floor displacement ratios and story drift ratios for 1 mode, two modes and 3 modes are summarized in Tables A.6 and A.7, and illustrated in Figures A.11 and A.12, respectively.

For response of the FDBF system combined by 3 modes, the errors of floor displacement ratios estimated by MPA compared with that by NL-RHA are between *–39.73%* and *8.54%*; and for story drifts ratios, the errors are from *–39.73%* to *55.85%*; i.e., the seismic responses at some levels are much underestimated and at other levels, they are much

overestimated. That is obviously not acceptable and it is necessary to introduce the improvement modal pushover analysis (IMPA) procedure.

A.4 COMPARISON OF RESULTS DETERMINED BY IMPA WITH NL-RHA

The differences between MPA and IMPA procedure were described in section 5.5.

As seen in Table A.8, for response of the FDBF system combined by 3 modes, the errors of floor displacement ratios estimated by IMPA compared with that by NL-RHA are between *1.69%* and *14.93%*. They are much better than that of MPA procedure.

As seen in Table A.9, for story drifts ratios, the errors of IMPA compared with NL-RHA procedure are from *1.69%* to *38.76%*. At first sight, they are not so correct but they are acceptable because they are overestimated and lead to a higher degree of safety.

As for the plastic slip in the friction bracing, the errors of IMPA compared with the NL-RHA procedure shown in Table A.10 and Figure A.15 are from *-100%* to *94.73%*. They are not good and therefore not acceptable.

A.5 COMPARISON OF RESPONSE BY IMPA, FEMA-273 WITH NL-RHA

The three force distributions for FEMA-273 pushover analysis are summarized in Table A.3.

The comparison of floor displacement ratios estimated by FEMA-273 pushover analysis with three force distributions, IMPA combined with 3 modes, and the NL-RHA procedure is illustrated in Figure A.16 and also summarized in Tables A.11. The errors for the FEMA-273 uniform force distribution are between *6.17%* and *54.22%*, *-5.65%* and *12.49%* for ELF force distribution, and *–6.44%* and *6.17%* for SRSS force distribution.

Similarly, for the story drift ratios summarized in Table A.12 and Figure A.17, the errors for the FEMA-273 uniform force distribution are between *–37.58%* and *53.49%*, *-12.70%* and *32.84%* for ELF force distribution, and *–10.04%* and *32.35%* for SRSS force distribution. For the plastic slip of friction bracing shown in Table A.13 and Figure A.18, the errors for the FEMA-273 uniform force distribution are between *–100%* and *210.5%*, *-100%* and *68.42%* for ELF force distribution, and *–100%* and *0.00%* for SRSS force distribution.

It is demonstrated again that the FEMA-273 and all three force distributions underestimate the seismic response of the FDBF system by more than IMPA, such as the floor displacements and story drifts. But for the plastic slips of friction bracing, all of these procedures cannot provide acceptable estimations.

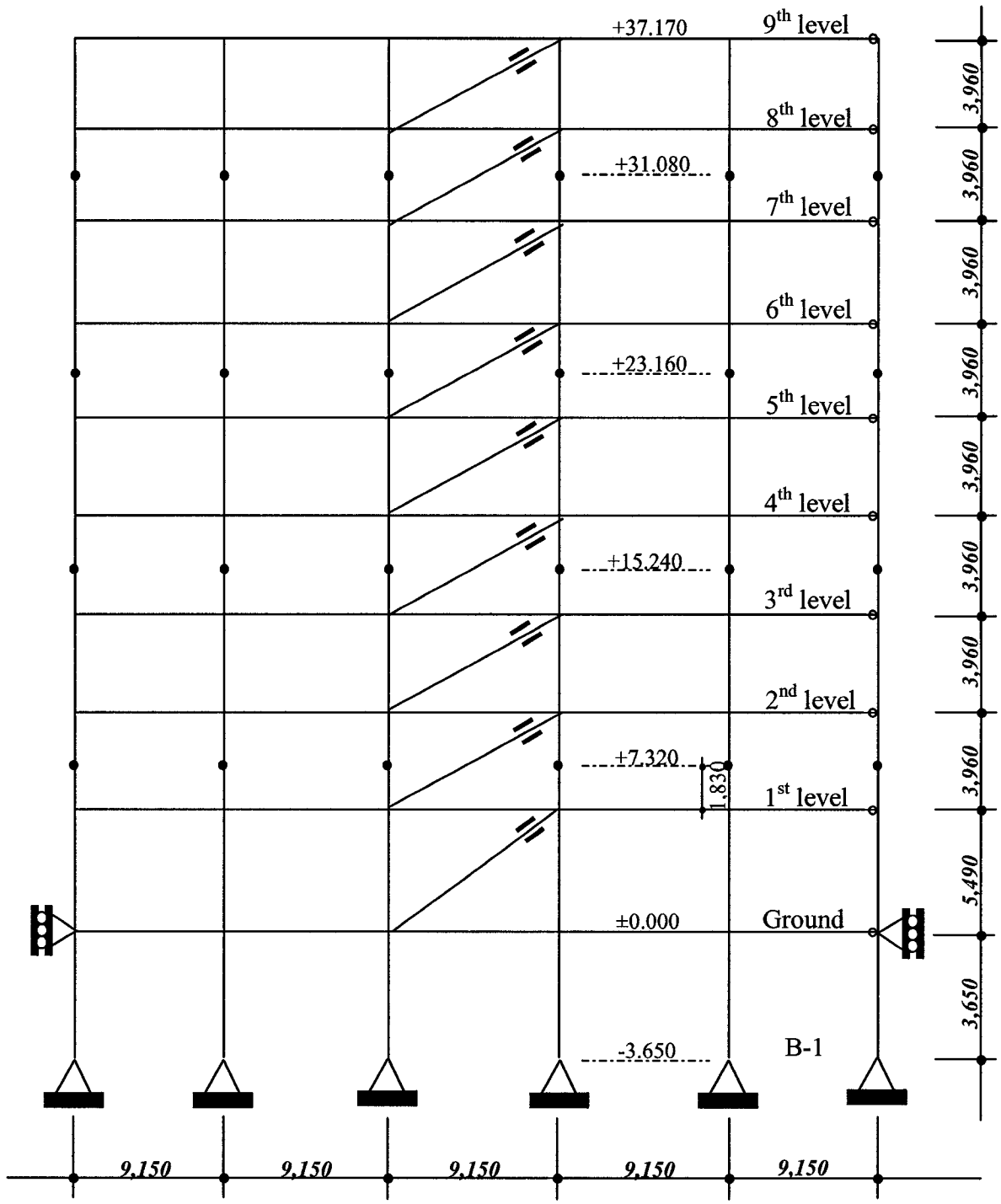

Figure A.1. 5-bay & 9-story FDBF System [Chopra and Goel, 2001]

Table A.1. System Description of 5-bay & 9-story MRF[Chopra and Goel, 2001]

<table>
<tr><td colspan="2">Beams (248MPa)</td><td colspan="2">Connections:</td></tr>
<tr><td>Ground-2nd level</td><td>W920x238</td><td colspan="2" rowspan="2">• indicate a moment resisting connection;
o indicate a simple (hinged) connection</td></tr>
<tr><td>3rd-6th level</td><td>W920x201</td></tr>
<tr><td>7th level</td><td>W760x147</td><td colspan="2">Dimensions:</td></tr>
<tr><td>8th level</td><td>W690x125</td><td colspan="2">all measurements are center line;</td></tr>
<tr><td>9th level</td><td>W610x101</td><td>basement level height</td><td>3.650 m</td></tr>
<tr><td colspan="2">Columns (345MPa)</td><td>Ground level height</td><td>5.490 m</td></tr>
<tr><td colspan="2">column size change at splices</td><td>1st-8th level heights</td><td>3.960 m</td></tr>
<tr><td>Level (m)</td><td>Section</td><td>bay widths (all)</td><td>9.150 m</td></tr>
<tr><td>-3.65~+7.32</td><td>W360x744</td><td colspan="2">Seismic Mass:</td></tr>
<tr><td>+7.32~+15.24</td><td>W360x677</td><td colspan="2">including steel framing, for one N-S MRF;</td></tr>
<tr><td>+15.24~+23.16</td><td>W360x551</td><td>Ground level</td><td>4.825×10^5 kg</td></tr>
<tr><td>+23.16~+31.08</td><td>W360x421</td><td>1st level</td><td>5.050×10^5 kg</td></tr>
<tr><td>+31.08~+37.17</td><td>W360x382</td><td>2nd-8th level</td><td>4.945×10^5 kg</td></tr>
<tr><td colspan="2">Splices:</td><td>9th level</td><td>5.350×10^5 kg</td></tr>
<tr><td colspan="2">denoted with•;are at 1.83m higher than 1st, 3rd,5th & 7th level</td><td>entire structure (above ground)</td><td>4.505×10^6 kg</td></tr>
<tr><td colspan="4">Restraints:</td></tr>
<tr><td colspan="4">columns pinned at base; structure laterally restrained at ground level</td></tr>
</table>

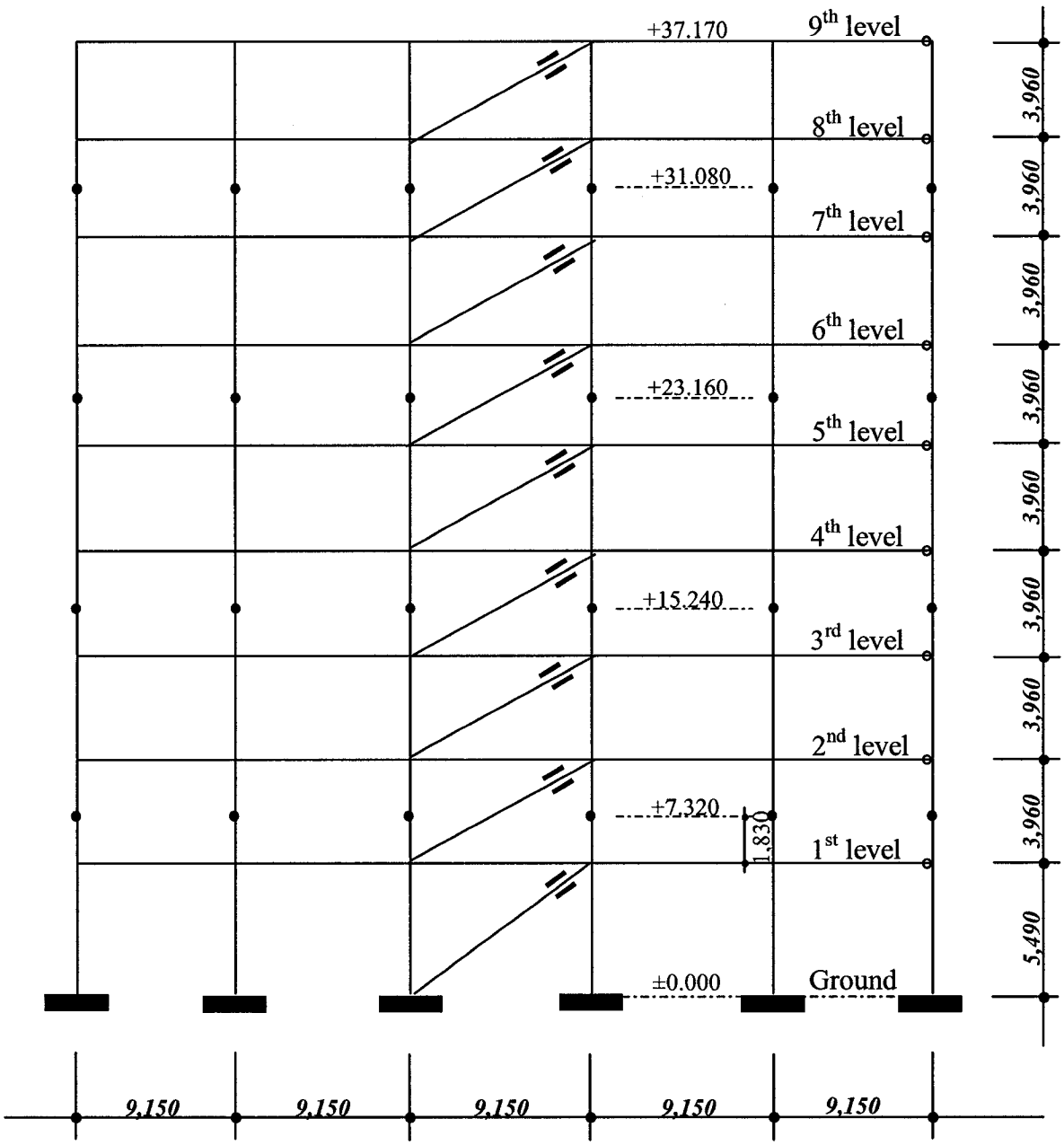

Figure A.2. Simplified 5-bay & 9-story FDBF System

Table A.2. System Description of Simplified 5-bay & 9-story MRF

Beams (248MPa)		**Connections:**	
Ground-2nd level	W920x238	• indicate a moment resisting connection; o indicate a simple (hinged) connection	
3rd-6th level	W920x201		
7th level	W760x147	**Dimensions:**	
8th level	W690x125	all measurements are center line;	
9th level	W610x101	No basement	
Columns (345MPa)		Ground level height	5.490 m
column size change at splices		1st-8th level heights	3.960 m
Level (m)	Section	bay widths (all)	9.150 m
±0.00~+7.32	W360x744	**Seismic Mass**:	
+7.32~+15.24	W360x677	including steel framing, for one N-S MRF;	
+15.24~+23.16	W360x551	Ground level	4.825×10^5 kg
+23.16~+31.08	W360x421	1st level	5.050×10^5 kg
+31.08~+37.17	W360x382	2nd-8th level	4.945×10^5 kg
Splices:		9th level	5.350×10^5 kg
denoted with•;are at 1.83m higher than 1st, 3rd,5th & 7th level		entire structure (above ground)	4.505×10^6 kg
Restraints:			
columns fixed at ground level			

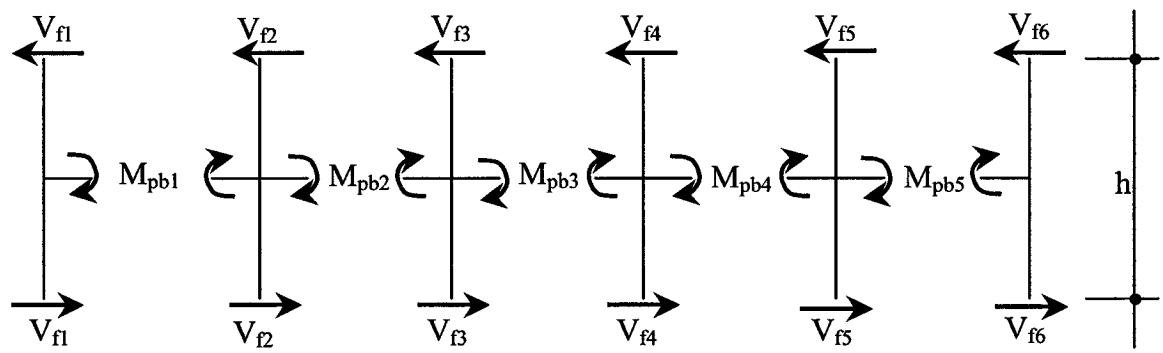

Figure A.3. Free-body Diagram of One Floor of MRF System

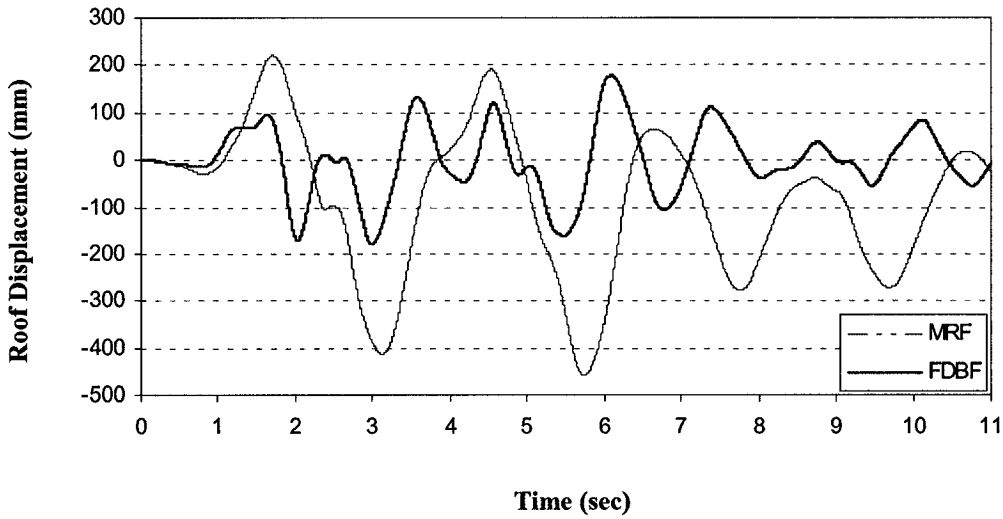

Figure A.4. Comparison of Roof Displacement History Response of 9-story FDBF with MRF to 1.5 El-Centro Ground Motion

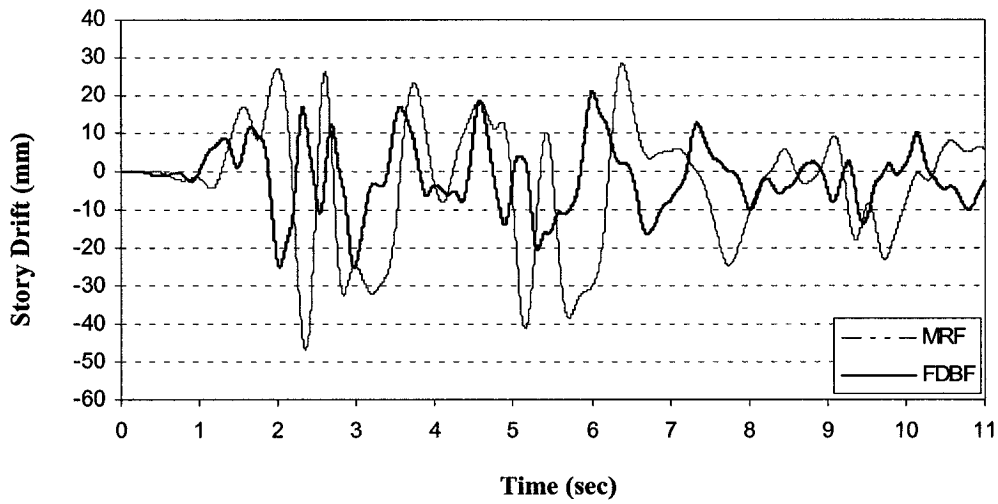

Figure A.5. Comparison of Top Story Drift History Response of 9-story FDBF with MRF to 1.5 El-Centro Ground Motion

Table A.3. Modal Properties for 9-story FDBF

Mode		1	2	3
Period, T_n (sec)		1.295	0.443	0.256
Frequency, ω_n (rad/sec)		4.853	14.177	24.572
Participation factor, Γ_n		1.402	0.58	0.289
Effective mass, M_n^* (k kg)		3400.0	637.4	211.7
Mode shape at story levels (normalized)	9(Roof)	1	1	1
	8	0.898	0.048	-0.238
	7	0.777	-0.093	-1.029
	6	0.653	-0.528	-0.905
	5	0.535	-0.771	-0.297
	4	0.413	-0.847	0.468
	3	0.291	-0.756	0.97
	2	0.177	-0.535	0.951
	1	0.074	-0.247	0.512
	Ground	0	0	0

Table A.4 Force Distributions

Floor	MPA			FEMA-273		
	Mode #1	Mode #2	Mode #3	Uniform	ELF	SRSS
9 (Roof)	1.000	1.000	1.000	1.000	1.000	1.000
8	0.831	0.444	-0.220	0.925	0.785	0.519
7	0.719	-0.086	-0.952	0.925	0.651	0.159
6	0.604	-0.489	-0.837	0.925	0.526	0.006
5	0.495	-0.713	-0.275	0.925	0.410	0.072
4	0.382	-0.784	0.433	0.925	0.304	0.237
3	0.269	-0.700	0.898	0.925	0.208	0.341
2	0.163	-0.495	0.880	0.925	0.125	0.302
1	0.070	-0.233	0.484	0.944	0.057	0.157
Ground	0.000	0.000	0.000	0.000	0.000	0.000

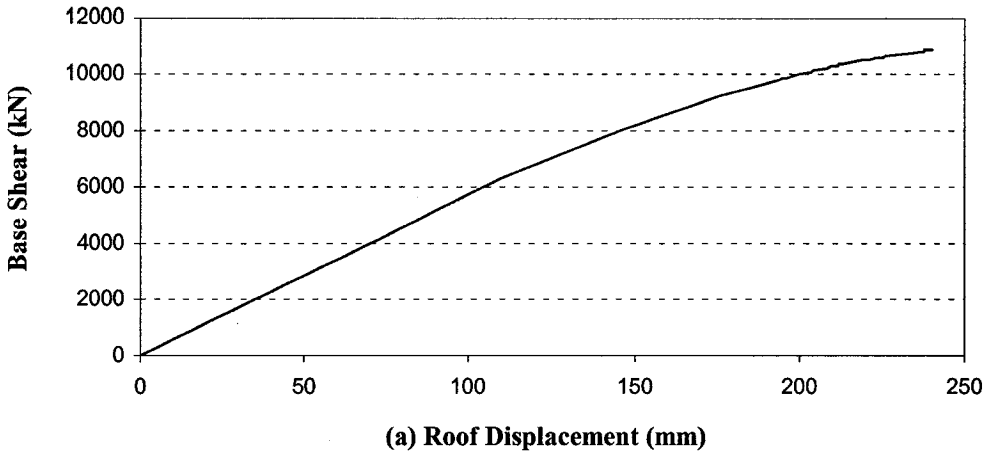

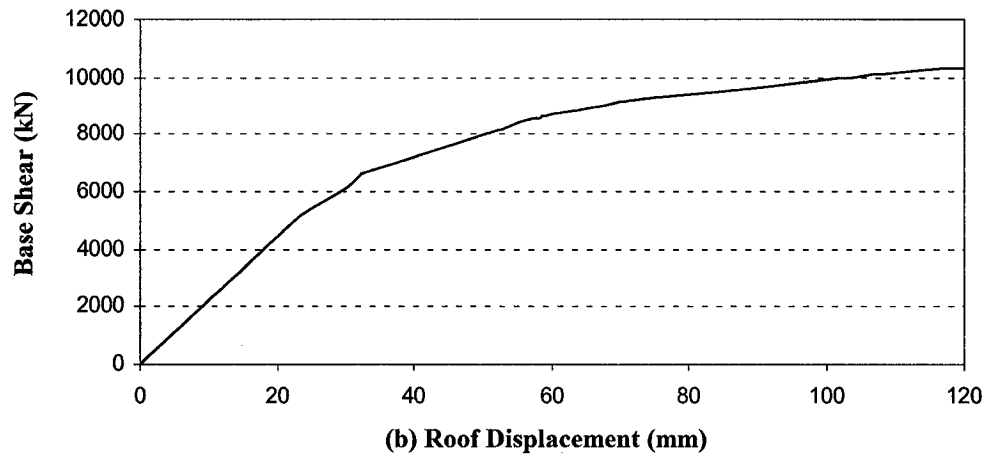

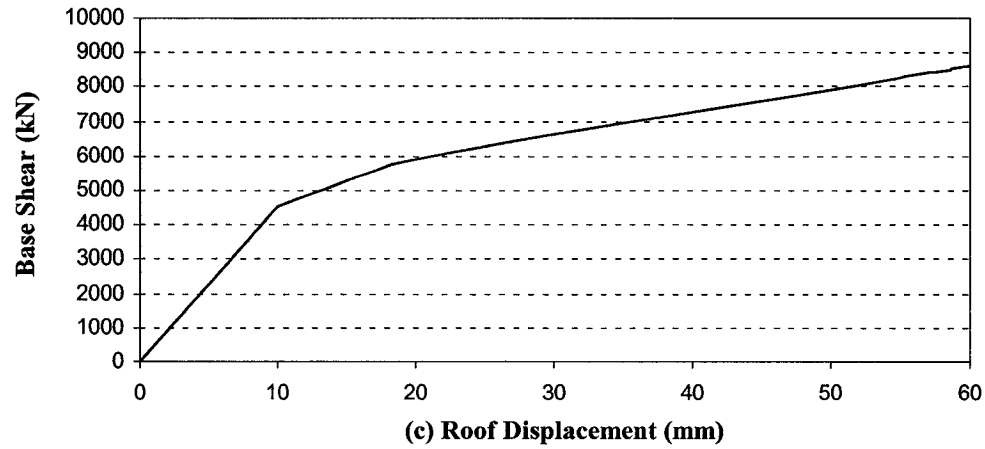

Figure A.6. Modal Pushover Capacity Curve for 9-story FDBF: (a) "Mode" 1, (b) "Mode" 2, (c) "Mode" 3

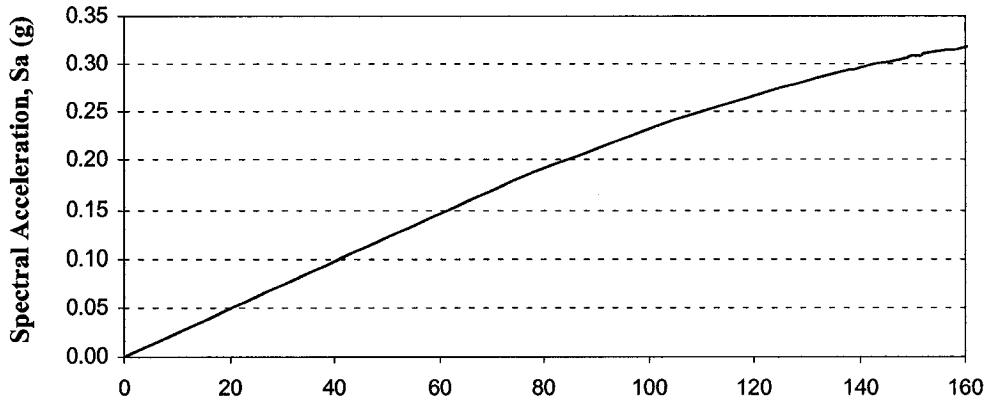

(a) Spectral Displacement, S_d (mm)

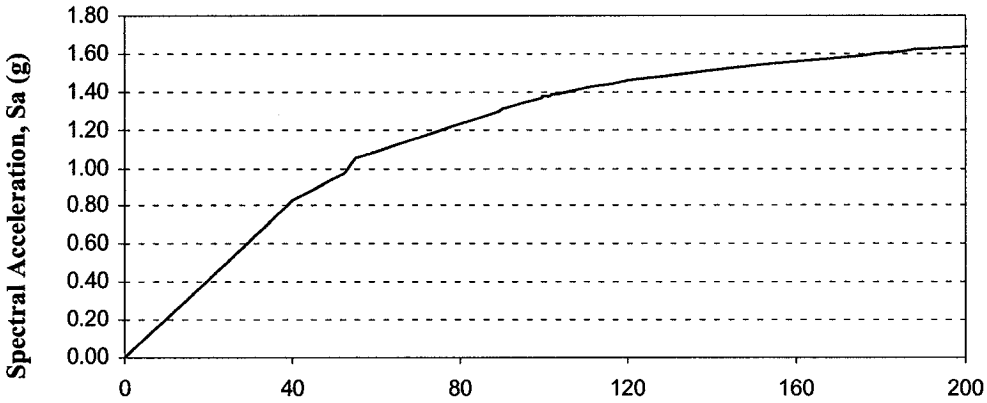

(b) Spectral Displacement, S_d (mm)

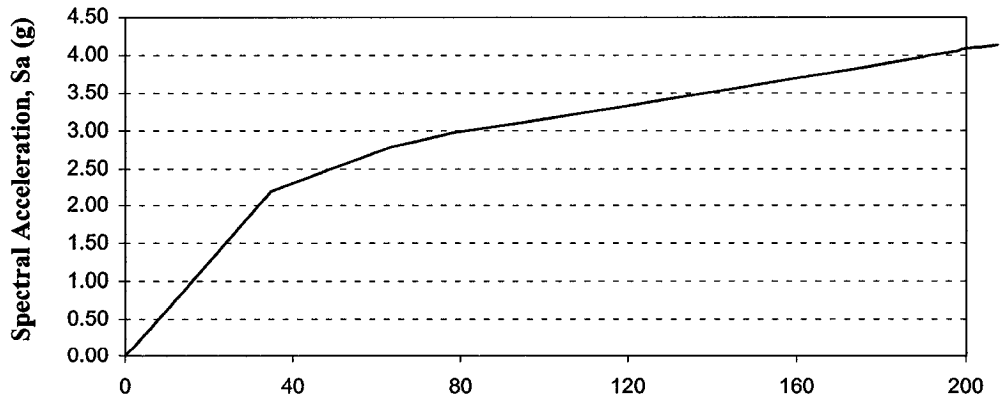

(c) Spectral Displacement, S_d (mm)

Figure A.7. Capacity Spectrum Curves for 9-story FDBF: (a) "Mode" 1, (b) "Mode" 2, (c) "Mode" 3

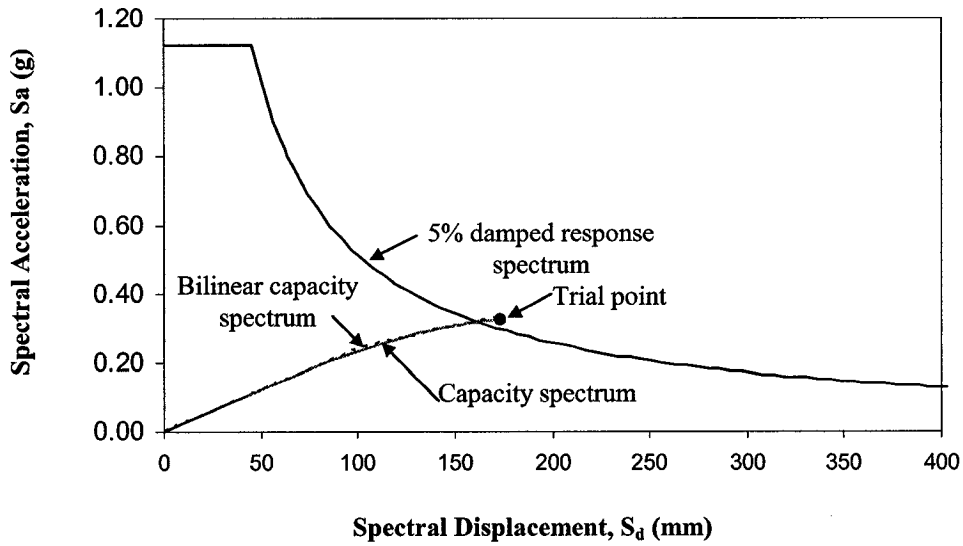

Figure A.8. Capacity Spectrum Procedure A after Step 4

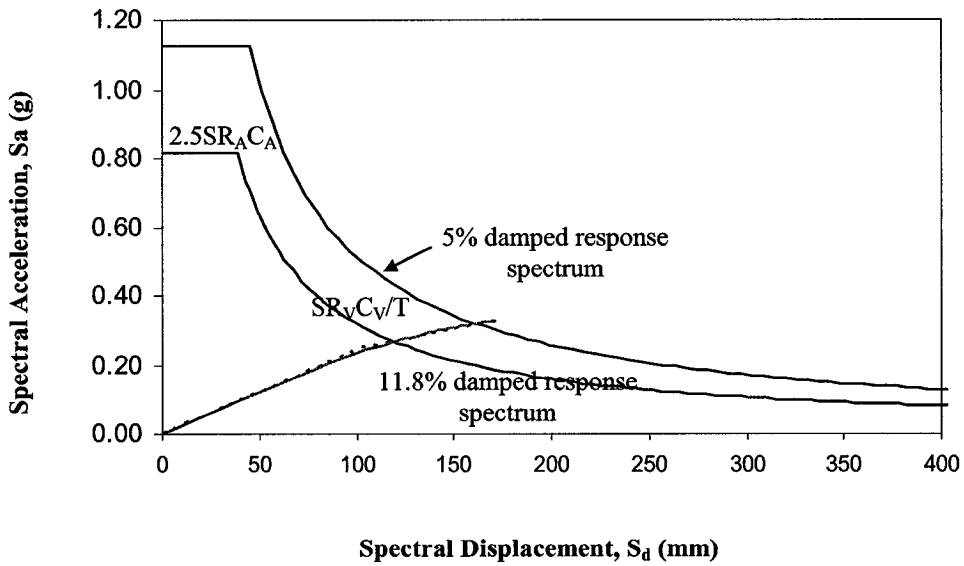

Figure A.9. Capacity Spectrum Procedure A after Step 5

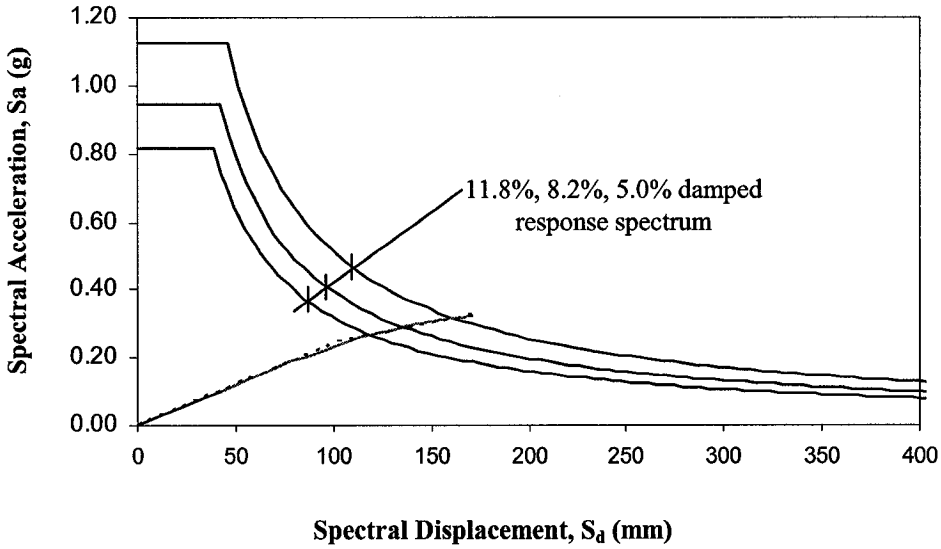

Figure A.10. Capacity Spectrum Procedure A after Step 7

Table A.5. Trial for Demand Performance Point for Mode 1

Trial	a_y(g)	d_y(mm)	a_{p1}(g)	d_{p1}(mm)	Error (%)	$\hat{\zeta}_{eq}$ (%)	SR_A	SR_V	Ts(sec)
0						5.0	0.998	1.000	0.401
1	0.2481	103.3	0.3257	171.2		11.8	0.724	0.788	0.435
2	0.2059	85.7	0.2757	125.5	-26.7	7.7	0.858	0.892	0.416
3	0.2203	91.7	0.2995	142.7	13.7	9.0	0.811	0.855	0.422
4	0.2133	88.8	0.2852	132.0	-7.5	8.2	0.839	0.877	0.418
Final			0.2920	135.0	2.3				

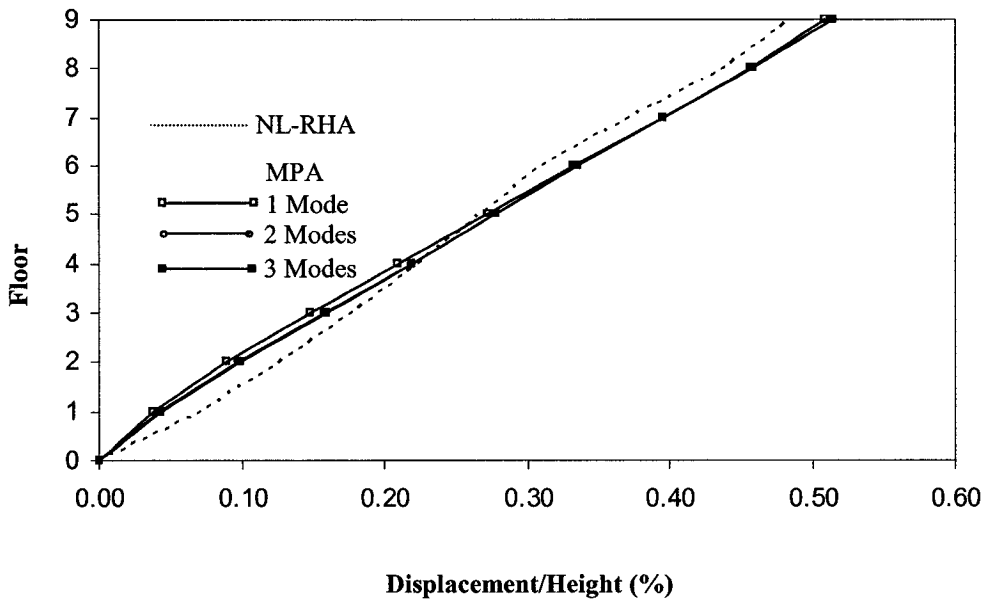

Figure A.11. Comparison of Floor Displacement Ratios Determined by MPA and NL-RHA for FDBF

Table A.6. Peak Values of Floor Displacement Ratios (as % of building height=37.17m) from MPA for 1.5x El Centro Ground Motion

Floor	Displacement/Height (%)							Error (%)		
	Modal Response			Combined (MPA)			NL-RHA			
	Mode #1	Mode #2	Mode #3	1 Mode	2 Modes	3 Modes		1 Mode	2 Modes	3 Modes
0	0.000	0.000	0.000	0.000	0.000	0.000	0.000	0.00	0.00	0.00
1	0.038	-0.018	0.009	0.038	0.042	0.043	0.071	-46.87	-41.02	-39.73
2	0.090	-0.040	0.016	0.090	0.098	0.100	0.127	-29.01	-22.44	-21.37
3	0.148	-0.056	0.017	0.148	0.158	0.159	0.178	-16.69	-10.95	-10.46
4	0.210	-0.063	0.008	0.210	0.219	0.220	0.224	-6.29	-2.22	-2.15
5	0.272	-0.057	-0.005	0.272	0.278	0.278	0.268	1.63	3.84	3.86
6	0.333	-0.039	-0.016	0.333	0.335	0.335	0.309	7.69	8.43	8.54
7	0.396	-0.007	-0.018	0.396	0.396	0.396	0.373	6.27	6.28	6.39
8	0.457	0.036	-0.004	0.457	0.459	0.459	0.439	4.30	4.61	4.62
9	0.509	0.074	0.017	0.509	0.515	0.515	0.485	4.93	6.03	6.09

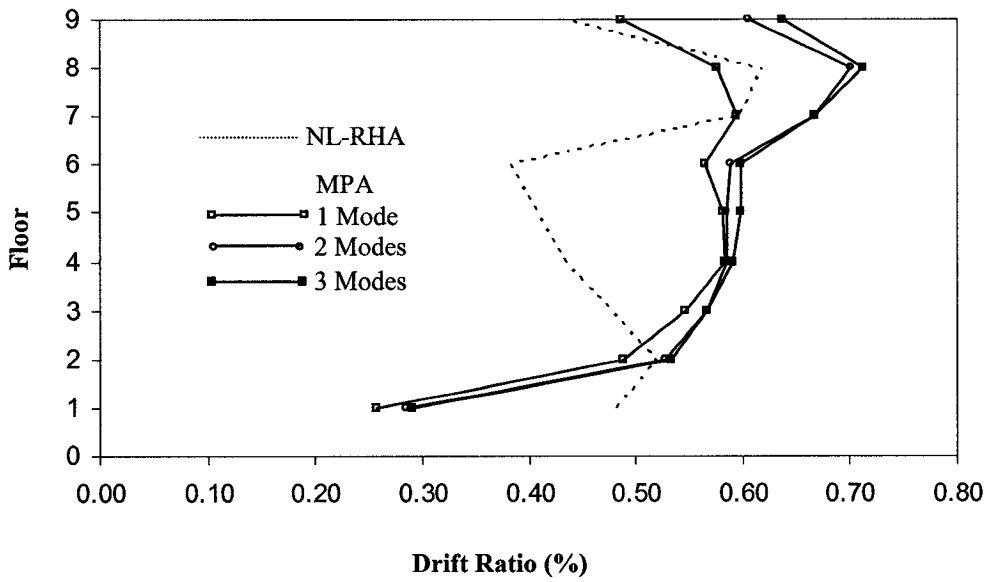

Figure A.12. Comparison of Drift Ratios Determined by MPA and NL-RHA for FDBF

Table A.7. Peak Values of Story Drift Ratios (as % of story height) from MPA for 1.5x El Centro Ground Motion

Floor	Drift Ratio (%)							Error (%)		
	Modal Response			Combined (MPA)			NL-RHA			
	Mode #1	Mode #2	Mode #3	1 Mode	2 Modes	3 Modes		1 Mode	2 Modes	3 Modes
1	0.256	-0.124	0.060	0.256	0.285	0.291	0.483	-46.87	-41.02	-39.73
2	0.489	-0.200	0.071	0.489	0.528	0.533	0.520	-6.04	1.54	2.45
3	0.546	-0.153	0.003	0.546	0.567	0.567	0.480	13.85	18.25	18.25
4	0.583	-0.063	-0.081	0.583	0.586	0.592	0.437	33.44	34.22	35.50
5	0.583	0.053	-0.124	0.583	0.585	0.598	0.409	42.45	43.04	46.20
6	0.566	0.168	-0.098	0.566	0.590	0.598	0.384	47.34	53.73	55.85
7	0.595	0.302	-0.020	0.595	0.667	0.668	0.598	-0.61	11.49	11.54
8	0.577	0.398	0.128	0.577	0.701	0.712	0.619	-6.81	13.24	15.10
9	0.487	0.361	0.200	0.487	0.606	0.638	0.439	10.86	37.98	45.30

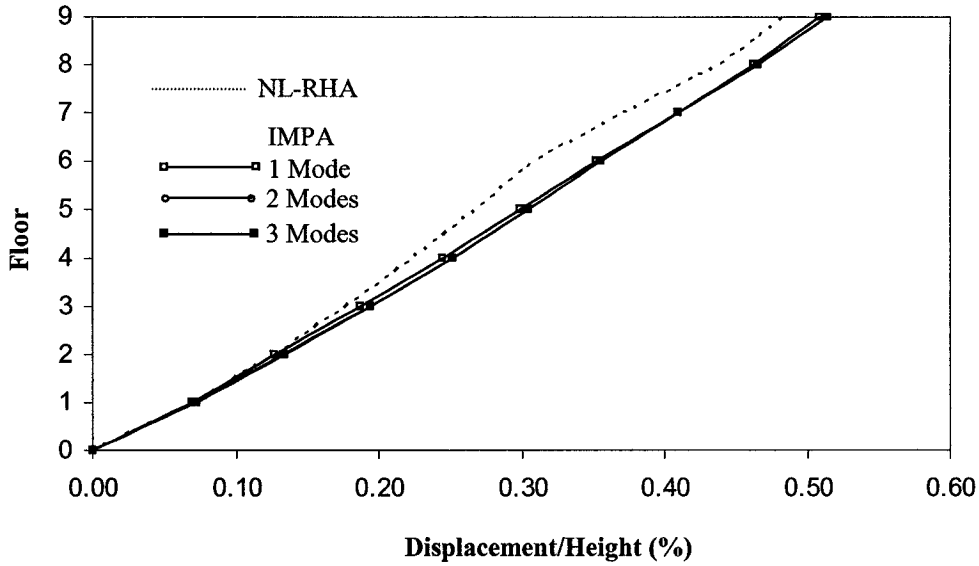

Figure A.13. Comparison of Floor Displacement Ratios Determined by IMPA and NL-RHA for FDBF

Table A.8. Peak Values of Floor Displacement Ratios (as % of building height=37.17m) from IMPA for 1.5x El Centro Ground Motion

Floor	Displacement/Height (%)							Error (%)		
	Modal Response			Combined (IMPA)			NL-RHA			
	Mode #1	Mode #2	Mode #3	1 Mode	2 Modes	3 Modes		1 Mode	2 Modes	3 Modes
0	0.000	0.000	0.000	0.000	0.000	0.000	0.000	0.00	0.00	0.00
1	0.070	-0.017	0.009	0.070	0.072	0.072	0.071	-2.01	0.93	1.69
2	0.128	-0.037	0.016	0.128	0.133	0.134	0.127	0.74	4.97	5.77
3	0.187	-0.053	0.017	0.187	0.194	0.195	0.178	5.05	9.18	9.58
4	0.245	-0.059	0.008	0.245	0.252	0.252	0.224	9.11	12.26	12.32
5	0.300	-0.054	-0.005	0.300	0.304	0.304	0.268	11.78	13.58	13.60
6	0.353	-0.037	-0.016	0.353	0.355	0.355	0.309	14.19	14.82	14.93
7	0.409	-0.007	-0.018	0.409	0.409	0.410	0.373	9.86	9.88	9.98
8	0.464	0.038	-0.004	0.464	0.465	0.465	0.439	5.71	6.07	6.07
9	0.509	0.074	0.017	0.509	0.515	0.515	0.485	4.93	6.03	6.09

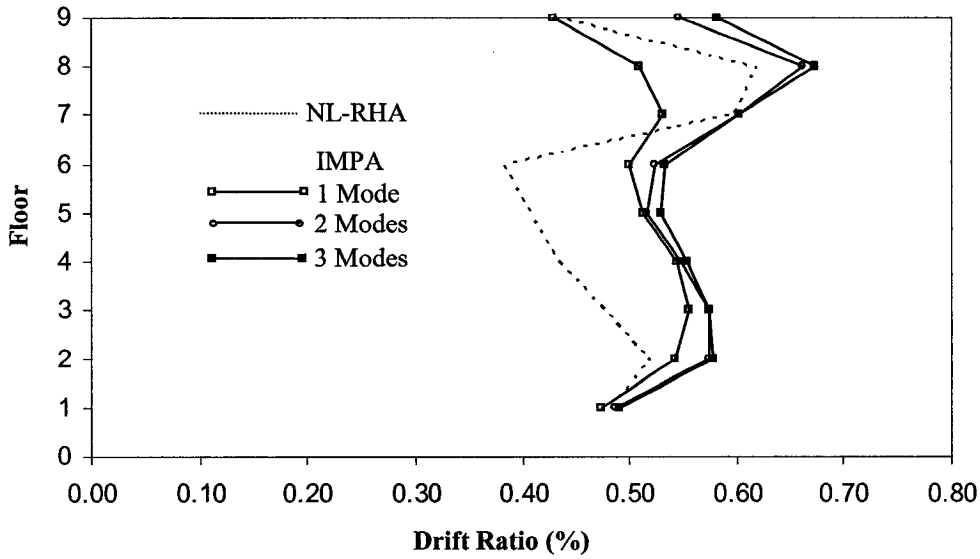

Figure A.14. Comparison of Drift Ratios Determined by IMPA and NL-RHA for FDBF

Table A.9. Peak Values of Story Drift Ratios (as % of story height) from IMPA for 1.5x El Centro Ground Motion

Floor	Drift Ratio (%)							Error (%)		
	Modal Response			Combined (IMPA)			NL-RHA			
	Mode #1	Mode #2	Mode #3	1 Mode	2 Modes	3 Modes		1 Mode	2 Modes	3 Modes
1	0.473	-0.117	0.060	0.473	0.487	0.491	0.483	-2.01	0.93	1.69
2	0.542	-0.189	0.071	0.542	0.574	0.579	0.520	4.28	10.44	11.27
3	0.555	-0.145	0.003	0.555	0.574	0.574	0.480	15.74	19.63	19.63
4	0.544	-0.060	-0.081	0.544	0.548	0.554	0.437	24.59	25.35	26.72
5	0.513	0.049	-0.124	0.513	0.516	0.530	0.409	25.52	26.09	29.66
6	0.499	0.158	-0.098	0.499	0.523	0.533	0.384	30.01	36.38	38.76
7	0.532	0.283	-0.020	0.532	0.603	0.603	0.598	-11.10	0.69	0.74
8	0.509	0.423	0.128	0.509	0.662	0.674	0.619	-17.76	6.95	8.93
9	0.429	0.338	0.200	0.429	0.546	0.581	0.439	-2.36	24.23	32.31

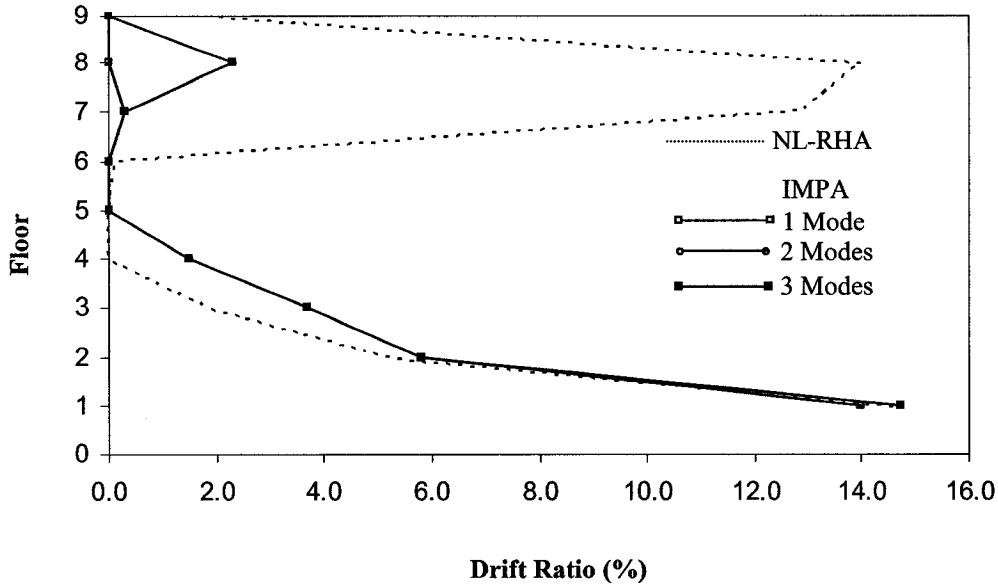

Figure A.15. Comparison of Plastic Slips of Braces Determined by IMPA and NL-RHA for FDBF

Table A.10. Peak Values of Plastic Slips of Braces Determined by IMPA for 1.5x El Centro Ground Motion

Floor	Plastic Extensions (mm)							Error (%)		
	Modal Response			Combined (IMPA)			NL-RHA			
	Mode #1	Mode #2	Mode #3	1 Mode	2 Modes	3 Modes		1 Mode	2 Modes	3 Modes
1	14.0	-4.6	0.0	14.0	14.7	14.7	14.6	-4.11	0.93	0.93
2	5.8	0.0	0.0	5.8	5.8	5.8	5.3	9.43	9.43	9.43
3	3.7	0.0	0.0	3.7	3.7	3.7	1.9	94.74	94.74	94.74
4	1.5	0.0	0.0	1.5	1.5	1.5	0.0	-	-	-
5	0.0	0.0	0.0	0.0	0.0	0.0	0.0	0.00	0.00	0.00
6	0.0	0.0	0.0	0.0	0.0	0.0	0.1	-100.00	-100.00	-100.00
7	0.3	0.0	0.0	0.3	0.3	0.3	12.9	-97.67	-97.67	-97.67
8	0.0	2.3	0.0	0.0	2.3	2.3	14.0	-100.00	-83.57	-83.57
9	0.0	0.0	0.0	0.0	0.0	0.0	1.9	-100.00	-100.00	-100.00

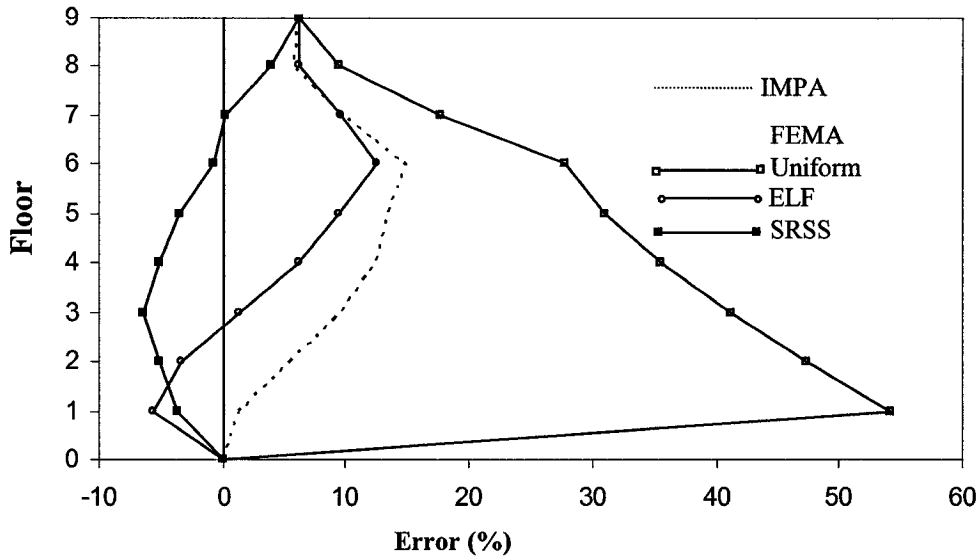

Figure A.16. Errors in Floor Displacement Ratios estimated by FEMA-273 and IMPA for FDBF

Table A.11. Peak Values of Floor Displacement Ratios (as % of building height=37.17 m) from FEMA and IMPA for 1.5 El-Centro Ground Motion

Floor	Displacement/Height (%)					Error (%)			
	FEMA			IMPA 3 modes	NL-RHA	FEMA			IMPA 3 modes
	Uniform	ELF	SRSS			Uniform	ELF	SRSS	
0	0.000	0.000	0.000	0.000	0.000	0.00	0.00	0.00	0.00
1	0.109	0.067	0.068	0.072	0.071	54.22	-5.65	-3.75	1.69
2	0.187	0.123	0.121	0.134	0.127	47.44	-3.40	-5.10	5.77
3	0.251	0.180	0.167	0.195	0.178	41.17	1.27	-6.44	9.58
4	0.303	0.238	0.213	0.252	0.224	35.48	6.17	-5.12	12.32
5	0.351	0.293	0.259	0.304	0.268	31.00	9.42	-3.53	13.60
6	0.395	0.348	0.307	0.355	0.309	27.81	12.49	-0.74	14.93
7	0.439	0.409	0.374	0.410	0.373	17.71	9.63	0.18	9.98
8	0.480	0.467	0.456	0.465	0.439	9.39	6.27	3.94	6.07
9	0.515	0.515	0.515	0.515	0.485	6.17	6.17	6.17	6.09

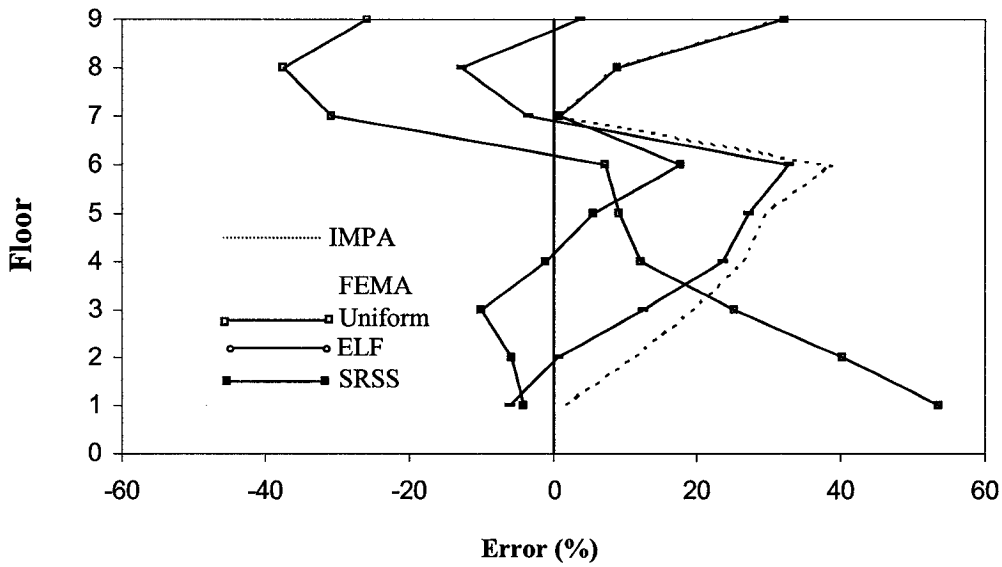

Figure A.17. Errors in Story Drift Ratios Estimated by FEMA-273 and IMPA for FDBF

Table A.12. Peak Values of Story Drifts Ratios (as % of story height) from FEMA and IMPA for 1.5 El-Centro Ground Motion

Floor	Drifts Ratio (%)					Error (%)			
	FEMA			IMPA 3 modes	NL-RHA	FEMA			IMPA 3 modes
	Uniform	ELF	SRSS			Uniform	ELF	SRSS	
1	0.741	0.454	0.463	0.491	0.483	53.49	-6.10	-4.21	1.69
2	0.730	0.523	0.490	0.579	0.520	40.35	0.52	-5.79	11.27
3	0.601	0.540	0.432	0.574	0.480	25.21	12.58	-10.04	19.63
4	0.490	0.540	0.432	0.554	0.437	12.11	23.66	-1.19	26.72
5	0.447	0.520	0.432	0.530	0.409	9.28	27.19	5.58	29.66
6	0.412	0.510	0.452	0.533	0.384	7.19	32.84	17.71	38.76
7	0.414	0.576	0.603	0.603	0.598	-30.75	-3.72	0.84	0.74
8	0.386	0.540	0.674	0.674	0.619	-37.58	-12.70	8.89	8.93
9	0.326	0.455	0.581	0.581	0.439	-25.80	3.54	32.35	32.31

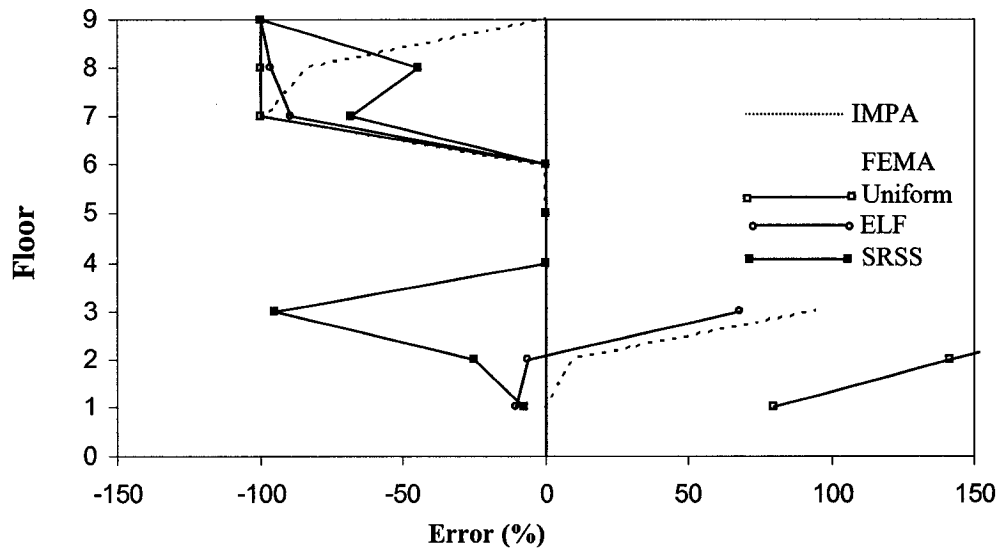

Figure A.18. Errors in Plastic Slips of Braces Determined by FEMA-273 and IMPA to 1.5 El-Centro Ground Motion for FDBF

Table A.13. Peak Values of Plastic Slips of Braces Determined by FEMA and IMPA for 1.5 El-Centro Ground Motion

Floor	Plastic Slip (mm)					Error (%)			
	FEMA			IMPA 3 modes	NL-RHA	FEMA			IMPA 3 modes
	Uniform	ELF	SRSS			Uniform	ELF	SRSS	
1	26.3	13.1	13.5	14.7	14.6	80.14	-10.27	-7.53	0.93
2	12.8	5.0	4.0	5.8	5.3	141.51	-5.66	-24.53	9.43
3	5.9	3.2	0.1	3.7	1.9	210.53	68.42	-94.74	94.74
4	0.9	1.2	0.0	1.5	0.0	-	-	0.00	-
5	0.0	0.0	0.0	0.0	0.0	0.00	0.00	0.00	0.00
6	0.0	0.0	0.0	0.0	0.1	-100.00	-100.00	-100.00	-100.00
7	0.0	1.4	4.0	0.3	12.9	-100.00	-88.98	-68.50	-97.64
8	0.0	0.5	7.8	2.3	14.0	-100.00	-96.43	-44.29	-83.57
9	0.0	0.0	0.0	0.0	1.9	-100.00	-100.00	-100.00	0.00

APPENDIX B

B.1. Seismic Coefficient, C_A

	Shaking Intensity, ZEN[1,2]					
Soil Profile Type	**= 0.075**	**= 0.15**	**= 0.20**	**= 0.30**	**= 0.40**	**> 0.40**
S_B	0.08	0.15	0.20	0.30	0.40	1.0(ZEN)
S_C	0.09	0.18	0.24	0.33	0.40	1.0(ZEN)
S_D	0.12	0.22	0.28	0.36	0.44	1.1(ZEN)
S_E	0.19	0.30	0.34	0.36	0.36	0.9(ZEN)
S_F	*Site-specific geotechnical investigation required to determine C_A*					

1. The value of E used to determine the product, ZEN, should be taken to be equal to 0.5 for the Serviceability Earthquake, 1.0 for the Design Earthquake, and 1.25 (Zone 4 sites) or 1.5 (Zone 3 sites) for the Maximum Earthquake

2. Seismic coefficient C_A should be determined by linear interpolation for values of the product ZEN other than those shown in the table.

B.2. Seismic Coefficient, C_V

	Shaking Intensity, ZEN[1,2]					
Soil Profile Type	**= 0.075**	**= 0.15**	**= 0.20**	**= 0.30**	**= 0.40**	**> 0.40**
S_B	0.08	0.15	0.20	0.30	0.40	1.0(ZEN)
S_C	0.13	0.25	0.32	0.45	0.56	1.4(ZEN)
S_D	0.18	0.32	0.40	0.54	0.64	1.6(ZEN)
S_E	0.26	0.50	0.64	0.84	0.96	2.4(ZEN)
S_F	*Site-specific geotechnical investigation required to determine C_V*					

1. The value of E used to determine the product, ZEN, should be taken to be equal to 0.5 for the Serviceability Earthquake, 1.0 for the Design Earthquake, and 1.25 (Zone 4 sites) or 1.5 (Zone 3 sites) for the Maximum Earthquake

2. Seismic coefficient C_V should be determined by linear interpolation for values of the product ZEN other than those shown in the table.

B.3. Values for Damping Modification Factor, κ

Structural Behavior Type[1]	ζ_{eq} (percent)	κ
Type A	□16.25	1.0
	>16.25	$1.13-\frac{0.51(a_y d_{pi} - d_y a_{pi})}{a_{pi} d_{pi}}$
Type B	□25	0.67
	>25	$0.845-\frac{0.446(a_y d_{pi} - d_y a_{pi})}{a_{pi} d_{pi}}$
Type C	Any Value	0.33

1. See Appendix B.5 for structural behavior types.

B.4. Minimum Allowable SR_A and SR_V Values[1]

Structural Behavior Type[2]	SR_A	SR_V
Type A[2]	0.33	0.50
Type B	0.44	0.56
Type C	0.56	0.67

1. Values for SR_A and SR_V shall not be less than those shown in this table.

2. See Appendix B.5 for structural behavior types.

B.5. Structural Behavior Types

Shaking Duration	Essentially New Building	Average Existing Building	Poor Existing Building
Short	Type A	Type B	Type C
Long	Type B	Type C	Type C